POLITECNICO DI TORINO

Corso di Laurea Magistrale in Ingegneria Edile

Tesi di Laurea Magistrale

EXPERIMENTAL AND NUMERICAL ASSESSMENT OF THERMAL BRIDGES IN BUILDING COMPONENTS

Relatore:
Prof. Ing. Marco Perino

Correlatori:
Prof. Arch. Stefano Fantucci
Prof. Arch. Elisa Fenoglio

Candidato:
Clarissa Carmagnini

29 Novembre 2018

Contents

List of figures

List of tables

1 Introduction

Nomenclature			
Φ	Heat flow, W	T_f	Temperature of the fluid, °C
φ	Specific heat flux, W/m^2	T_r	Radiative temperature, °C
λ	Thermal conductivity, W/(mK)	h_e	External heat transfer coefficient, W/(m^{2}K)
T_a	Surface temperature, °C	h_i	Internal heat transfer coefficient, W/(m^{2}K)
T_b	Surface temperature, °C	ΔT	Temperature difference, K
U	Thermal transmittance, W/(m^{2}K)	Φ_{1D}	One-dimensional heat flow, W
R	Thermal resistance, m^{2}K/W	Φ_{2D}	Two-dimensional heat flow, W
h	Heat transfer coefficient, W/(m^{2}K)	Φ_{tb}	Thermal bridge heat flow, W
h_c	Convective heat transfer coefficient, W/(m^{2}K)	φ_{1D}	One-dimensional specific heat flux, W/m^2
h_r	Radiative heat transfer coefficient, W/(m^{2}K)	φ_{2D}	Two-dimensional specific heat flux, W/m^2
Ψ	Linear thermal transmittance, W/(mK)	$R_{add,up}$	Upper additional resistance, m^{2}K/W
X	Point thermal transmittance, W/K	$R_{add,low}$	Lower additional resistance, m^{2}K/W
H_{tr}	Transmission heat transfer coefficient, W/K	R_x	Total thermal transmittance, m^{2}K/W
φ_n	Heat flux by *n* elements, W/m^2	T_{up}	Upper temperature, °C
φ_{2n}	Heat flux by *2n* elements, W/m^2	T_{low}	Lower temperature, °C

In the past few decades, the research in the building sector focused on the improvement of the thermal performances of building components and materials in order to increase the thermal efficiency of buildings.

This trend aims at accomplishing the EU targets of the Directive 2010/31/UE, in which it has been introduced the concept of Nearly Zero-Energy Buildings (nZEBs). 'Nearly Zero–Energy Buildings' means a building that has a very high energy performance, Annex 1 of the Directive, and in which "the nearly zero or very low amount of energy required should be covered to a very significant extent by energy from renewable sources, including energy from renewable sources produced on-site or nearby".

All new private buildings will have to achieve these standards by 31st December 2020 and by 31st December 2018 for public ones.

From this perspective, the European Union demands ever lower energy requirements as regard building heating and cooling, thereby putting the focus of engineers and architects on specific solutions in order to improve the energy efficiency of buildings. This focus is mainly on the building envelope, in particular on the new solution of assembly and on high insulating materials, in order to decrease the issue of thermal losses, which is closely linked with localized phenomena of components, one of them the thermal bridges. A thermal bridge is an area of an envelope characterized by lower thermal resistance than closer materials, which therefore can be identified whenever a multilayer wall, roof or floor shows discontinuities about thermal performance. These discontinuities shall be represented by an interruption of material, a classic is that of a pillar inside a masonry, or geometry chance, for instance the joint between balcony and wall or simply the intersection between two envelopes. Hence, where the building has a thermal bridge the heat loss is higher than the points where the multilayer envelope, for example, is homogeneous. Moreover, these thermal bridges, linked to the heat losses, shall be expressed by means of the linear thermal transmittance, Ψ, or the point thermal transmittance, χ. The first parameter is useful to calculate the two-dimensional heat flow, whereas the second one the three-dimensional heat flow.

Baghero S. *et al*. [28] have studied the impact of thermal bridge on the heat flux of an existing building in six different cases: the linear thermal bridges between the current wall and the pillar (pc), between the window and the curtain wall (wc), between the roller shutter box and the curtain wall (rc), between the beam and the curtain wall (bc), between the balcony and the curtain wall (bac) and between the roller shutter box, the balcony and the window (rbaw). The total percentage contribution determined by Baghero S. *et al*. [28] was about 60%, whereas focusing on the single contributes the following percentages were established: about 20% by rbaw-joint, about 15% by bc-joint and pc-joint separately, about 4% by bac-joint, 5% by wc-joint and 0.2 % is given by rc-joint.

Sadauskiene J. *et al.* [29] have investigated the influence of point thermal bridges on the thermal transmittance, U, of a ventilated façed system with aluminium fastener. They have highlighted the difficulty of calculating the χ-value, since it requires not only the knowledge of thermal properties and dimensions of faster but also the thermal property and the dimensions of the materials employed in the external wall layers. The results obtained by Sadauskiene J. *et al.* [29] revelated an influence of point thermal transmittance on the U-value of the entire wall investigated of 30%. Furthermore, Sadauskiene J. *et al.* explained that the biggest influence of the χ-value and the U-value of the whole wall are the thermal conductivity, λ, of the bearing multilayer envelope and the thickness of the insulating materials.

Theodosiou T.G. *et al.* [30] have studied the double brick wall building, that is largely employed in Greece and the influence of thermal bridges on the heating need of three typical apartments. The authors show that the percentage contribution of thermal bridges on the heating need can reach 30%, although the building presents a high insulation level.

Owing to the importance of the assessment of thermal bridges, the aim of the present thesis is to research and establish an experimental methodology in order to determine the linear thermal transmittance, Ψ, through two types of thermal bridges.

The proposed methodology is introduced as an alternative procedure to assess the Ψ-value, since is based on the analysis of one-dimensional and two-dimensional heat flows by means of only one experimental measurement by heat flux meter. Furthermore, the methodology is carried out employing one additional resistance, R_{add}, and without the knowledge of the equivalent thermal conductivity of the envelope. Hence, by using this additional resistance it is possible to measure by heat flux meter the φ_{1D}-value and the φ_{2D}-value at the same time, that are necessary in order to estimate the Ψ-value. This methodology is in addition to the assessment of the linear thermal transmittance by two experimental measurements using heat flux meter for the one-dimensional and two-dimensional heat fluxes separately.

Subsequently, the experimental methodology is validated by several numerical simulations, by using Physibel Bisco software according to EN ISO 10211:2017 [1].

The first type of thermal bridge investigated refers to a dry envelope composed of several materials, which have different thermal properties. In particular, this envelope, the so-called assembly, consists of plasterboard panels, insulating materials, metallic frames and filler layers. In this case, the presence of elements with different thermal conductivities engenders a structural thermal bridge, which is specifically caused by the metallic frame and the filler layer and it is assessed by the linear thermal transmittance, Ψ. The experimental test was carried out by a heat flux meter apparatus at the Department of Energy (DENERG) of Politecnico di Torino and then validated by numerical simulations on Physibel Bisco in several configurations. The latter concern variations on the R_{add} value and that of the thermal conductivity of filler, λ_{filler}.

The second envelope studied consists of two masonry walls composed of traditional and high-performance insulation materials filled bricks, respectively. In this case, the structural thermal bridges are due to the joint between consecutives bricks and thus the focus was calculated the Ψ-values caused by them. In particular, the horizontal linear thermal transmittance, Ψ_h, linked to the horizontal joint, and the vertical linear thermal transmittance, Ψ_v, referred to the vertical joint were determined. The experimental tests were carried out into a thermostatic chamber, in the DENERG laboratory, by heat flux analysis, according to ISO 9869-1:2014 [4], and by IR thermography. In this case, the values of thermal transmittance, thermal conductance and thermal conductivity of the traditional and high-performance insulation materials bricks were also assessed.

2 State of the art

The base of this work was careful research through the international scientific publications in order to understand what was the knowledge so far learned. Hence, the study of these papers focused on finding cases similar to the two investigated and then their reproducibility was evaluated.

In particular, in the first case the focus was on the assessment of dry envelope and how the structural thermal bridges were assessed. In the second one, scientific research was more articulated due to the issues encountered during the experimental procedure, as will be illustrated in the chapter devoted.

As regards the proposed methodology, widely explained in Chapter 4, no reference to past research served as a basis. In this case, a study of the heat flows, one-dimensional and two-dimensional, was only conducted.

2.1 Dry envelope

The main researches taken as a reference were those of Zalewski L. *et al.* [11], Sprengard C. *et al.* [16], Prata J. *et al.* [17], Baldinelli G. *et al.* [18], Isaia F. *et al.* [19], Lorenzati A. *et al.* [20].

The first case is the one that is closest to the one in question in the thesis, since the layer of the envelope is comparable with those used for the investigated assembly. Zalewski L. *et al.* performed an experimental and numerical study in order to evaluate the linear thermal transmittance of the wall. The experimental procedure was carried out by a thermostatic chamber and by IR thermography and the numerical simulation by Physibel Trisco. The focus of this research was on the concept of equivalent thermal conductivity, that is the parameter excluded in this thesis, as mentioned above.

Also Sprengard C. *et al.,* Isaia F. *et al.* and Lorenzati A. *et al.* started from the assessment of the equivalent thermal conductivity even if the experimental set-up and the numerical model were the same ones used in this work. Indeed, the Ψ-value performed by HFM apparatus and by Physibel Bisco were compared.

In the other two studies, the experimental procedures were performed by a calibrated hot box and by IR thermography.

2.2 Masonry brick

In this case, the following articles were added to those previously mentioned: Nardi I. *et al.* [14], Asdrubali F. *et al.* [21], Evangelisti L. *et al.* [22], Asdrubali F. *et al.* [23], Wernery J. *et al.* [24], Nagy B. [25], Sassine E. *et al.* [26].

The direct comparison was only possible with Wernery J. *et al.* [24], since in this article a study about aerogel-filled insulating brick was conducted. In particular, the research assessed and compared a brick with perlite filling and a brick with aerogel filling by means of experimental and numerical methods for evaluating the thermal conductivities. The experimental procedures were carried out by a guarded hot plate device, while the numerical ones by Physibel Bisco.

In addition to this approach, the other articles highlighted the possibility of evaluating the influence of linear thermal bridges by heat flux meter method (HFM) and by Infrared thermography (IRT). The former, which can assess the thermal transmittance in situ, works with several conditions, for example, a minimum temperature difference between the two sides of the wall, and without anomalies, for instance, humidity between the heat flux sensor and the wall. Indeed, the IR thermography was introduced over the last few years in order to assess the thermal transmittance. This method, however, is still complicated to apply today due to the determination of several parameters employed in IR image reading. In this context Avdelidis N.P. *et al.* [27] studied the role of the emissivity on the temperature reading, and Dactu S. *et al.* evaluated the influence of reflected radiation on the accuracy of temperature measurements. The reflected temperature, in fact, allow eliminating the contribution of the reflected radiation in order to achieve the correct value of temperatures.

Asdrubali F. *et al.* [21] provided a methodology to assess thermal bridges by an *incidence factor of the thermal bridges*, which was not applied due to the hypotheses of the method. Finally, Asdrubali F. *et al.* [23] proposed a mathematical approach, based on the sampling Kantorovich algorithm, in order to improve the thermographic images.

3 The thermal bridges

3.1 Heat transfer

The heat transfer is defined as the propagation of thermal energy due to a temperature difference, from a high-temperature reservoir to a lower temperature reservoir according to the second law of thermodynamics. From the macroscopic point of view, this phenomenon is classified into three modes:

- Thermal conduction: through molecular agitation within a continuous medium without any motion of the material as a whole;
- Thermal convection: by movement of a heated fluid, liquid or gaseous;
- Thermal radiation: a process by which a heated surface emits electromagnetic radiation in all directions. This mode does not require an intervening medium to carry it.

The fundamental quantities in this field are the heat flow, Φ, defined as the quantity of heat that crosses a building envelope in the unit of time, and the specific heat flux, φ, obtained by Eq. (1) where A is the area of the building envelope.

$$\varphi = \frac{\Phi}{A} \qquad [\mathrm{W/m^2}] \qquad (1)$$

Taking into consideration an infinitesimal surface of the continuous medium, dA, the specific heat flow, that crosses the isothermal surfaces, is obtained by Fourier's law, Eq. (2):

$$\varphi = \frac{d\Phi}{dA} = -\lambda \frac{\partial t}{\partial n} \qquad [\mathrm{W/m^2}] \qquad (2)$$

where the proportionality constant, λ, is the so-called thermal conductivity, the t-parameter is the temperature and the parameter n is the normal coordinate to the isothermal surface. The above-mentioned isothermal surface is a surface characterized by an identical temperature in all its points at a given moment.

In the case of a flat wall with its height and length of dimensions higher than its thickness and a series of homogeneous and isotropic parallel flat layers, the general equation of thermal conductivity can be written, by applying the principle of energy conservation, as shown Eq.(3):

$$\lambda\left(\frac{\partial^2 t}{\partial x^2}+\frac{\partial^2 t}{\partial y^2}+\frac{\partial^2 t}{\partial z^2}\right)+\dot{q}=\rho c\frac{\partial t}{\partial \tau} \qquad \text{[W/m}^2\text{]} \qquad (3)$$

where $\dot{q}$ is the volumetric thermal flow generated by Joule effect, ρ is the density and c is the specific heat.

In steady-state conditions, $\frac{\partial t}{\partial \tau}=0$, and without internal generation, $\dot{q}=0$, Eq. (3) becomes Eq. (4).

$$\left(\frac{\partial^2 t}{\partial x^2}+\frac{\partial^2 t}{\partial y^2}+\frac{\partial^2 t}{\partial z^2}\right)=0 \qquad \text{[W/m}^2\text{]} \qquad (4)$$

In the case of the temperature ranges only by *x*-coordinate, Eq. (4) becomes Eq. (5), the so-called Laplace's equation, and the heat flow, Φ, by conduction across an isothermal surface is perpendicular to every point at the surface itself.

$$\frac{\partial^2 t}{\partial x^2}=0 \qquad \text{[W/m}^2\text{]} \qquad (5)$$

In this way, by integrating Eq. (5), for a flat multilayers wall with thickness-*s* and constant temperatures, T_a and T_b, on the two opposite surfaces the specific heat flux is assessed by means of Eq. (5):

$$\varphi=\frac{\Phi}{A}=\frac{|T_a-T_b|}{\sum_{j=1}^{k}\frac{s_j}{\lambda_j}} \qquad \text{[W/m}^2\text{]} \qquad (6)$$

where k is the number of layers, s_j and λ_j are the thickness and the thermal conductivity of the j-th homogeneous layer respectively.

Moreover, considering the same wall in contact with air, the heat exchange between the boundary surface and the environment is of two types, by convection and radiation. In the case of the temperature of the fluid, T_f, is the same as the radiant temperature, T_r, the heat flow is evaluated as:

$$\Phi=(h_c+h_r)A\left(T_a-T_{r=f}\right)=hA\left(T_a-T_{r=f}\right) \qquad \text{[W]} \qquad (7)$$

where T_a is the temperature on the boundary surface, h_c is the convective heat transfer coefficient, h_r is the radiative heat transfer coefficient, and h is the heat transfer coefficient, which assumes different values concerning the slope of the wall and the environmental conditions.

Hence, a wall dividing two environments at a different temperature is subject to a global heat transfer involving conduction, convection and radiant at the same time. Eq. (6) can be rewritten as Eq. (7):

$$\Phi = UA|T_1 - T_2| \qquad \text{[W]} \qquad (8)$$

where T_1 and T_2 are the temperature value of the two environments and U is the thermal transmittance, which is the heat flow that, in steady-state conditions, crosses the unit area of the building envelope. Due to a temperature difference, T_1 - T_2, between the two environments. The thermal transmittance of a building envelope is assessed by Eq. (9), in which h_e and h_i are the external heat transfer coefficient and internal heat transfer coefficient respectively.

$$U = \frac{1}{h_e + \sum_{j=1}^{k} \frac{s_j}{\lambda_j} + h_i} \qquad \text{[W/m}^2\text{K]} \qquad (9)$$

Nevertheless, the building envelope is not perfectly homogeneous, and several discontinuities arise, both geometrical and material. According to EN ISO 10211:2017 [1], the thermal bridge is the part of the envelope where the thermal transmittance changes significantly as a result of deviation of one-dimensional heat flow. The types of the thermal bridge can be distinguished as follows:

- Geometrical thermal bridge, due to a discrepancy between the opposite sides of a wall, e.g. at the corner of the building;
- Structural thermal bridge, caused by one type of material with different thermal resistance, e.g. at the joint between pillar and bricks;
- Mixed type thermal bridge, when both geometrical and structural thermal bridge exists.

Consequently, the hypothesis of one-dimensional conditions is no longer valid and as a consequence of this, issues regarding the heat losses across thermal bridges and how to assess them arise. In the case of a linear thermal bridge, which in general has a more significant influence on heat losses than the point thermal bridges, the linear thermal transmittance, ψ, is the parameter used to evaluate the two-dimensional heat flow. The point thermal transmittance, χ, is instead used to assess the three-dimensional heat flow.

3.2 The linear transmittance of the thermal bridge

According to EN ISO 14683:2014 [2], the possible methods for determining ψ-value are:

- Numerical calculations, with a typical accuracy of ± 5%, when full details of the different elements of the building envelope are known. In this case, the linear thermal transmittance shall be calculated by EN ISO 10211:2017 [1] guidelines;
- Thermal bridges catalogues, with a typical accuracy of ± 20%, when sufficient information is available. The value of ψ from the catalogue may be used when dimensions and thermal properties of the examples are similar or less favourable than those of the designed detail;
- Manual calculation, with a typical accuracy of ± 20%, when sufficient information is available. The method shall provide information regarding types of constructional details, dimensional limits, values of surface resistance, limits of thermal conductivity of materials, method accuracy;
- Default values, with a typical accuracy of ± 20%, where the details are not designed but the size and the main form of the building are already defined. Tables of values of linear thermal transmittance are given in the Annex of EN ISO 14683:2014 [2]. The use of default values involves several approximations, that lead to overestimating the heat losses.

3.2.1 Numerical calculations

The methodology proposed by EN ISO 10211:2017 [1] is based on a division of building into flat surfaces, characterised by their thermal transmittance, U, linear thermal bridges, ψ, and point thermal bridges, χ, that in this discussion will not be considered.

The transmission heat transfer coefficient, H_{tr}, is calculated through the building envelope is defined by Eq. (10):

$$H_{tr} = \sum_i A_i U_i + \sum_k l_k \Psi_k \qquad \text{[W/K]} \qquad (10)$$

where A_i is the area of element i of the building envelope, U_i is the thermal transmittance of the element i of the building envelope, l_k is the length of linear thermal bridge k, Ψ_k is the linear thermal transmittance of the linear thermal bridge k.

The area of the building elements shall be calculated by a three-dimension system in according to EN ISO 13789:2008 [3]: internal dimension, excluding the thickness of internal partitions, overall internal dimension, including the thickness of internal partitions and external dimension.

By multiplying each term by the temperature difference, ΔT, between the two environments, Eq. (10) may be rewritten as Eq. (11), where Φ_{2D} is the two-dimensional heat flow of the building envelope, Φ_{1D} is the one-dimensional heat flow calculated by Eq. (8).

$$\Phi_{2D} = \sum_i \Phi_{1D,i} + \left(\sum_k l_k \Psi_k\right) \Delta T \qquad \text{[W]} \qquad (11)$$

Hence, the linear thermal transmittance, Ψ, shall be evaluated by Eq (12).

$$\Psi = \frac{\Phi_{2D} - \Phi_{1D}}{l \Delta T} \qquad \text{[W/(mK)]} \qquad (12)$$

In order to assess the two-dimensional heat flow, Φ_{2D}, it is necessary to use a methodology, so-called finite element analysis, that divides the designed detail into several elements of homogeneous material and solves the equations for each individual element. Usually, this methodology shall be performed using software, like Physibel Bisco or Trisco.

The numbers of homogeneous material must be such as to observe the convergence criteria, which is reflected respecting either of these two hypotheses:

- Doubling the subdivisions number of the element, the calculated heat flow cannot differ for more than 1%, by means of Eq. (12).

$$1 - \frac{\varphi_n}{\varphi_{2n}} \leq 0.01 \qquad (13)$$

- Doubling the subdivisions number, the temperature factor, f_{Rsi}, on the internal surface cannot differ for more than 0.005.

4 Experimental methodologies

In order to assess the linear thermal transmittance, Ψ, the experimental procedure, that are already known according to EN ISO 10211:2017 [1] and EN ISO 14683:2014 [2], is based on two experimental measurements by means of heat flux meter method. More specifically, one measurement aims to determine the one-dimensional heat flow, Φ_{1D}, and the other one to measure the two-dimensional heat flow, Φ_{2D}.

By applying this methodology to a multilayer envelope composed by several materials, the two experimental measurements can be carried out by a heat flux meter apparatus (HFM apparatus) and by a thermostatic chamber, called Building Envelope Test Cell (BET cell). Hence, regardless of the experimental instrument employed, the assessment of the Ψ-value is only possible through two measurements: the first by the investigated envelope without the thermal bridge and the second one by the envelope with the thermal bridge.

The result of the first measurement will allow obtaining the φ_{1D}-value, whereas the result of the second one the φ_{2D}-value. The latter must be multiplied by the measurement areas of the heat flux sensors, in order to achieve the Φ_{1D}-value and the Φ_{2D}-value respectively. Having assessed these two values by two different measurements, and taking into account the length, l, of the linear thermal bridge, Eq. (12) can be applied.

In the present thesis, an alternative experimental methodology is proposed in order to assess the φ_{1D}-value and the φ_{2D}-value by means of only one measurement, and thus to calculate the Ψ-value by Eq. (12). Taking into account the same envelope described above, this means that the single measurement is carried out on the envelope with the thermal bridge. Furthermore, this methodology is based on the knowledge of the thermal resistance of an additional resistance, R_{add}, and of the set temperature on the opposite surfaces, T_{up} and T_{low}.

To better explain the proposed methodology and to underline the differences with that by means of two experimental measurements, the following cases are investigated:

- HFM A, referred to two measurements by HFM apparatus;
- HFM B, referred to one measurement by HFM apparatus;
- BET A, related to one measurement into the thermostatic chamber by HF analysis;
- BET B, related to one measurement into the thermostatic chamber by IR thermography;

In this chapter, these four cases will be studied and applied with a reference sample composed by several materials, so-called multilayer envelope, and in the following chapters, they will be employed on the two types of thermal bridges investigated.

4.1 HFM A

The multilayer envelope composed by several materials, with a total thermal resistance R_x, two additional resistances, with $R_{add,up}$-value and $R_{add,low}$-value, and liable to a temperature difference, T_{up} - T_{low}, is showed in Figure 1 below. Furthermore, Figure 1 displays the multilayer envelope without the thermal bridge and subjected to the one-dimensional conditions. This configuration is called one-dimensional assembly (1D assembly).

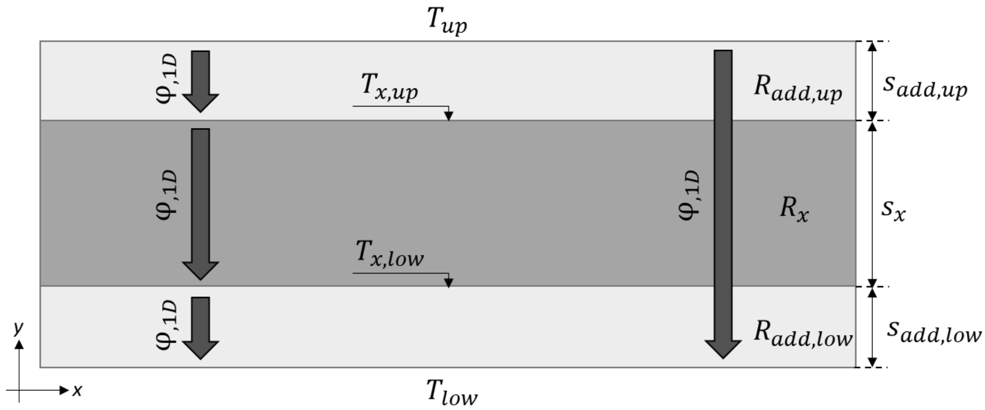

Figure 1_ Multilayer wall horizontal section.

In steady-state conditions and without internal generation, the one-dimensional specific heat flux, φ_{1D}, can be assessed by one experimental measurement by HFM apparatus, by imposing a temperature difference, T_{up} - T_{low}, at the boundary of the layer (Figure 1).

In case of a structural thermal bridge, this example becomes a heterogeneity sample, which is characterized by materials with different R-value, R_{tb} and R_x, in the x-direction (Figure 2), and the hypotheses of two-dimensional conditions are now reported. Figure 2 shows this configuration called two-dimensional assembly (2D assembly).

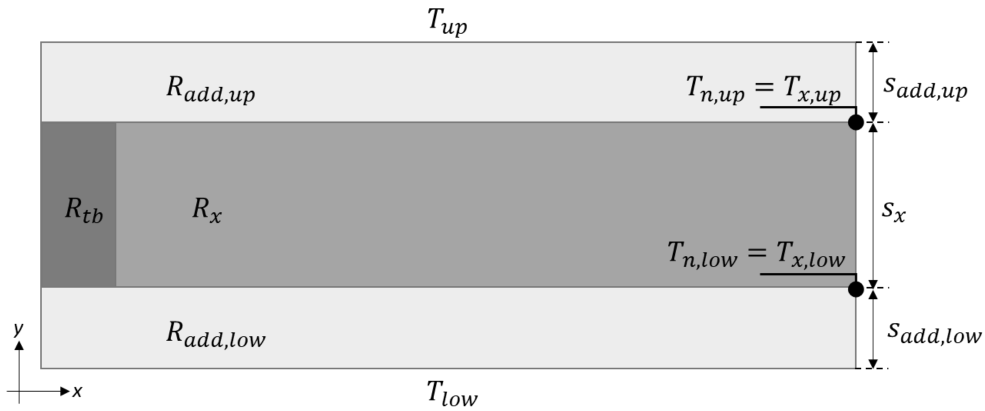

Figure 2_ Structural thermal bridge.

By using the same additional resistance, $R_{add,up}$ and $R_{add,low}$ and by setting the same temperature difference, T_{up} - T_{low}, than the previous measurement on the 1D assembly, the two-dimensional specific heat flux, φ_{2D}, can be assessed by one experimental measurement by HFM apparatus.

After the φ_{1D}-value and the φ_{2D}-value must be multiplied by the measurement area of the heat flux sensor in order to obtain the Φ_{1D}-value and the Φ_{2D}-value. At this point, the Ψ-value is calculated by Eq. (12). Hence, the linear thermal transmittance, in this case, shall be assessed by means of two experimental measurements.

4.2 *HFM B*

Taking into account the same 1D and 2D assemblies (Figure 1 and Figure 2, respectively) of the HFM A case, the following observations can be made.

As regards the 1D assembly (Figure 1), in steady-state conditions and without internal generations, the φ_{1D}-value is the same in each layer and can be calculated as the ratio between the temperature difference, T_{up} - T_{low}, at the boundary of the layer, and its thermal resistance, Eq.(14).

$$\varphi_{1D} = \frac{|T_{up} - T_{low}|}{R_{add} + R_x} = \frac{|T_{up} - T_{x,up}|}{R_{add,up}} = \frac{|T_{x,up} - T_{x,low}|}{R_x} = \frac{|T_{low} - T_{x,low}|}{R_{add,low}} \quad [\text{W/m}^2] \qquad (14)$$

with:

$$R_{add} = R_{add,up} + R_{add,low} = \frac{s_{add,up}}{\lambda_{add,up}} + \frac{s_{add,low}}{\lambda_{add,low}} \quad [\text{m}^2\text{K/W}]$$

$$R_x = \frac{s_x}{\lambda_x}$$

In case of a structural thermal bridge (Figure 2), the opposite side of the linear thermal bridge may be the undisturbed zone of the sample, in which the one-dimensional conditions are still verified, the temperatures, $T_{n,up}$ and $T_{n,low}$, are the same as the one-dimensional conditions. In the other points, the temperatures at the interface between the upper or lower material, with $R_{add,up}$-value and $R_{add,low}$-value, and the core material, with R_x-value, are no longer the same along the x-axis. Hence, Eq. (14) can be written as Eq. (15), underlining that this equation is only valid where the one-dimensional conditions are observed.

$$\varphi_{1D} = \lambda_{add,up} \frac{|T_{up} - T_{n,up}|}{s_{add,up}} \quad [\text{W/m}^2] \quad (15)$$

At this stage, the proposed methodology needs a number of thermocouples, which must be connected to the HFM apparatus in order to assess the temperatures between the envelope and the upper, or lower, additional resistance. In this proposal, the upper additional resistance was taken as a reference.

On this basis, it is possible to adopt the following procedure, in order to calculate the two-dimensional specific heat flux, φ_{2D}, by means of one experimental measurement:

- Place the thermocouples between the envelope and the upper additional resistance;
- Divide the sample into k elements of known influence area d_k;
- Assess the temperature of each influence area, from $Tc_{up,1}$ to $Tc_{up,k}$;

The thermocouples must be positioned progressively subdividing the horizontal section of the sample, as indicated in the scheme below (Figure 3).

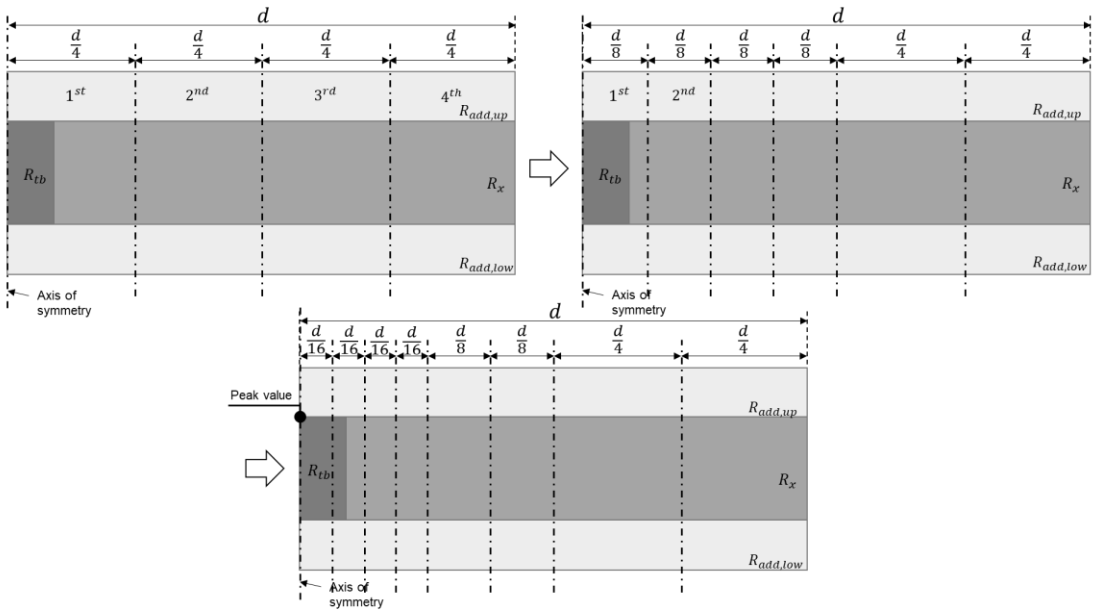

Figure 3_ Subdivision of the sample.

If the sample has a symmetrical geometry, as in the reference sample, it is only possible to consider half of the geometry in order to simplify the calculations. According to Figure 3, it is necessary to divide into equal part the section, following three steps:

- Split the section into four equal areas;
- Split the 1st and the 2nd areas, which are in the side of the thermal bridge, into two equal areas;

- Split the new first two, into another two areas.

This subdivision is due to the temperatures trend at the interface between the envelope and the upper additional resistance. As can be seen from Figure 4, the temperatures have a qualitative U-shape, considering the symmetry of the sample. In fact, Figure 4 presents the temperatures trend only if the sample has an axis of symmetry, as shown in Figure 3. This means that the peak value of the graph corresponds to the position x=0, namely the point between the envelope and the upper additional resistance on the axis of symmetry, as displayed in Figure 3.

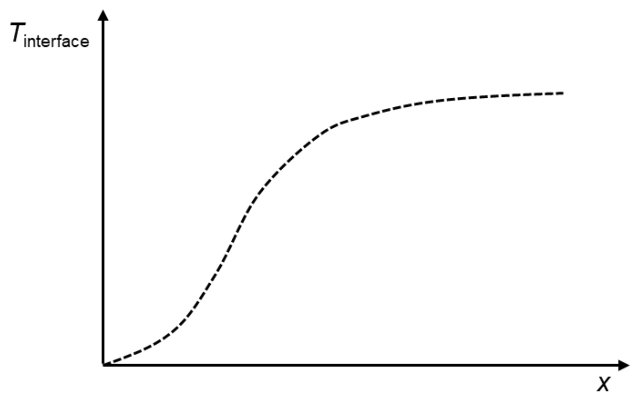

Figure 4_ Temperatures trend.

Figure 5 is instead useful to show the specific method of the placement of the thermocouples on the upper surface of the sample: the drawn seven lines plus the two boundary lines match the thermocouples positions.

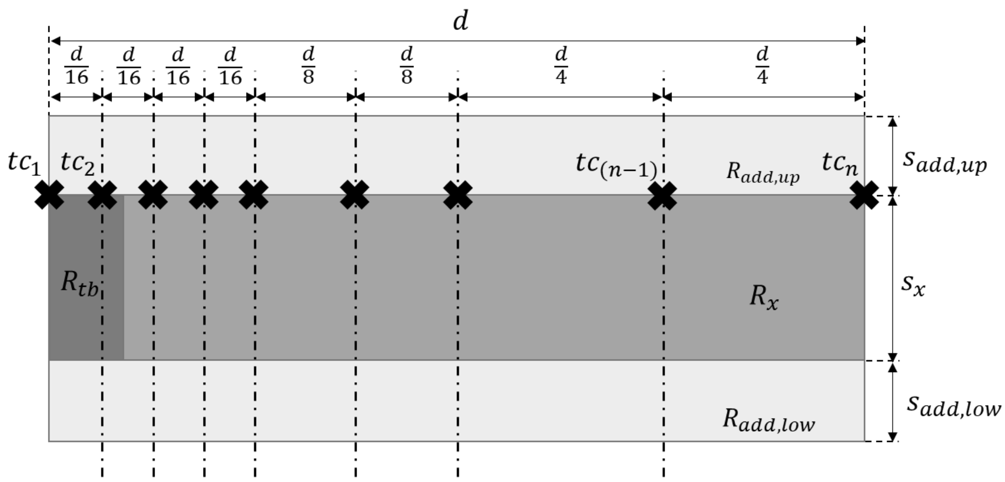

Figure 5_ Placement of the thermocouples.

Finally, the influence areas are determined by splitting half the distance between the thermocouples, as shown in Figure 6.

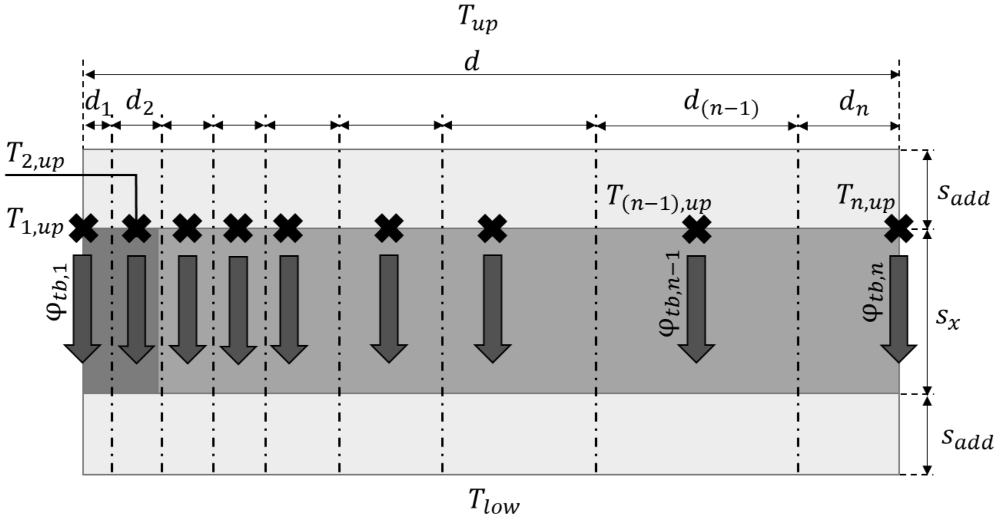

Figure 6_ Defining of the influence areas.

The one-dimensional specific heat flux in each influence area, called specific heat flux of the *i*-th thermal bridge, can be calculated by Eq (16), where $T_{i,up}$ is the temperature of the *i*-th influence area. This equation is the result of a simplification of the total influence area *d*, subjected to two-dimensional heat flow, in *n* areas d_i subjected to one-dimensional heat flow, $\Phi_{tb,i}$, as displayed in Figure 6.

$$\varphi_{tb,i} = \lambda_{add,up} \frac{|T_{up} - T_{i,up}|}{s_{add,up}} \qquad [W/m^2] \qquad (16)$$

It is clear that the greater the number of the influence areas, the lower the approximation of the $\varphi_{tb,i}$-value. The choice of splitting the area close to the thermal bridge in greater detail is quite aimed at increasing the accuracy of the methodology.

It is also important to clarify that in this process the number of the influence area and thus the number of the thermocouples are based on the material available in the laboratory of Politecnico di Torino, that is sixteen thermocouples. This limitation led to the placement of the thermocouples on the upper surface of the sample in order to avoid reducing the overall precision.

By equating $s_{add,up}$ from Eq.(15) and Eq. (16), Eq (17) is obtained. Hence, the $\varphi_{tb,i}$-value may be assessed as a multiplication of three terms, as Eq. (18) shows:

- The one-dimensional specific heat flux, φ_{1D}, calculated by Eq.(15);
- The ratio between two temperature differences: between the set temperature, T_{up}, and the temperature measured by the *i*-th thermocouples, $T_{i,up}$, and between the set temperature, T_{up}, and the temperature of the thermocouple placed in the undisturbed zone of the sample, $T_{n,up;}$
- The ratio between the same λ_{add}-values, that in this case is elided and worth 1.

The next step is to evaluate the two-dimensional specific heat flux, φ_{2D}, by means of Eq. (19), where *l* is the unit length of the sample.

$$\lambda_{add,up}\frac{|T_{up}-T_{i,up}|}{\varphi_{tb}}=\lambda_{add,up}\frac{|T_{up}-T_{n,up}|}{\varphi_{1D}} \qquad [\mathrm{W/m^2}] \qquad (17)$$

$$\varphi_{tb,i}=\varphi_{1D}\frac{|T_{up}-T_{i,up}|}{|T_{up}-T_{n,up}|}\frac{\lambda_{add,up}}{\lambda_{add,up}} \qquad [\mathrm{W/m^2}] \qquad (18)$$

$$\varphi_{2D}=\frac{\sum_{i=1}^{n}\varphi_{tb,i}\,A_i}{A}=\frac{l\left(\sum_{i=1}^{n}\varphi_{tb,i}\,d_i\right)}{ld}=\frac{\sum_{i=1}^{n}\varphi_{tb,i}\,d_i}{d} \qquad [\mathrm{W/m^2}] \qquad (19)$$

With the previously calculated two-dimensional specific heat flux, Eq. (19), it is possible to assess the linear thermal transmittance, Ψ, due to the thermal bridge as the ratio between the extra-flow, $\Phi_{2D}-\Phi_{1D}$, and the set temperature difference by Eq. (20). In the case of the thermal bridge of unit *l*-value, Eq. (20) becomes Eq. (21).

$$\psi=\frac{\Phi_{2D}-\Phi_{1D}}{|T_{up}-T_{low}|l} \qquad [\mathrm{W/mK}] \qquad (20)$$

$$\psi=\frac{\Phi_{2D}-\Phi_{1D}}{|T_{up}-Tc_{n,up}|} \qquad [\mathrm{W/mK}] \qquad (21)$$

To summarise, the methodology proposed can be applied in the following hypotheses:

- Presence of a linear thermal bridge;
- Availability of an additional resistance, which simulates the surface resistance;
- A temperature trend as displayed in Figure 4: U-shape;
- The sample must contain the linear thermal bridge and as undisturbed zone together;

Hence, this experimental methodology (HFM B) allows calculating the Ψ-value by means of one experimental measurement of the 2D assembly. The procedure aims to avoid the assessment of the Ψ-value by two measurements, previously explained in HFM A case, and introduces for this purpose the combined use of an additional resistance and thermocouples. It is important to highlight again that the nine thermocouples do not represent a maximum limit, but rather a minimum limit.

Moreover, in order to validate the methodology, the thermocouples can be replaced by other means. In the case of simulation by software, the purpose will be to find the temperatures of the points where the thermocouples would be placed. The validation will be explained in Chapter 5.2.

4.3 BET A

This case is referred to experimental measurements into the BETcell in order to assess the Ψ-value.

Considering the same reference samples of the previous cases, this methodology aims to calculate the linear thermal transmittance, Ψ, of the 2D assembly (Figure 6) by means of only one measurement. Hence, the BET A methodology is based on the same procedure of the HFM B case, but by means of different instrument. In fact, the HFM B methodology is carried out by HFM apparatus and thermocouples connected to the latter, the BET A one by heat fluxes sensors and thermocouples, into the BETcell, and connected to an acquisition instrument. In both cases, however, the Ψ-value can be calculated, by only one measurement of the 2D assembly (Figure 6).

More specifically, the 2D assembly placed into BETcell should be monitored in steady-state conditions and during an acquisition period. As explained in Paragraph 6.2, in the second case study (Chapter 6), this period was considered by two different methods : the first linked to the hours preceding the entry into the thermostatic chamber and the second refers to the data collected during the IR thermography. This choice is due to verify the influence of an operator during data collection.

It is important to underline that the sample must split the thermostatic chamber into the zones, in which two different environmental conditions are set: the hot and cold side. Moreover, the sample must not include the additional resistance, since it is already represented by the air of the two sides. As the previous case (HFM B), the choice will be done according to the available instruments. In this methodology, the placement of thermocouples follows the same procedure previously explained (Figure 3, Figure 5 and Figure 6). These thermocouples can be placed on both surfaces of the sample investigated or on only one.

But, in this case the placement of the heat flux sensors must be decided. The latter should be placed on the surface of the sample and in both sides. Moreover, in order to measure the one-dimensional heat flux, φ_{1D}, the sensors must be placed on the undistributed zone by the thermal bridge. In the 2D assembly (Figure 3, Figure 5 and Figure 6) this zone is on the opposite side of the linear thermal bridge.

Finally, the air thermocouples should be placed close to the sample in order to measure the air temperatures of the two sides.

In this experimental procedure, Eq. (18) can be applied directly, since the heat flux measured by the heat flux sensor is one-dimensional. Then, Eq. (19) (20) (21) are still valid in order to assess the Ψ-value.

4.4 BET B

In this case the 2D assembly (Figure 3, Figure 5 and Figure 6) is placed into the thermostatic chamber, as in the previous case (BET A). Also in this procedure, the Ψ-value can be assessed by means of one measurement, but the data are obtained by IR camera and by the air thermocouples. Hence, the heat flux sensors and the surface thermocouples are not necessary, and they are replaced by the IR camera. The latter can provide thermographic images of the sample investigated, and by using a specific software the temperatures of each pixel are display.

The single thermographic image shall record the nine values of temperatures required to apply the experimental methodology explained in Paragraph 4.2. Hence, by the temperatures of the IR camera Eq. (18) can be applied only after calculating the φ_{1D}-value by means of Eq. (7).

5 First case study: plasterboard assembly

In this analysis, the thermal bridge of a plasterboard envelope was evaluated. The investigated sample is made of several building materials. As explained in Chapter 4 the 1D assembly refers to the envelope subjected to the one-dimensional conditions, whereas the 2D assembly liked to the two-dimensional conditions. The first was needed to assess the one-dimensional specific heat flux, φ_{1D}, and the second the two-dimensional specific heat flux, φ_{2D}, in order to assess the linear thermal transmittance, Ψ, of the plasterboard envelope.

The Ψ-value was evaluated by numerical simulations and experimental procedures, which were performed in parallel and by several pre-defined configurations, as described in the paragraphs below.

The two procedures were started from the single materials measurement and characterization adopted for the assembly: plasterboard panels, metallic frames, mineral wool panels, unimproved/improved filler and additional resistances, that were different rubber mats.

5.1 Preliminary materials characterization and instrument

The first step was to measure the previously cut materials with a meter and caliber. Table 1 presents the measurements of each material:

- Plasterboard panel: due to the issue linked to its shape, two thicknesses and the distance between these were measured. Figure 7 displays the difference in height between the two opposite sides: around three-quarters of the panel has a steady thickness and then it decreases to the thinner side;

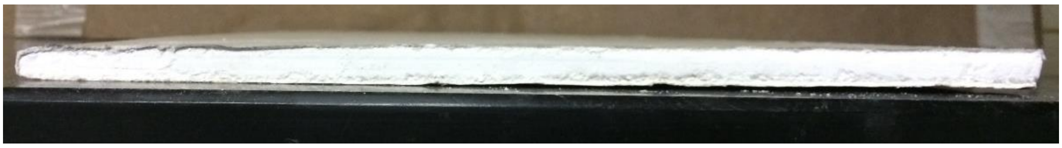

Figure 7_ Plasterboard panel.

- Metallic frame: thickness[1] and width profile;
- Mineral wool: it was not necessary to take any thickness measures due to its property to squeeze into the plasterboard panels;
- Rubber mat: thickness measured by Heat Flux Meter apparatus. The mats, arranged on the opposite sides of the assembly, had four roles: the first was

[1] Due to the thickness of the metallic frame, an arithmetic average of five values was calculated.

closely linked to follow the procedure described in Chapter 4; the second was that to reproduce the environmental conditions, or rather to add two additional resistances which could simulate the surface resistance; the third role was to reduce the heat flow dissipation; the last was to recreate a smooth and coplanar surface in order to avoid air joints, that cause of unnecessary resistances.

The experimental setup follows the UNI EN 12667:2002 [6]. For this first case study, the “LASERCOMP FOX600” was used, a Heat Flux Meter apparatus (HFM) characterized by two plates, heated and cooled site of (600x600) mm (Figure 8). The measurement area, located in the center of the plates, is of (254x254) mm. One heat flux sensor is integrated into each plate and is used to monitor the specific heat flux, φ, generated due to the temperature difference, T_{up}-T_{low}, between the top and bottom plate at regular intervals, since steady-state heat flux is reached. The device must be calibrated with materials having similar heat transfer characteristics as the materials to be evaluated. This value is saved in the calibration file of the software. The experimental setup follows the UNI EN 12667:2002 [6].

HFM apparatus was used to assess the λ-value and R-value of each material and these data are shown in Table 2. Regarding the metallic frame, due to its c-shape, a measurement was not possible to perform, thus the λ-value, 52 W/(mK), was taken from literature.

Measured Sizes		
Material	**Thickness [mm]**	**Width [mm]**
Metallic frame	0.656	49.05
Mineral wool	49.05	/
Plasterboard	6.50	60.20
	9.50	
Dist. Between plast.	1.60	/
	1.66	
Black rubber	13.895	/
Red rubber_3mm	3.16	/
Red rubber_5mm	4.845	/
Red rubber_10mm	9.735	/

Table 1_ Material measurements.

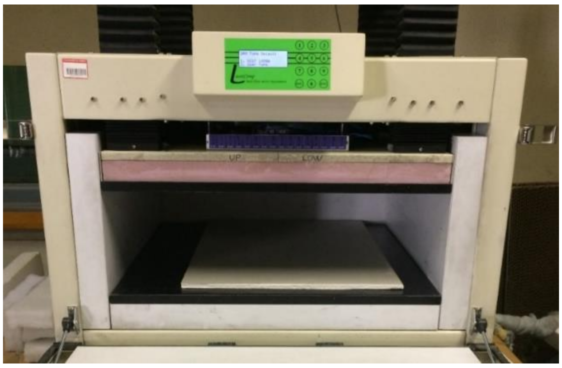

Figure 8_ HFM apparatus.

HFM results			
Material	**Thickness [mm]**	**Conductivity [W/(mK)]**	**Resistance [m²K/W]**
Plasterboard panel	9.49	0.188	0.0505
Mineral wool	47.97	0.0326	1.472
Black rubber	27.79	0.0520	0.535
Red rubber_5mm	9.69	0.199	0.0487
Red rubber_10mm	19.47	0.199	0.0978
Traditional filler	20.48	0.276	0.0742

Insulating filler	23.22	0.06529	/
Metallic frame	/	52	/

Table 2_ HFM results.

The traditional gypsum filler sample was made by several mixtures with a ratio of 100 g of water per 285 g of plaster (Figure 9). The filler sample was created with the aid of a polystyrene frame, previously cut in the center and pasted on a rigid support (Figure 10). The square in the center was (300 x 300) mm. The filler was placed into the frame with the aid of a spatula and trowel (Figure 11). The last coat of filler was given after a few hours when the filler had dried up a little and it was useful for covering any superficial holes and to make the surface as polished as possible (Figure 12).

Figure 9_ Preparation of mixtures.

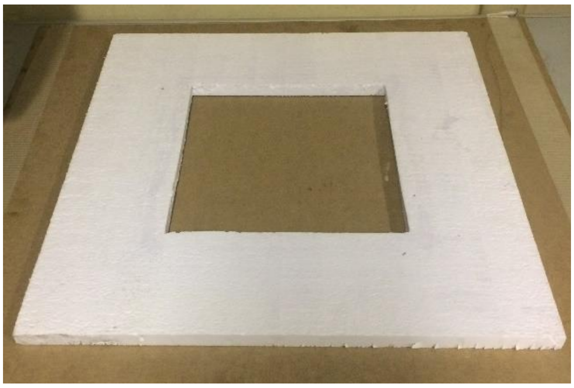

Figure 10_ Polystyrene frame.

Figure 11_ Drafting filler.

Figure 12_ Filler sample.

The insulating filler is an interior patching filler with the addition of aerogel grans and it is developed in order to increase thermal performance in walls buildings. The advantages declared by the company using this product should be to fix all defects and imperfections, to delete the thermal bridges and VOC emission. In this analysis, the focus was on the thermal bridges and how the filler can avoid energy loss.

The filler was mixed in the laboratory with a ratio declared by the company of 140 g of water per 100 g of powder (

Figure 13). The mixture sample was created with the aid of an EPS frame as in the case of unimproved filler but with a larger area, (340 x 340) mm (Figure 14).

The result is shown in Table 2.

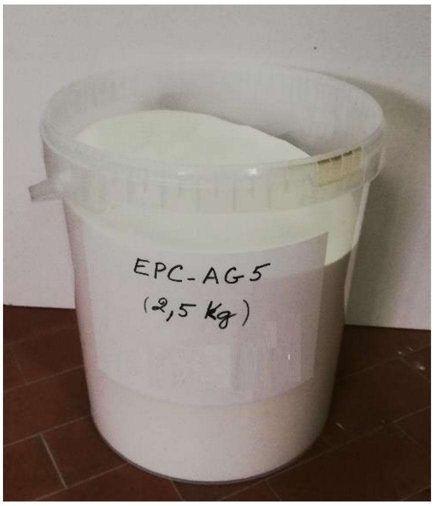

Figure 13_ Patching filler powder.

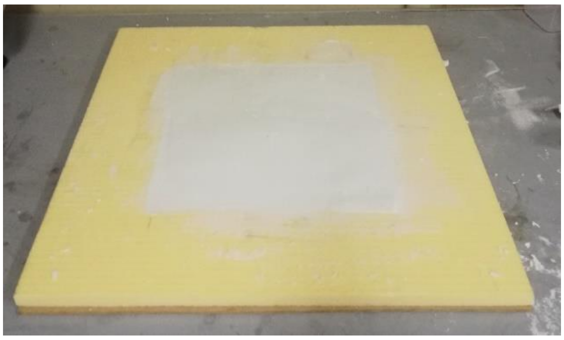

Figure 14_ Filler sample.

5.2 *Experimental procedure*

As in the materials characterization, HFM apparatus was used in order to assess the one-dimensional and two-dimensional heat flux, φ_{1D} and φ_{2D}, and the temperatures of the two assemblies, 1D and 2D.

The 1D Assembly (Figure 15), used to evaluate the one-dimensional conditions, was made with two rubber mats, two mineral wool panels and three plasterboard panels, two of which were located on the lower plate and matched to the thicker side, in order to make a coplanar surface.

Figure 16 shows the 2D assembly composed of four plasterboard panels, three metallic frames, four mineral wool panels and filler. Moreover, two rubber mats were used as additional resistances.

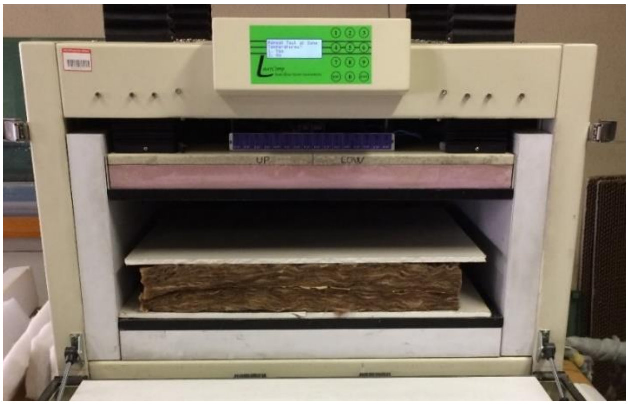

Figure 15_ 1D Assembly.

Figure 16_ Plasterboard assembly

The assembly was realized by introducing two mineral wool panels between the prefabricated c-shaped metallic frameworks. The outside surfaces of the envelope are composed of two plasterboard panels for each side, which were placed above the middle of the frame and fixed on it by screws, as shown in Figure 17. The two plasterboard panels were positioned by centring the separation groove as much as possible with half of the metallic frame. A coin, of 1 or 2 cents, was used to measure the space between the two plasterboard panels and to determine the distance between the two panels. This gap had to be maintained as much as possible to fix the panels to the framework (Figure 18).

The assembly also includes two layers of gypsum filler, internally and on the joints of the opposite plasterboard panels (Figure 16), which was necessary to make a flat surface, due to the characteristic plasterboard-shape, and to prepare the surface for further finishing layers in order to avoid a step through the different thicknesses of the panel. Figure 7 displays this discrepancy between the two opposite sides: about three-quarters of the panel has a steady thickness and then it decreases to the thinner side.

Figure 17_ Plasterboard fixing

Figure 18_ Plasterboard spacing.

5.2.1 ExpA and ExpB procedures

In this case, the linear thermal transmittance, Ψ, was assessed in only one configuration: with 1 additional resistance, which consisted of two rubber mats, R_{add}= 0.535 m^{2}K/W and with the gypsum filler previously measured.

The ExpA procedure refers to the measurements by HFM apparatus of the one-dimensional and two-dimensional heat flows, separately. Hence, this methodology is the application of HFM A case reported in Paragraph 4.1.

The ExpB is linked to the methodology addressed in Paragraph 4.2 (HFM B). As Figure 19 illustrates, the ExpA procedure has 1 φ_{1D}-value, 1 φ_{2D}-value and thus 1 Ψ-value; the ExpB procedure has 1 φ_{1D}-value, 1 φ_{2D}-value and 1 Ψ-value.

The first method was carried out by two experimental measurements, conducted separately, and the second by only one measurement. Moreover, in both cases the set temperatures of the top and bottom plates were T_{up}= 35°C and T_{low}=15°C, respectively.

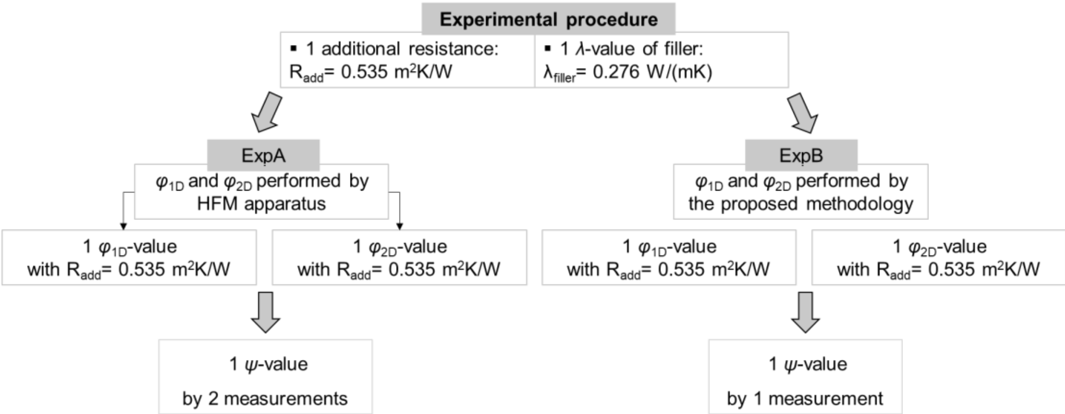

Figure 19_ Experimental procedure sketch.

In order to assess φ_{1D}-value and the φ_{2D}-value for the ExpB procedure, 16 thermocouples were placed into a square of (254x254) mm, at the same distance x_i and with the same influence areas of the pixels taken into account in the NumB procedure (Figure 20), as will be widely explained in Paragraph 5.3. This means that each thermocouple matches the point of measurements of the numerical simulation.

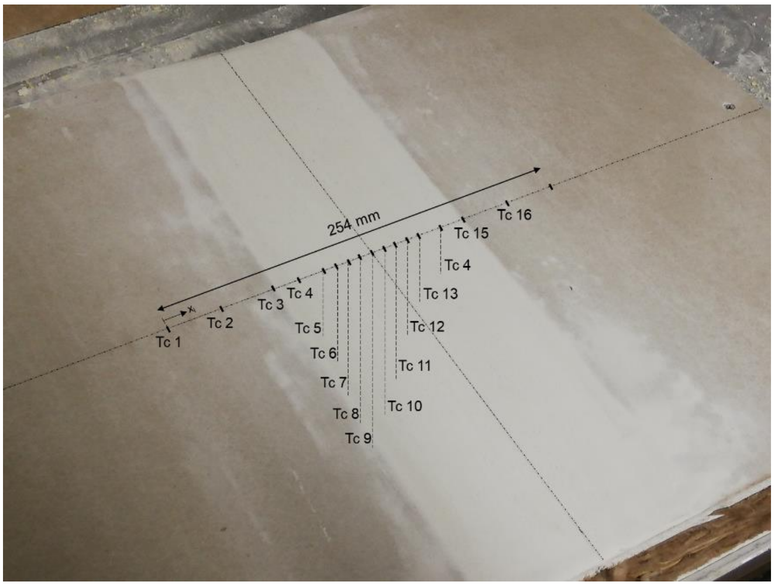

Figure 20_ Thermocouple distance.

After that, the thermocouples were connected to HFM apparatus (Figure 21) and, due to the available number of thermocouples, that is 16, the 17th temperature was evaluated as the first one. This application was supported by the fact that the 1st and the 17th thermocouples were placed on the two areas undisturbed by the linear thermal bridge.

In the ExpB procedure, the temperature trend follows a U-shape, as Figure 22 shows, therefore the hypothesis of the numerical methodology, proposed in Paragraph 4.2 (HFM B), was met. Furthermore, the center of element, the dotted line, does not correspond to the peak value of the temperatures trend. This is due to the geometry of the layers: as shown in Figure 16 or Figure 18, the metallic framework is not symmetrical along the y-axis. Hence, in this case it was not possible to apply the methodology of Paragraph 4.2

considering half of the 2D assembly. For this reason, all 2D assembly was taken into account, as shown in Figure 20.

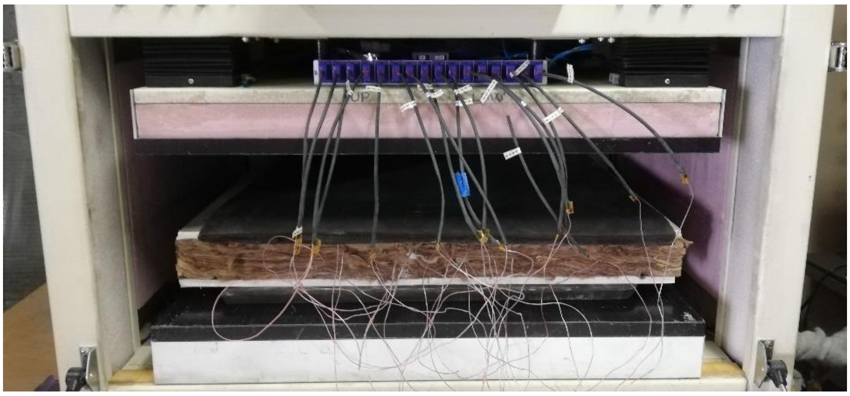

Figure 21_ Thermocouples connecting.

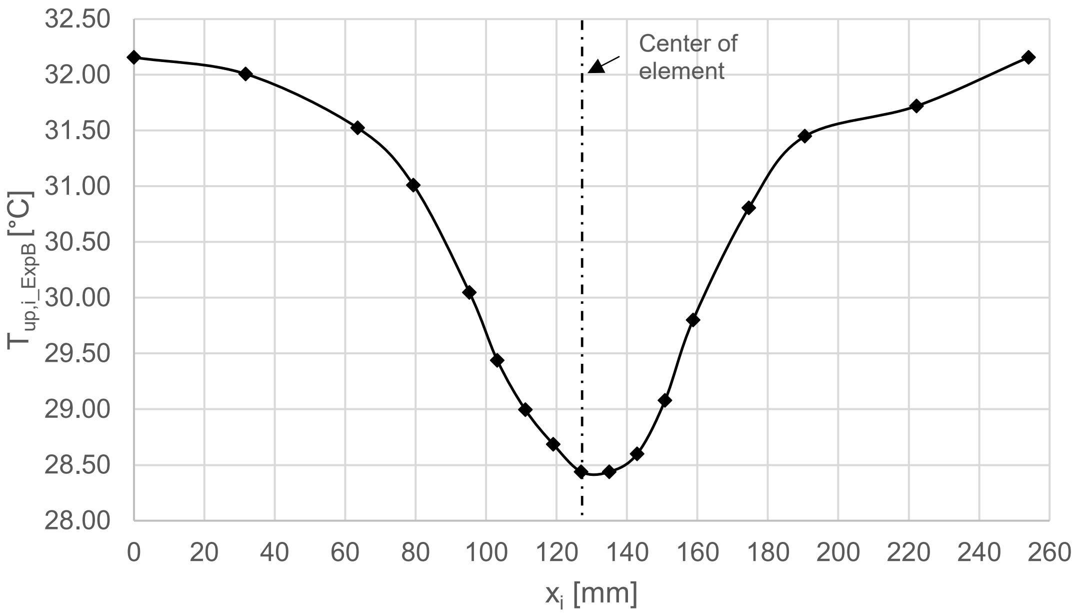

Figure 22_ Temperatures U-shape, HFM results. Average values of the last 10 data.

5.2.2 Results

Table 3 shows the results obtained by HFM apparatus. Table 17 in Annex B presents the thermocouples temperatures, where the last line refers to the average values of the last 10 data, corresponding the last 10 blocks, in which steady values of heat flux were reached. The trend of this temperatures will be presented in Paragraph 5.4.

Moreover, the result of ExpA and ExpB procedures are illustrated in Table 18 and Table 19 of Annex B.

HFM results	**Heat flux [W/m^2]**
1D Assembly	9.588
2D Assembly	15.050

Table 3_ 1D and 2D Assembly results.

5.3 Numerical simulations

The numerical thermal analysis was performed by Physibel Bisco [15], a software used for steady-state heat transfer in two-dimensional geometries and for different boundary conditions, according to EN ISO 13789:2008 [3].

As already mentioned in Paragraph 4.2 these numerical simulations were carried out in order to validate the experimental methodology (HFM B) explained in Paragraph 4.2.

The input of Bisco needs a 2D drawing of the element to simulate, which must be converted to a coloured image (called bitmap) in 256 colours, any one of which is linked to a boundary condition or homogeneous material. Moreover, the pixel of this bitmap is a square with a fixed physical length.

In all the simulations described in this study, the pixel size was 0.165 mm and therefore each value showed in Table 1, was scaled by 0.165 mm unit, as shown in Table 4, in order to import the bitmap file into Bisco. Moreover, Table 5 and Table 6 present the percent errors and the multiplicative factors of the measurements.

The designs made were set the whole design in a rectangle of (254x100) mm also containing the environmental conditions, and then converted in a 256-colours BMP file.

Scaled Sizes	Scale factor [mm]= 0.165	
Material	**Thickness [mm]**	**Width [mm]**
Metallic frame	0.66	49.17
Mineral wool	49.17	/
Plasterboard	6.44	60.23
	9.57	
Dist. Between plast.	1.65	/
	1.65	
Black rubber	13.86	/
Red rubber_3mm	3.135	/
Red rubber_5mm	4.785	/
Red rubber_10mm	9.735	/

Table 4_ Scaled Sizes. Unit= 0.165 mm.

Percent Error		
Material	**Thickness [mm]**	**Width [mm]**
Metallic frame	0.6%	0.2%
Mineral wool	0.2%	/
Plasterboard	1.0%	0.00%
	0.7%	
Dist. Between plast.	3.1%	/
	0.6%	
Black rubber	0.25%	/
Red rubber_3mm	0.79%	/
Red rubber_5mm	1.24%	/
Red rubber_10mm	0.00%	/

Table 5_ Percent Error.

Multiplicative Factor		
Material	**Thickness [mm]**	**Width [mm]**
Metallic frame	4	298
Mineral wool	298	/
Plasterboard	39	365
	58	
Dist. Between plast.	10	/
	10	
Black rubber	84	/
Red rubber_3mm	19	/
Red rubber_5mm	29	/
Red rubber_10mm	59	/

Table 6_ Multiplicative Factor.

Legend
Grey: plasterboard panel;
Green: mineral wool;
Light blu: metallic frame;
Yellow: filler;
Black: additional resistance;
Red/violet: environmental conditions.

Figure 23_ 1D BMP file.

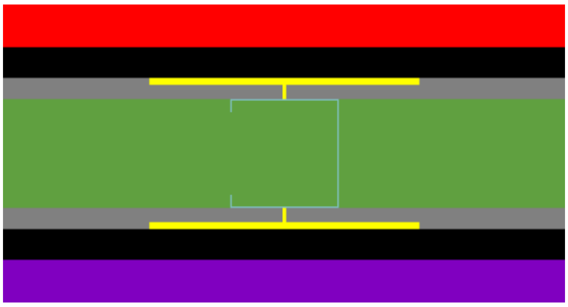

Figure 24_ 2D BMP file.

Figure 23 and Figure 24 show two example upload files in the case of one-dimensional (1D assembly) and two-dimensional conditions (2D assembly).

In the graphics return, an approximation of the plasterboard shape was conducted. In fact, the plasterboard panel has a graduated improvement of thickness from the thin to thick side, but this is not correctly reproduced by Bisco. The mash in the slope-side, so-called hypotenuse, would be denser than the other section. Hence, the plasterboard shape was assessed with a stair: in other words, a constant thickness from the thin side to the thick side was plotted (Figure 17)[2].

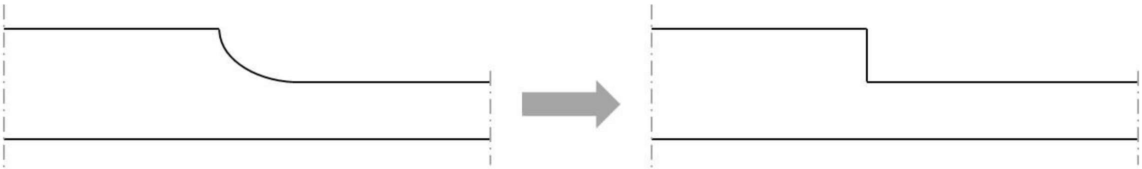

Figure 17_ Plasterboard approximation.

The BMP file was uploaded in Bisco, where whole materials are defined by its colour type and corresponding thermal properties, e.g. thermal conductivity, λ. In these simulations, the colour type used was MATERIAL*,* for materials, and BC_SIMPL, for boundary conditions.

The bitmap image is converted by Bisco into a vector image, to create a calculation better. All area materials are then triangulated with a mesh and the vertices of this triangulation mesh are the nodes of the thermal system. In the cases examined, the uniform triangulation mesh size for all materials was calculated through three cases: mesh-value of 5, 3 and 2. Therefore, by Eq. (13) mesh-value equal to 2 was the correct design detail and validated the mash dependence analysis.

[2] Zalewski L. et al. [11] used the same geometry transformation for the inclined parts of the hat profiles.

Moreover, the result of the system calculation is the temperatures of all system nodes and the heat flow values. The first values produce the isothermal lines and the seconds the heat flow lines that they follow orthogonal direction to the isothermal lines. Finally, the output displays the input data values and calculation results, e.g. numbers of system nodes or flow in and flow out.

5.3.1 NumA and NumB procedures

In order to assess the linear thermal transmittance, Ψ, in several configurations, 4 different additional resistances and 10 different λ-values of filler, from 0.30 W/m^{2}K to 0.03 W/m^{2}K by steps of 0.03, were performed.

Furthermore, two procedures, so-called numerical A (NumA) and numerical B (NumB) were conducted:

- NumA refers to numerical simulations by Bisco for the one-dimensional and two-dimensional heat flow separately. This procedure is the numerical validation of the HFM A methodology explained in Paragraph 4.1. In fact, both determine the φ_{1D}-value and the φ_{1D}-value separately, but the HFM A employs the HFM apparatus, so experimental measurements, and the NumA the simulation by Bisco.;
- NumB is linked to numerical calculations, in accordance with the methodology addressed in Paragraph 4.2, for the one-dimensional and two-dimensional heat flows. In this specific instance, the proposed methodology was applied by deriving the $T_{i,up}$-values from Bisco temperatures output, which are the temperatures of the pixels placed at the distance x_i, as shown in Figure 26. The figure also presents the influence areas, *a b c d e f*, which were determined according to the procedure explained in Paragraph 4.2. Hence, the NumB procedure is necessary in order to validate the experimental methodology explained in Paragraph 4.2 (HFM B).

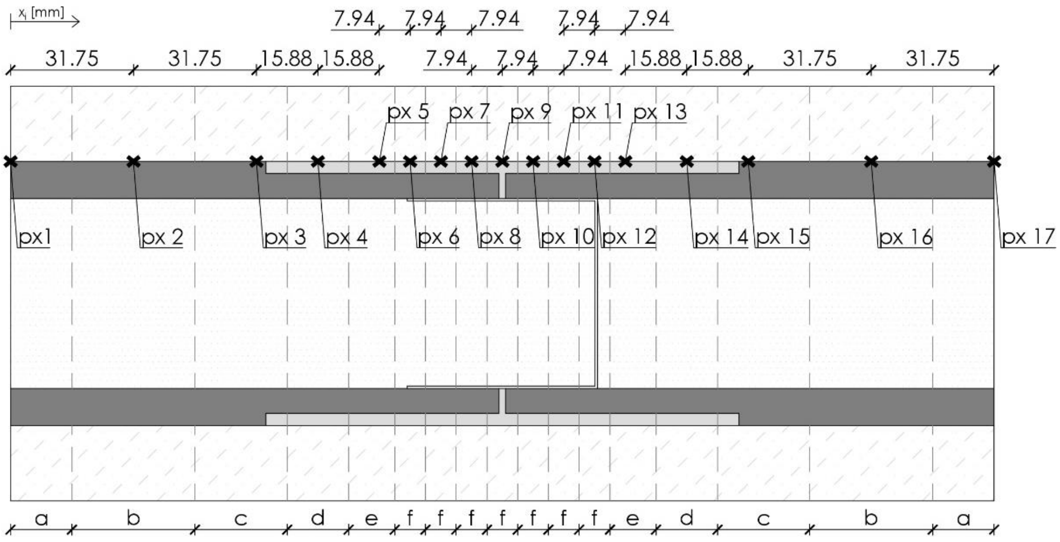

Figure 26_ Pixel distance.

the NumA procedure has 4 Φ_{1D}-values and 40 Φ_{2D}-values, calculated by Bisco, which allow obtaining 40 Ψ-values. The NumB procedure has 3 Φ_{1D}-values and 30 Φ_{2D}-values, established by the Proposed methodology, which can provide 30 Ψ-values. In this last case, it was not possible to assess the linear thermal bridge by R_{add}= 0 m^{2}K/W, since the additional resistance is required to apply the methodology.

Figure 27 sketches the two employed procedures and the results of the one-dimensional and two-dimensional heat flows performed by Bisco are shown in Annex A. It is also important to highlight that, the 40 Ψ-values of the NumA procedure were obtained by means of two simulations for each additional resistance and, instead, the 30 Ψ-values of the NumB procedure by means of one simulation for each additional resistance. In this last case, the simulation by Bisco was required in order to obtain the pixels temperatures and not for the one-dimensional or two-dimensional heat flow (Figure 22). Moreover, in all combinations, the T_{up}-value and the T_{low}-value were the same as those imposed in the ExpA and ExpB procedures: T_{up}=35°C and T_{low}=15°C.

The two methods were compared in order to validate the NumB procedure, by calculating the percent differences between the Φ_{1D}-values, the Φ_{2D}-values and the Ψ-values in the examined cases. This matter will be dealt with in the following chapter.

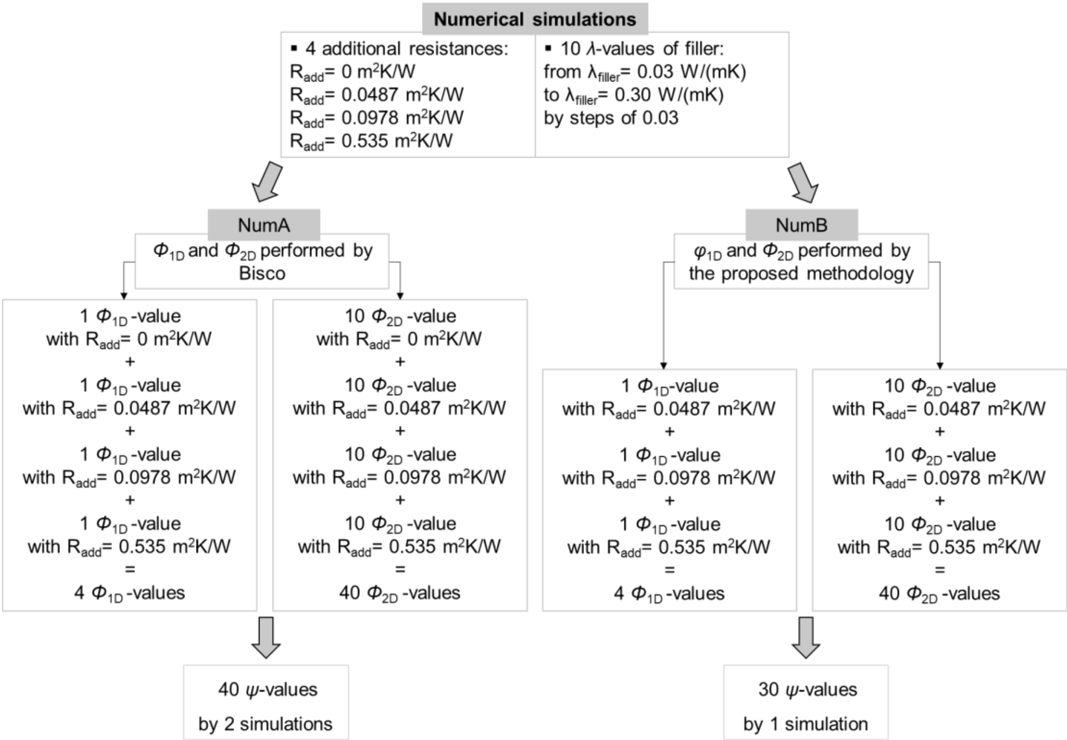

Figure 27_ Numerical simulations sketch.

Analysing the temperature output, it can be observed that in the one-dimensional conditions, the isothermal lines are parallels through themselves and with the assembly surfaces, as Figure 28 displays. Instead, in the two-dimensional conditions, the temperatures trend has a U-shape (Figure 29), caused by the linear thermal bridge.

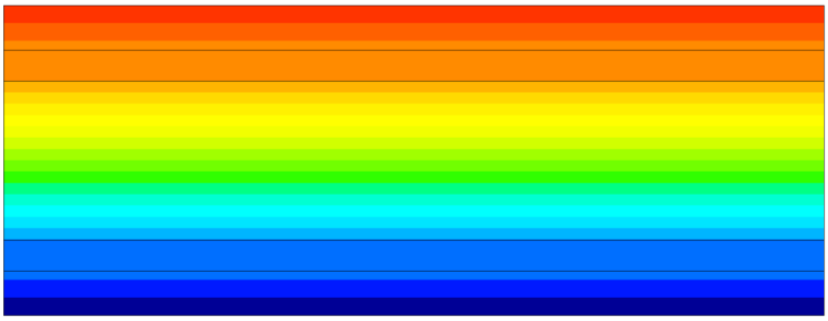

Figure 28_ 1D isothermal lines.

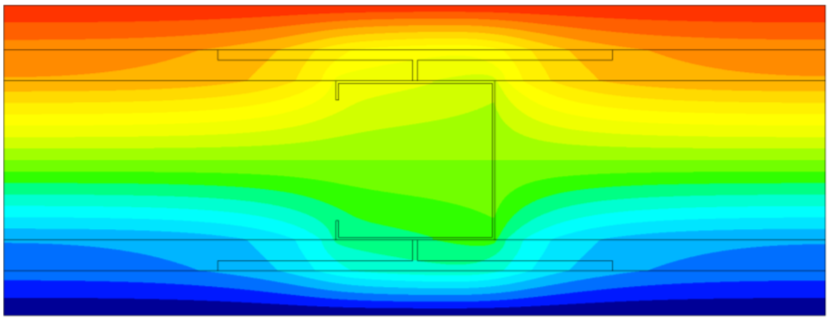

Figure 29_ 2D isothermal lines.

For example, Figure 30 displays the temperatures trend, between the upper additional resistance and the plasterboard panel and with λ_{filler}= 0.27 W/mK, performed by Bisco. This trend has allowed the application of the methodology proposed in Paragraph 4.2. Moreover, as is noticeable from Figure 30 the center of element of the 2D assembly section does not correspond to the peak value of the temperatures trend which is slightly shifted to the right. This is due to the geometry of the layers: as shown in Figure 24 or Figure 26, the metallic framework is not symmetrical along the *y*-axis. Hence, in this case, it was not possible to apply the methodology of Paragraph 4.2 considering half of the 2D assembly. For this reason, all 2D assembly was taken into account, as shown in Figure 26.

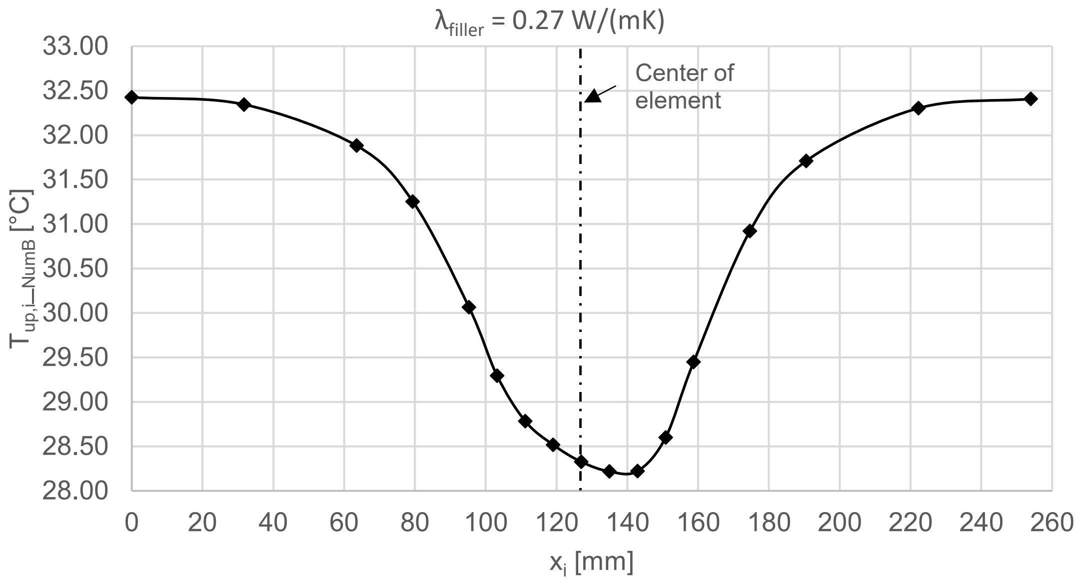

Figure 30_ Temperatures U-shape (Bisco).

After the hypotheses of the methodology have been validated, the linear thermal transmittance, ψ, in all the configuration previously described was assessed.

5.3.2 Results

Table 12 and Table 16 in Annex A present the Φ_{2D}-values and the Ψ-values for NumA and NumB procedure. In all cases, the linear thermal transmittance increases when the thermal conductivity of the filler raises and when the additional resistance decrease, as shown in Figure 31 and Figure 32.

Taking into account an additional resistance, the trend of Ψ-value confirms the concept that by increasing the resistance of the filler, or rather by decreasing the λ_{filler}-value, the linear thermal bridge reduces due to a decrease of the two-dimensional heat flow. The same reasoning follows the comparison through the curves of different additional resistances.

Furthermore, the dotted lines related to the λ-values of gypsum and insulating filler, display the Ψ-values of different R_{add}-values: the Ψ-value is higher for greater λ_{filler}-values and lower R_{add}-values. The line charts also show that the greater the additional resistance, the lower the difference between the Ψ-values evaluated by the unimproved and improved filler. In the case of R_{add}= 0.535 m^2K/W, this specific trend is particularly highlighted.

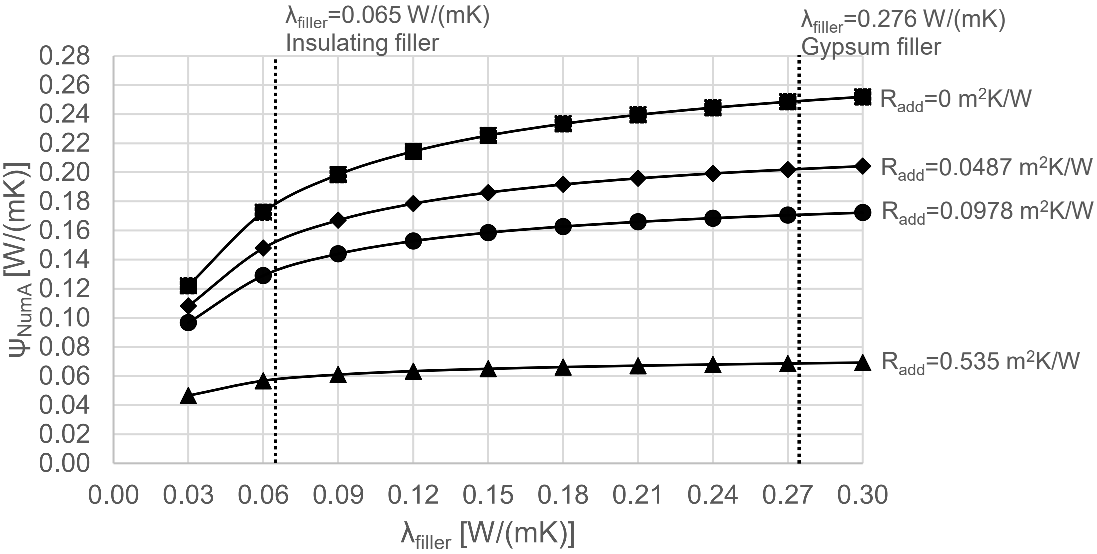

Figure 31_ Ψ-values when λ_{filler}-value and R_{add} change (NumA).

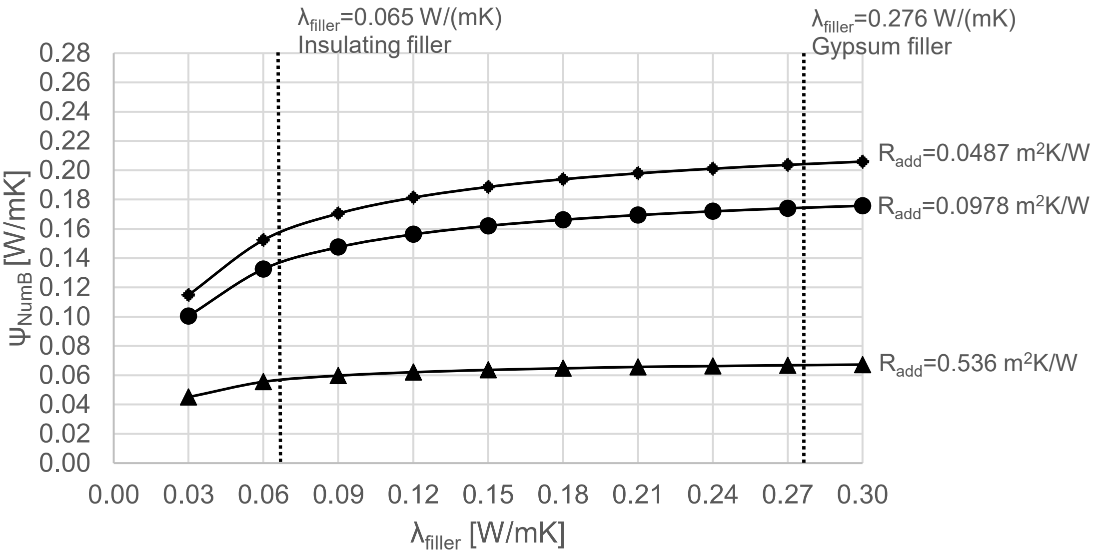

Figure 32_ Ψ-values when λ_{filler}-value and R_{add} change (NumB).

Moreover, Figure 33 and Figure 34 present the percent difference between the NumA and NumB procedure for φ_{2D}-values and Ψ-values in order to validate the proposed methodology and to assess its precision level. It can be seen from the charts that the NumB procedure is more accurate for higher λ_{filler}-values: in this case, the φ_{2D}-values differ by no more than 1.2% (Figure 33) and the Ψ-values by no more than 3% (Figure 34). In the worst case, that corresponds to λ_{filler}= 0.03 W/m^{2}K, the two percent differences are less than 2% and 6.4% respectively. This trend can be explained by a reason that the two-dimensional heat flow is lower for low values of filler and, consequently, the lower the value of a physical quantity, the greater will be difficult to find an alternative methodology aimed at the assessment of this value.

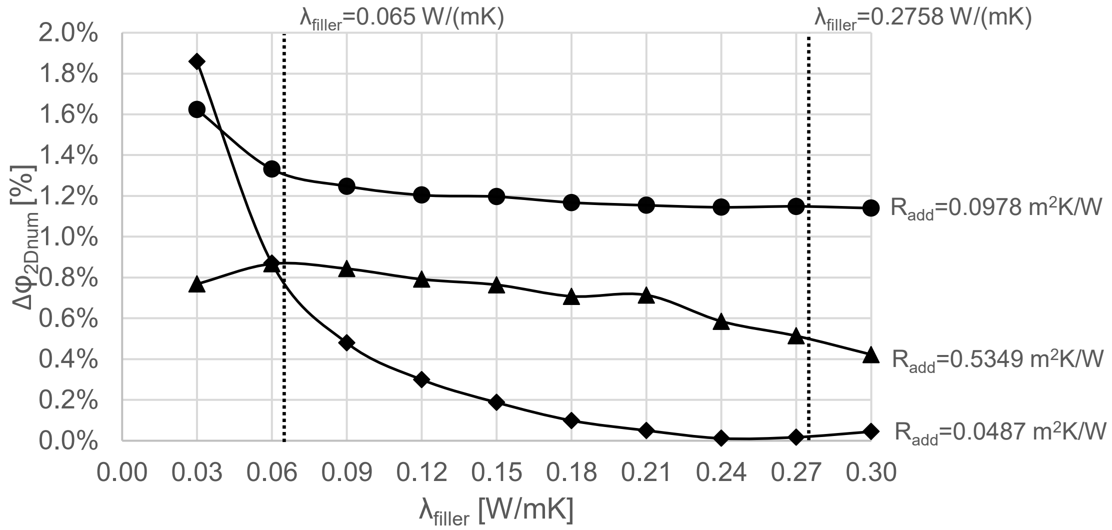

Figure 33_ $\Delta\varphi_{2DNum}$.

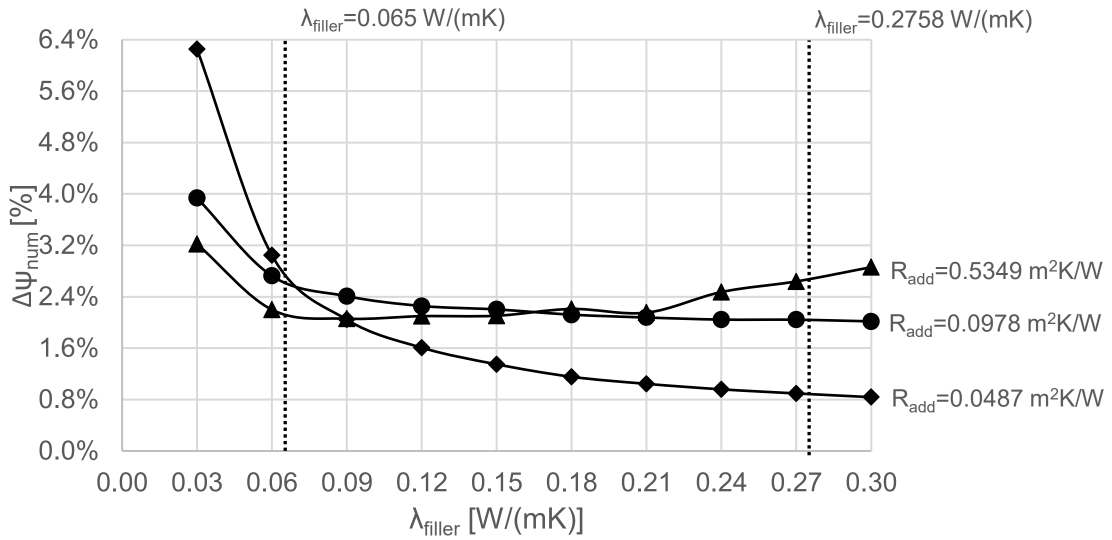

Figure 34_ $\Delta\psi_{Num}$.

Finally, Figure 35 and Figure 36 provide the linear thermal bridge values related to the gypsum and insulating filler, when the additional resistance changes. As explained above, the simulated values of filler were conducted from 0.03 W/(mK) to 0.30 W/(mK) by steps of 0.03. The λ_{filler}=0.27 W/(mK) and λ_{filler}=0.06 W/(mK) were taken as reference rather than the real values, 0.276 W/(mK) and 0.0653 W/(mK), of the fillers with the HFM apparatus. The dotted lines refer to the additional resistance in a real building application of the assembly: a horizontal heat flow and an internal surface resistance same as that external, R_i+ R_e = (0.13+0.13) m^{2}K/W = 0.26 m^{2}K/W according to UNI EN ISO 6946:2008 [4]. As is evident from the charts, the employment of the insulating filler, by means of numerical simulations, can reduce the linear thermal transmittance, Ψ, of about 23% both in the NumA procedure and the NumB.

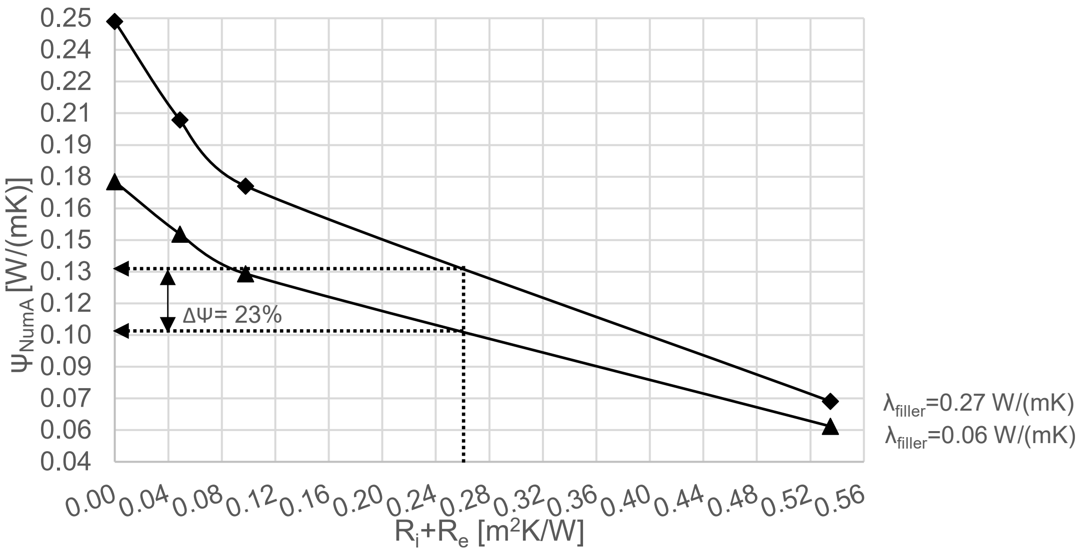

Figure 35_ Ψ_{NumA}-values depending on the additional resistance.

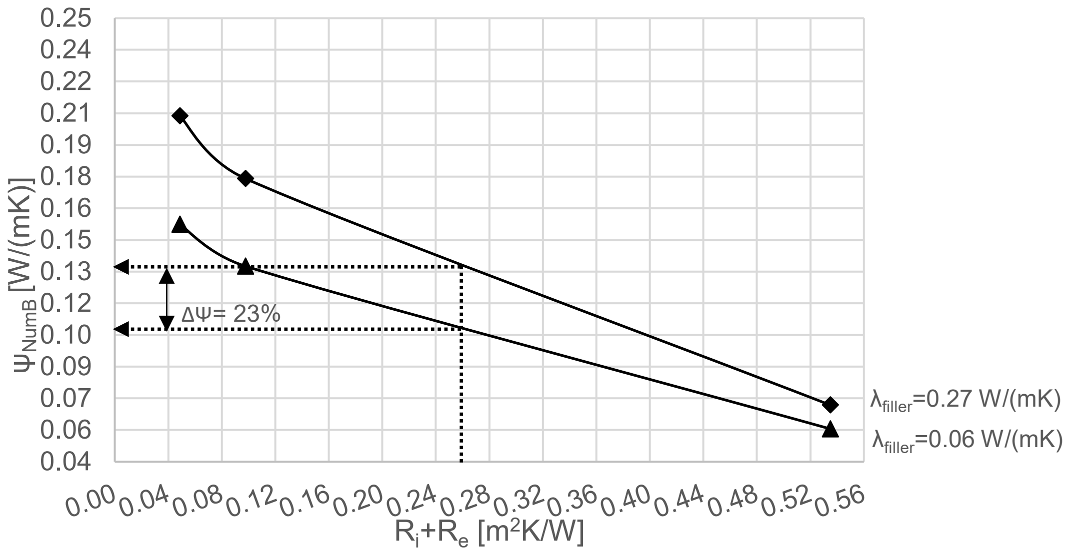

Figure 36_ Ψ_{NumB}-values depending on the additional resistance.

5.4 Comparison

Table 7 presents the percent difference between the six possible combinations, considering the gypsum filler, λ_{filler}= 0.276 W/(mK), and R_{add}=0.5349 m^{2}K/W, that are the values used for the experimental procedures (ExpA and ExpB).

The aim of this comparisons was to evaluate which procedure, between NumB and ExpB, was the most reliable. The focus was paid to these two because, as already explained, they are the ones that allow assessing the linear thermal transmittance, Ψ, by only one simulation by Bisco or one HFM test.

ΔT [K]	20
λ_{filler} [W/(mK)]	0.2758
R_{add} [m^{2}K/W]	0.5349

	NumA	NumB	ExpA	ExpB	NumA	ExpA	NumB	ExpB	NumA	ExpB	NumB	ExpA
φ_{1D} [W/m]	2.391	2.447	2.435	2.701	2.391	2.701	2.447	2.701	2.391	2.701	2.447	2.435
φ_{1D} [W/m^2]	9.413	9.632	9.588	10.632	9.413	10.632	9.632	10.632	9.413	10.632	9.632	9.588
φ_{2D} [W/m]	3.764	3.783	3.823	3.932	3.764	3.823	3.783	3.932	3.764	3.932	3.783	3.823
φ_{2D} [W/m^2]	14.819	14.895	15.050	15.481	14.819	15.050	14.895	15.481	14.819	15.481	14.895	15.050
Ψ [W/(mK)]	0.0687	0.0668	0.0694	0.0616	0.0687	0.0694	0.0668	0.0616	0.0687	0.0616	0.0668	0.0694
$\Delta\varphi_{1D}$	2.27%		9.82%		1.82%		9.41%		11.47%		0.46%	
$\Delta\varphi_{2D}$	0.51%		2.79%		1.54%		3.79%		4.28%		1.03%	
Δψ	2.71%		12.64%		1.03%		8.54%		11.48%		3.64%	

Table 7_ Percent difference between the numerical simulation and the experimental procedure.

It is evident how the NumB simulation, compared to the NumA, is more accurate than the ExpB, compared to the ExpA. The major difference concerns the one-dimensional heat flow: 2.27% for numerical simulation and 9.28% for the experimental procedure.

In the first case, this may be due to the accuracy of the HFM apparatus: the conductivity values of each material were assessed by the instrument and then employed as input on Bisco. The absolute thermal conductivity accuracy declared by the company is ±1%.

Furthermore, another cause shall be the imperfect one-dimensionality of the flow at the end of the investigated area.

However, as regard the φ_{2D}-value, two other causes add to those already mentioned:

- An inaccuracy during the thermocouples placement on the 2D assembly;
- The tolerance of the thermocouples of ±0.25 °C. As can be seen from the Figure 37, which shows the temperatures trend in the NumB and ExpB procedure, the display of the error bars (±0.25 °C) almost completely cancels the difference through the values between the two procedures. This observation represents a crucial issue because the methodology applied, both in the NumB and the ExpB case, refers to the values of temperature.

Moreover, Figure 38 indicates the $\varphi_{tb,i}$-values, always in the cases NumB and ExpB, which do differ by no more than 18% (Figure 39).

Overall, the second combination (ExpA_ExpB, Table 7) appears to be the worst possible and, therefore, those referring to the ExpB have a greater $\Delta\Psi$-value.

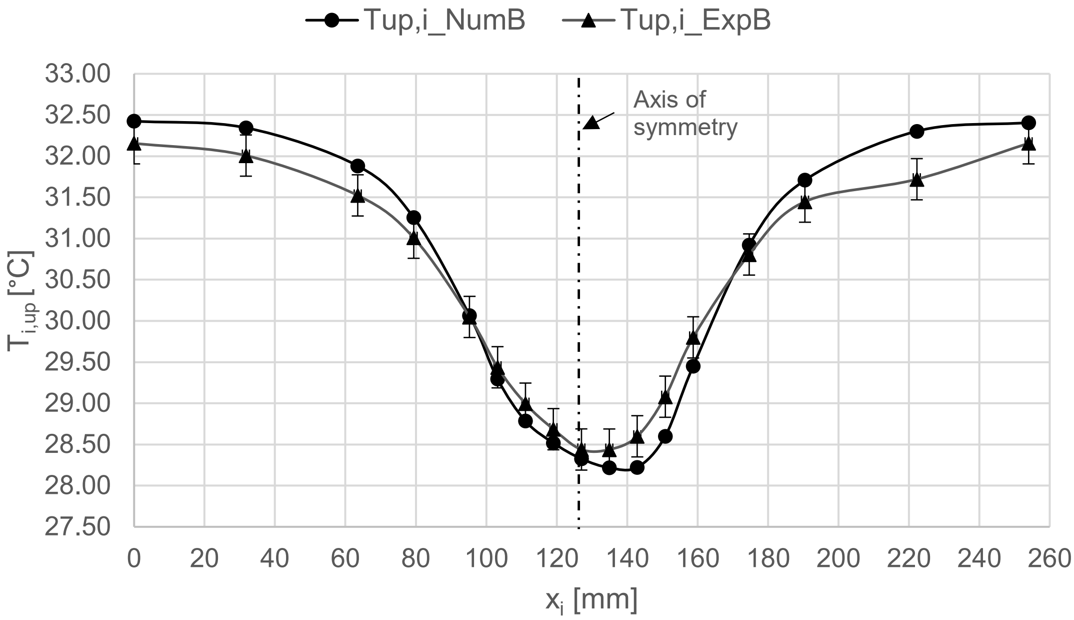

Figure 37_ T_{up,i_NumB} and T_{up,i_ExpB}.

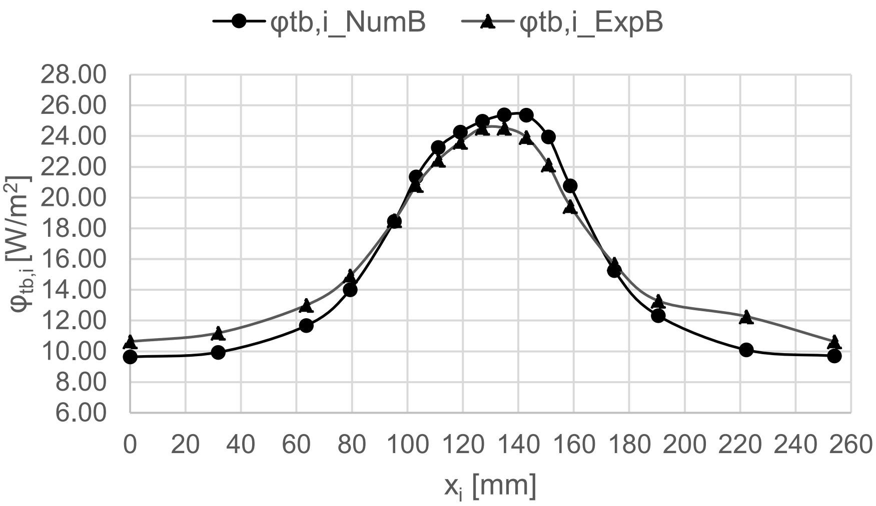

Figure 38_ φ_{tb,i_NumB} and φ_{tb,i_ExpB}.

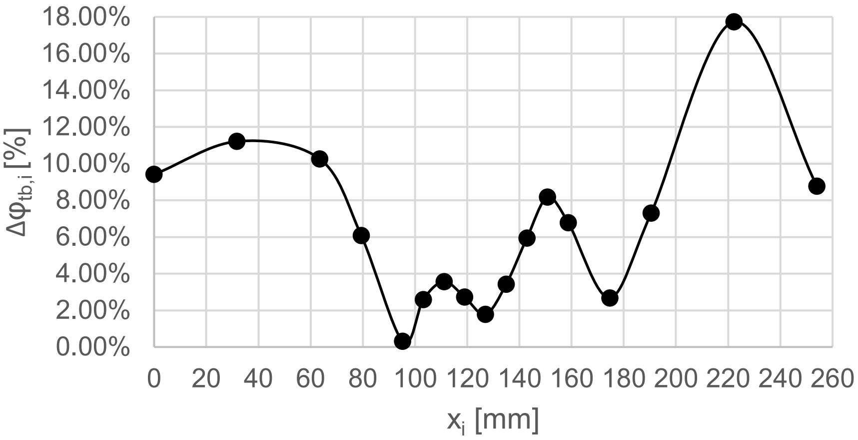

Figure 39_ $\Delta\varphi_{tb,i}$.

In order to reproduce the experimental methodology proposed (HFM B) for other building components, it is also important to highlight the difference, not only in numerical terms, between the NumB and ExpB procedure:

- The first requires the knowledge of all layers λ-values, in order to insert them into Bisco;
- The second needs an envelope sample of a maximum size of heat flux sensors, a linear thermal bridge that remains within the measurement area of the sensors, along with the undisturbed area due to evaluate the one-dimensional heat flow.

Hence, the choice between the two procedures will be based on the characteristics of the envelope, its thermal bridge and whether a sample can be produced.

6 Second case study: high-performance insulation material filled brick

The second investigated envelope was two walls composed of filled bricks developed in order to improve massive construction and to fulfil the requirements for passive houses, reducing the wall thickness at the same time.

The filling is an aerogel mixture similar to that analysed in the first case study, placed into the cavities of the bricks, as shown in Figure 40.

The company has provided both the filled bricks (Figure 40), with dimensions of (246x248x368) mm, and those without the filling with the same dimensions (Figure 41).

Figure 40_ Filled brick.


Figure 41_ Brick without filling.

The aim of this assessment was to evaluate:

- The thermal transmittance, *U*, the thermal conductance, *C*, and the thermal conductivity, *λ*, of the two bricks;
- The heat transfer coefficient, *h*;
- The linear thermal bridge, *Ψ*, caused by joints between the bricks.

The assessment of these thermophysical values was initially carried out by the heat flux analysis, according to the standards ISO 9869-1:2014 [4], and, subsequently, enhanced by means of IR thermography.

6.1 Experimental setup and instrument

The experimental tests were performed by the thermostatic chamber, called BET cell (Building Envelope Test Cell, Figure 42), in which it is possible to test building components or measurement methods in controlled thermal conditions. The cell has the following dimensions: length of 4.84 m, width 2.74 m, height 2.34 m.

Two walls were built inside the cell in order to divide the environment into two air-conditioned zones using two independently air-conditioners.

The first zone, called side A, has been set as the hot side by a radiator with a PID controller, the side B instead has been set as the cold side by an air conditioner. Moreover, a fan has been placed, close to the radiator, in order to minimize the air stratification and, in both sides, a plastic curtain has been arranged at a distance of about 1 m from the walls with the aim of reducing the convective heat flow near these.

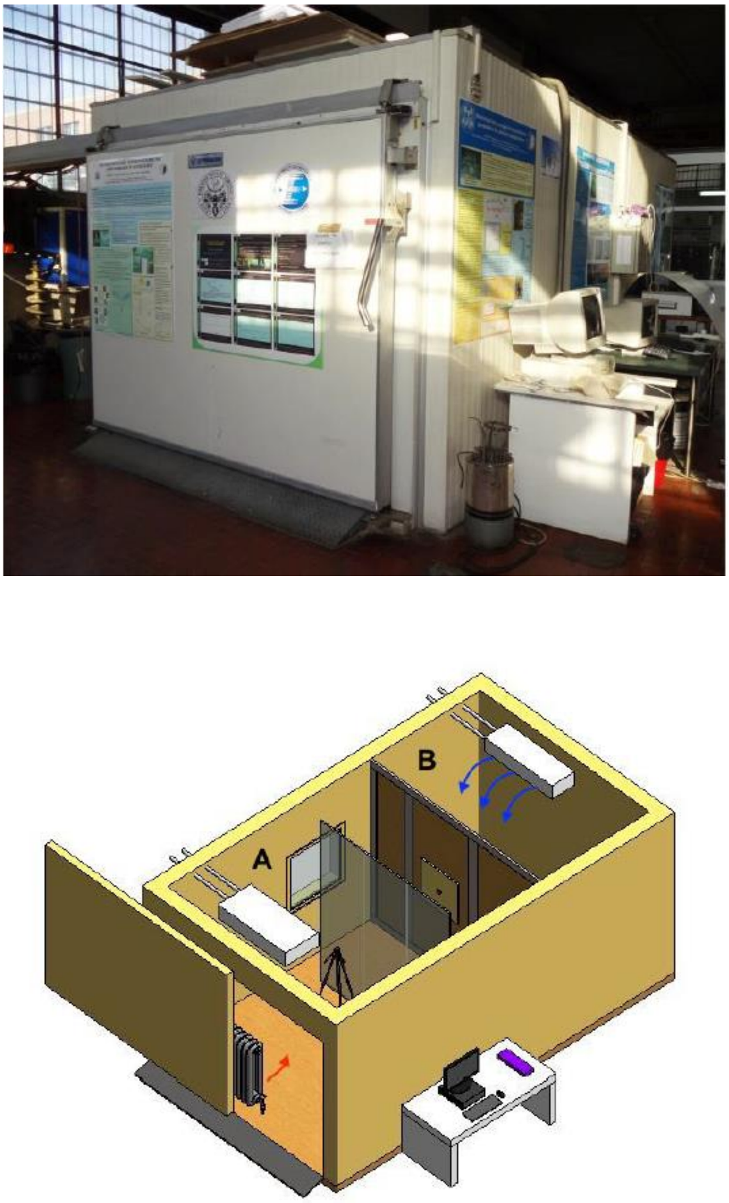

Figure 42_ Thermostatic chamber picture [32] and schematic representation.

The two investigated walls were each constituted of 27 bricks: the left one, called Reference, has all bricks without filling, the one on the right, called Filled, has the four central rows of filled bricks. Figure 43 presents the two walls for reference and filled sides, where in both cases, the four central rows of bricks were joined with mortar in order to recreate the real condition of use; in the others rows the joints were filled by PET films.

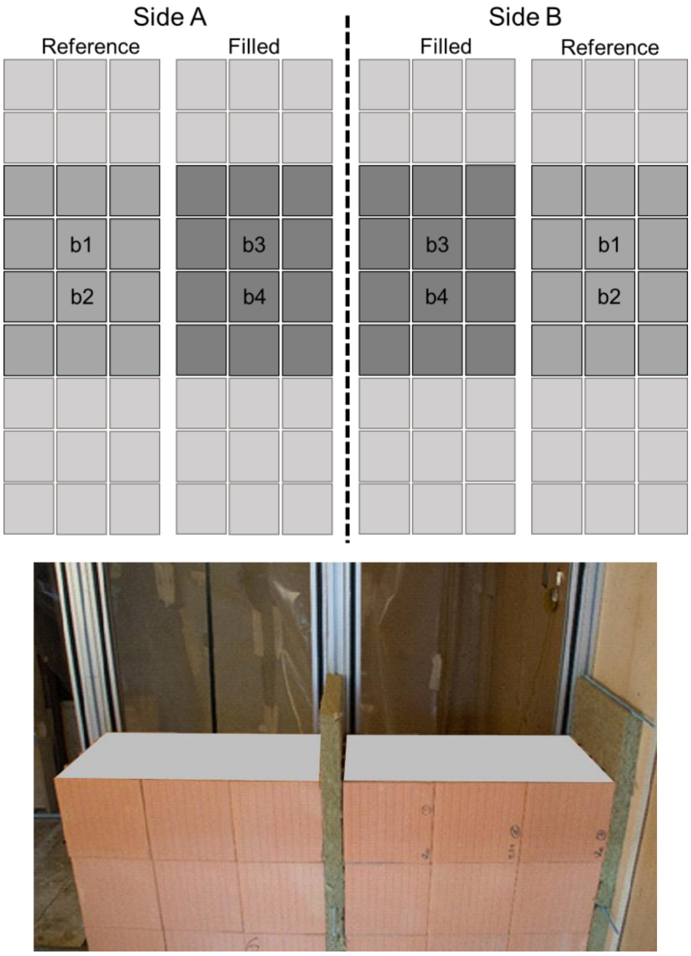

Figure 43_ Reference and filled side.

Furthermore, from Figure 43, it is possible to notice how the gaps between the two walls and between the envelope of the thermostatic chamber were filled by means of mineral wool. This chooses aimed to avoid heat losses.

Moreover, the walls were fixed to metallic frames by three planks of wood and the passage between the sides was closed by a wood panel (Figure 44).

Figure 44_ Experimental setup.

Two heat flux sensors and 32 thermocouples have employed the analysis.

The thermocouples (TT type) were used to measure both the air temperature and the temperature on the bricks and were placed, according to the sketch shown in Figure 45.

This arrangement follows the methodology proposed in Chapter 4: the horizontal alignment was used to assess the vertical linear thermal transmittance, Ψ_v, the vertical one to evaluate the horizontal linear thermal transmittance, Ψ_h. The last alignment, the diagonal one, was placed in order to determine a mapping temperature designed to assess the equivalent thermal conductivity of the two bricks.

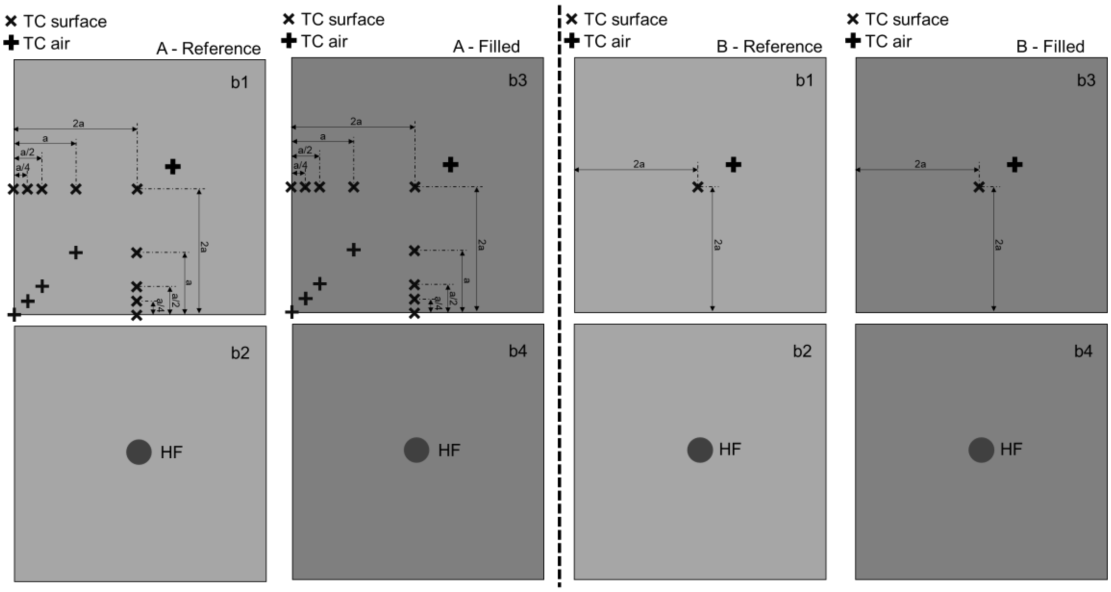

Figure 45_ Thermocouples positioning.

The heat flux sensors used were the HFP01-10 type produced by Hukseflux, which works by means of a thermopile measuring the differential temperature across the measurement area of the sensor (Figure 46). The output is a voltage that can be converted into the heat flux.

Figure 46_ Heat flux sensor.

Figure 47_ Datataker.

Figure 48_ IR camera

A Datataker, dT85 type, was used to acquire the temperatures and the heat fluxes data (Figure 47).

As regards the IR thermography, the measurements were performed by an IR camera (TESTO 825-2i) which require the continuous presence of an operator. This camera can convert the infrared radiation, IR, emitted from the sample into a thermal image using visible light. The emission, the reflection and the transmission of infrared rays are detected and acquired by the IR camera, as shown in Figure 49. The technical data declared by the company are shown in Table 8.

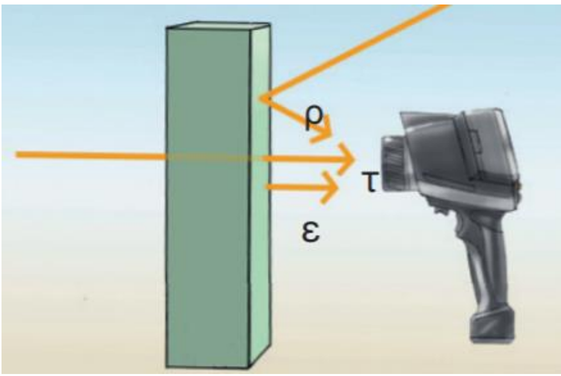

Figure 49_ Emissivity, reflection factor, transmission factor [10].

IR camera	
Type of detector	160 x 120 pixel
Thermal sensitivity	< 50 mK to 30 °C
Field of view	32° x 23°
Min. distance of focus	0.1 m
Accuracy	±2°C

Table 8_ IR camera technical data.

The data were assessed conducting three experimental campaigns:

- The first was performed with HF analysis and applying a temperature difference between the sides, $\Delta T_{setpoint}$, of 40°C: T_{sideA}= 40 °C, T_{sideb}= 0 °C;
- the second was carried out by $\Delta T_{setpoint}$=30°C and the IR thermography: T_{sideA}= 30 °C, T_{sideb}= 0 °C;
- the third by $\Delta T_{setpoint}$=28°C and the IR thermography; T_{sideA}= 28 °C, T_{sideb}= -3 °C.

6.2 Heat flux analysis

With regard to the heat flux analysis, the values investigated for each campaign were calculated by the average method according to ISO 9869-1:2014 [4].

Moreover, the thermal conductance, *C* (Eq. (22)), the thermal transmittance, *U* (Eq. (23)) and the heat transfer coefficient, *h* (Eq. (24)) were assessed both in the side A and in the side B and both for the reference side and the filled one. All the equations concern quantities calculated in the center of the brick. Taking into account the side A, the φ_{1D_A}-values, that are the heat fluxes measured by the HF sensors on the side A, were considered. Whereas taking into account the side B, the φ_{1D_B}-values, that are the heat fluxes measured by the HF sensors on the side B, were used.

$$C_A = \frac{\sum_j \varphi_{1D\_A,j}}{\sum_j |T_{s\_A\_c,j} - T_{s\_B\_c,j}|} \qquad [W/(m^2K)] \qquad (22)$$

$$U_A = \frac{\sum_j \varphi_{1D\_A,j}}{\sum_j |T_{a\_A\_c,j} - T_{a\_B\_c,j}|} \qquad [W/(m^2K)] \qquad (23)$$

$$h_A = \frac{\sum_j \varphi_{1D\_A,j}}{\sum_j |T_{a\_A\_c,j} - T_{s\_A\_c,j}|} \qquad [W/(m^2K)] \qquad (24)$$

In these equations, $T_{s\_A\_c}$ and $T_{s\_B\_c}$ are the surface temperatures of the brick, on the side A and on the side B; $T_{a\_A\_c}$ and $T_{a\_B\_c}$ are the air temperatures and j is the individual measurement of the acquisition period. The latter had to start when steady-state conditions were observed, and it was assessed by two different cases:

- Case A: the reference period considers the hours preceding the entry into the thermostatic chamber for the first and the third campaign. In particular, the first campaign covers a period of 54 hours and the third of 48 hours. In the second campaign, it was not possible to use this method, due to a problem regarding their acquisition.
- Case B: the reference period refers to the data collection time by IR camera during the third campaign, as explained in paragraph 6.3.

The thermal conductivity, λ, of the filled and unfilled brick was calculated by Eq. (28) and Eq. (29) and with regard the side A due to the unsteady-state conditions into the side B. In this respect, Figure 50 shows the trend temperature of the air in the side B.

$$\lambda_{A\_fil} = C_{A\_fil} s \qquad [W/(m^2K)] \qquad (28)$$

$$\lambda_{A\_ref} = C_{A\_ref} s \qquad [W/(m^2K)] \qquad (29)$$

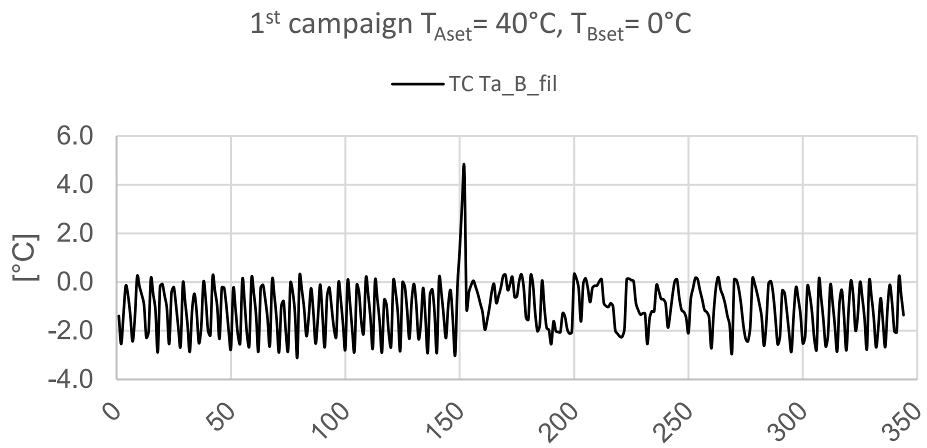

Figure 50_ Trend temperature, side B.

6.2.1 Results

In this case study, the methodology proposed in Chapter 4 was not applied due to the temperatures trend on the surface displayed in the figures below: Figure 51 and Figure 52 refer to the horizontal and vertical alignment on the reference side.

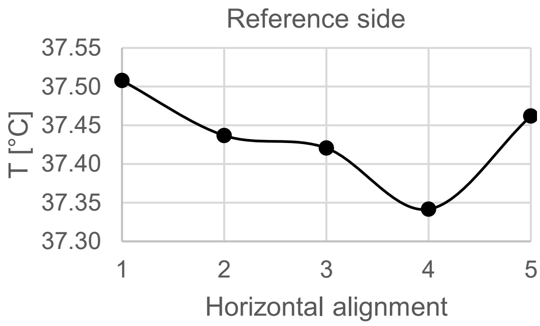

Figure 51_ Temperatures trend, horizontal alignment.

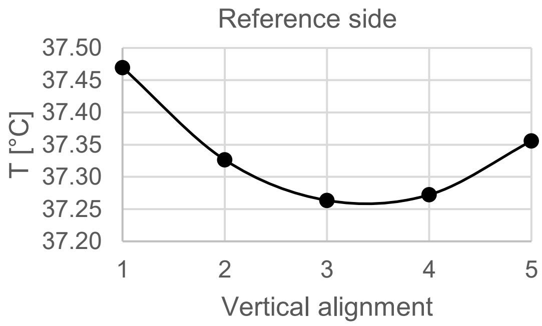

Figure 52_ Temperatures trend, vertical alignment.

Hence, the hypothesis of the proposed methodology was not established, and the Ψ_v-value and the Ψ_h-value were not calculated.

The results related to the calculations of *h*-values, *C*-values, *U*-values of the case are presented in Figure 53.

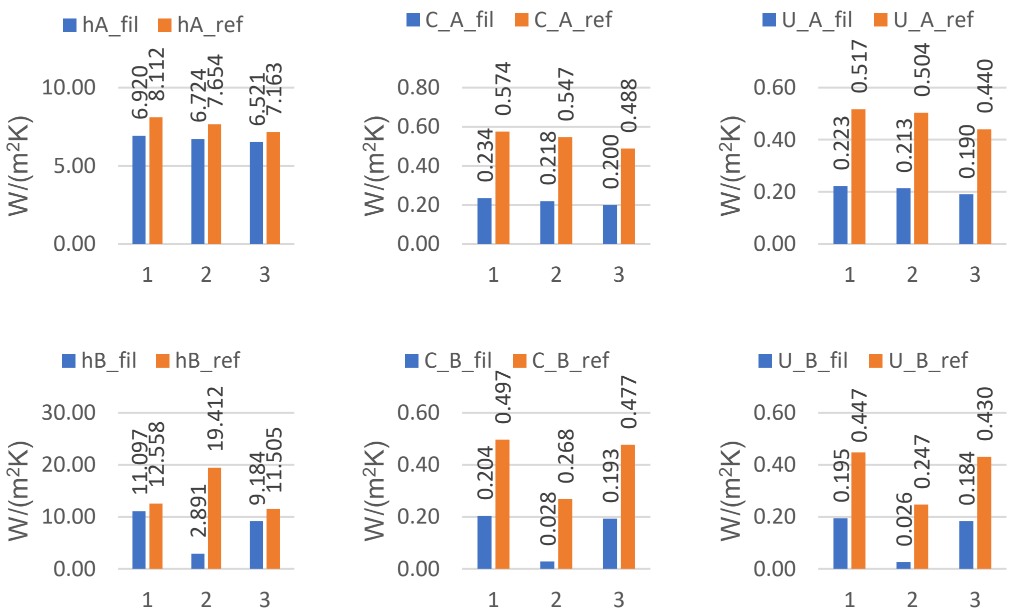

Figure 53_ HFM results, case A.

As is evident from the charts, the values referred to the side B vary considerably, due to the temperatures trend explained in the previous paragraph. For this reason, side B was not taken into account to assess the thermal conductivity, λ: Figure 54 presents the λ-values, which affect the filled brick and the unfilled one.

Moreover, by comparing the three campaigns, it is evident that all three determined quantities, *h*-values, *C*-values and *U*-values, decrease when the temperature difference, $\Delta T_{setpoint}$, decreases: a direct proportion between temperature and the thermal conductivity was observed. This trend is also shown in Figure 54 and the results are comparable with those obtained by Werney J. *et al.* [13], which they have measured the thermal conductivity of a similar brick in different conditions: using a temperature difference of 10 K the brick with aerogel filling has the thermal conductivity in the center is (59.00 ± 1.2) mW/(mK). This value, referring to a lower temperature difference than those applied in this assessment, would be positioned on the right to the bars of the third campaign and verify the thesis according to which the lower the temperature difference, the smaller the thermal conductivity of the filled brick. In the case of unfilled brick, this reduction of the *λ*-value is due to the presence of several cavities, as can be seen from Figure 41.

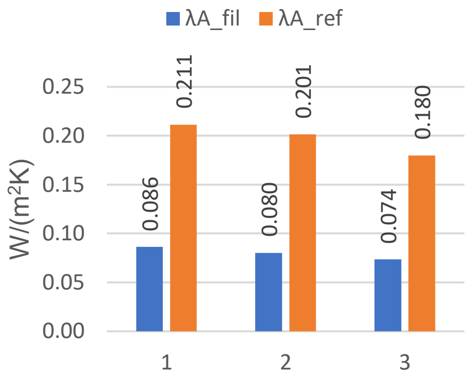

Figure 54_ Thermal conductivity, case A.

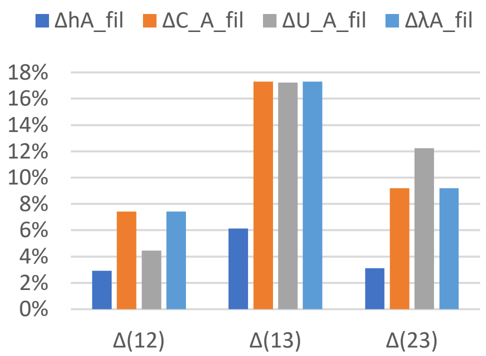

Figure 55_ Percent difference, filled side, case A.

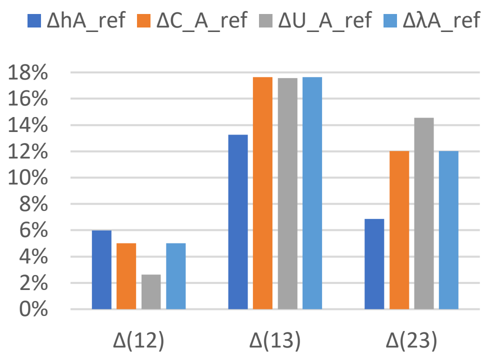

Figure 56_ Percent difference, reference side, case A.

Figure 55 and Figure 56 display the percent difference between the three campaigns, showing the highest value between the first and the last campaign and the lowest between the first and the second one. These results are linked to the $\Delta T_{setpoint}$ of each campaign: the biggest the difference between the $\Delta T_{setpoint}$-value of two campaign, the highest will be the percent difference shown in Figure 55 or Figure 56.

Taking into account the center of bricks, the thermal transmittance, *U*, of the filled brick is about 60% lower than the unfilled one, as well as the *C*-value and the *λ*-value. The percent difference of heat transfer coefficient, indeed, decreases when the T_{sideA}-values reduces. This trend could be connected with the heating mode of the side A, that is radiator plus flan, and, therefore, with the convective motions of the air.

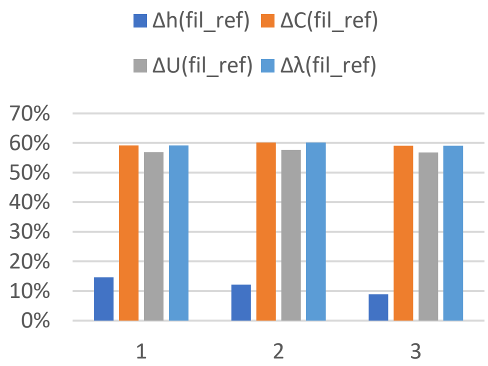

Figure 57_ Percent difference between the filled and reference side, case A.

As regards the case B, the tables related to the calculations of *h*-values, *C*-values, *U*-values are in Annex C, whereas the results of case A are presented in Figure 58. As in the case A, all values refer to the center of brick.

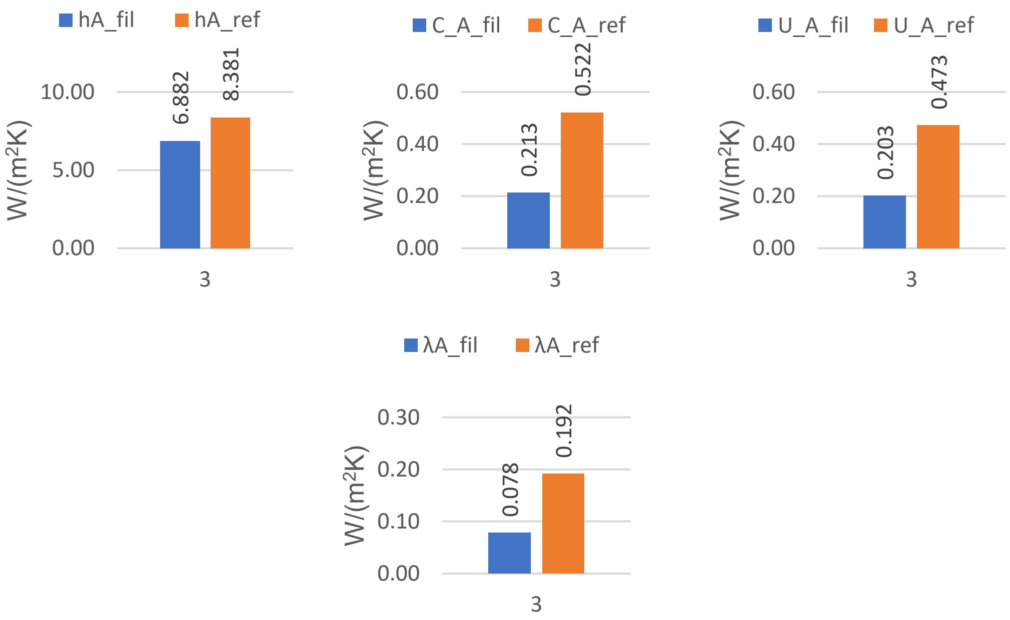

Figure 58_ HFM results, case B.

Moreover, Figure 59 displays the percent differences between the filled and reference side, which are comparable to those of the case A (Figure 59). Also in this case, the *U*-value, *C*-value and *λ*-value of the filled brick are 60 % lower than the unfilled one.

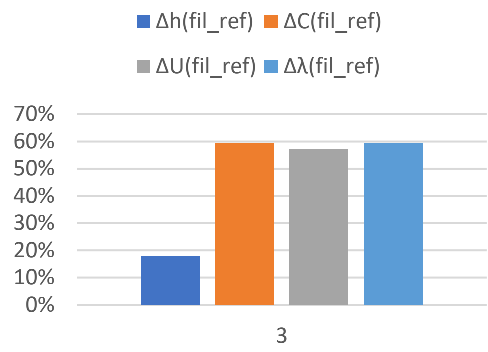

Figure 59_ Percent difference between the filled and reference side, case B.

6.3 IR Thermography

The thermal images were collected during the second and third campaign in order to compare this data with those obtained from the heat flux analysis and to assess the average values of thermal conductance, thermal transmittance and conductivity. The images were obtained positioning the IR camera in front of the plastic curtain cut close to the investigated bricks and shooting every five minutes in a synchronized manner with the datataker. After the second campaign fulfilled on the lower bricks, those marked in red in Figure 60, the last campaign was carried out on the upper bricks, the two marked in black in Figure 60. This decision was supported by the fact that, in the second campaign, the thermographic images appeared disturbed by the air stratification, as is evident from Figure 61. This, however, did not happen with the upper bricks, as Figure 62 shows. Hence, for this reason, the second campaign was not taken into account for the calculation of the *C*-values, *U*-values and *λ*-values.

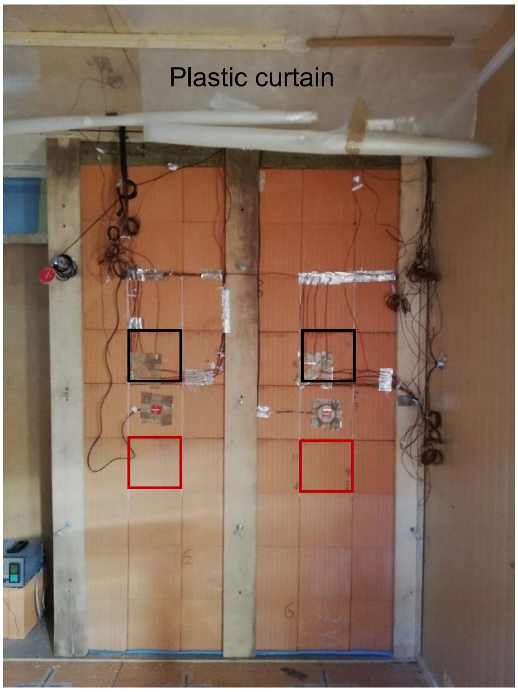

Figure 60_ IR thermography setup.

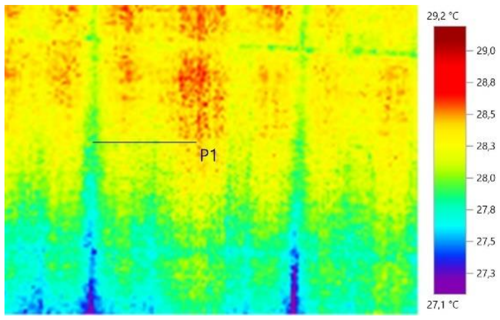

Figure 61_ Thermographic image refers to the second campaign and the reference side.

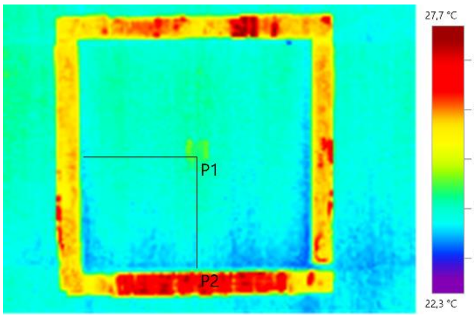

Figure 62_ Thermographic image refers to the third campaign and the reference side.

Moreover, the thermal images confirmed the non-applicability of the methodology proposed in Chapter 4 to assess the linear thermal transmittance, Ψ_h and Ψ_v. In this respect, as can be seen from Figure 63 and Figure 64, the temperatures trends of the horizontal alignment and the vertical one do not comply the hypothesis of the methodology, that is a trend qualitatively similar that of Figure 21 or Figure 36.

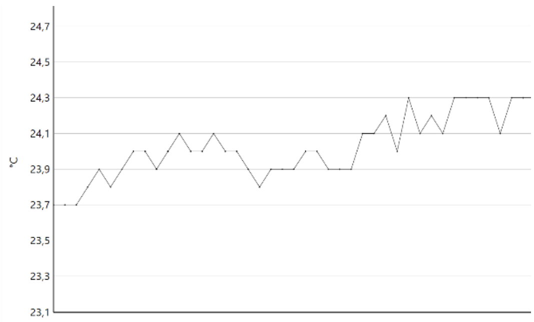

Figure 63_ Horizontal alignment.

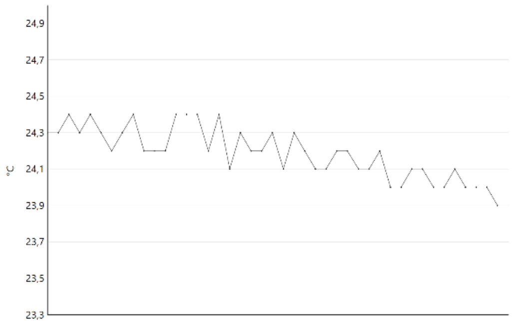

Figure 64_ Vertical alignment.

In order to evaluate the *C*-values, *U*-values and *λ*-values, using the thermographic images only, the heat transfer coefficient was considered as a known value and the same as those calculated during the third campaign in the HFM analysis: h_{A_fil}=6.724 W/(m^{2}K) and h_{A_ref}=7.163 W/(m^{2}K). This condition aims to simulate a real application of the IR thermography, in which the *h*-values are derived from UNI EN ISO 6946:2008 [4].

Hence, the one-dimensional heat flux can be assessed by Eq. (30), referred to the filled side, and Eq. (31) for the reference side, where the subscript *a* indicates the air temperature, the subscript *s* the surface temperature and the subscripts *fill* and *ref* the filled and the reference side. The air temperatures were obtained by the same thermocouples used in the HFM analysis and the surface temperatures by the thermographic images.

$$\varphi_{1D\_fil} = h_{A_{fil}}(T_{a\_A\_fil} - T_{s\_A\_c\_fil}) \quad [\mathrm{W/m^2}] \qquad (30)$$

$$\varphi_{1D\_ref} = h_{A_{ref}}(T_{a\_A\_ref} - T_{s\_A\_c\_ref}) \quad [\mathrm{W/m^2}] \qquad (31)$$

The *C*-values were evaluated by means of Eq. (32) and Eq. (33), where the surface temperatures of the side B was achieved by the thermocouples employed in the HFM analysis. Hence, the λ-values were calculated by Eq. (34) and Eq. (35), where the s-value is the thickness of the brick.

$$C_{A\_fil} = h_{A_{fil}} \frac{\sum_j (T_{a\_A\_fil,j} - T_{s\_A\_c\_fil,j})}{\sum_j (T_{s\_A\_c\_fil,j} - T_{s\_B\_c\_fil,j})} \quad [\mathrm{W/(m^2K)}] \quad (32)$$

$$C_{A\_ref} = h_{A_{ref}} \frac{\sum_j (T_{a\_A\_ref,j} - T_{s\_A\_c\_ref,j})}{\sum_j (T_{s\_A\_c\_ref,j} - T_{s\_B\_c\_ref,j})} \quad [\mathrm{W/(m^2K)}] \quad (33)$$

$$\lambda_{A\_fil} = C_{A\_fil}\, s \quad [\mathrm{W/(mK)}] \quad (34)$$

$$\lambda_{A\_ref} = C_{A\_ref}\, s \quad [\mathrm{W/(mK)}] \quad (35)$$

The U-values were assessed by Eq. (36) and (37), where the air temperature was obtained by the thermocouples.

$$U_{A\_fil} = h_{A_{fil}} \frac{\sum_j (T_{a\_A\_fil,j} - T_{s\_A\_c\_fil,j})}{\sum_j (T_{a\_A\_fil,j} - T_{a\_B\_fil,j})} \quad [\mathrm{W/(m^2K)}] \quad (36)$$

$$U_{A\_ref} = h_{A_{ref}} \frac{\sum_j (T_{a\_A\_ref,j} - T_{s\_A\_c\_ref,j})}{\sum_j (T_{a\_A\_ref,j} - T_{a\_B\_ref,j})} \quad [\mathrm{W/(m^2K)}] \quad (37)$$

Due to the considerable difference between the surface temperatures in the center of brick collected by the IR camera and those obtained by the thermocouples, it was necessary to improve the results obtained (Figure 65 and Figure 66) according to the method proposed by Nardi I. *et al.* [14].

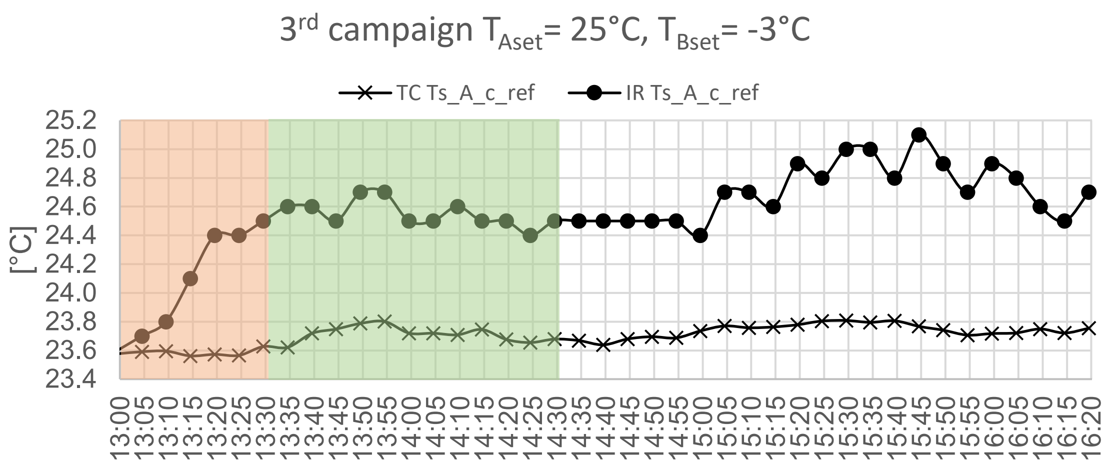

Figure 65_ Comparisons between the temperatures of the thermocouples and those of the IR thermography, reference side.

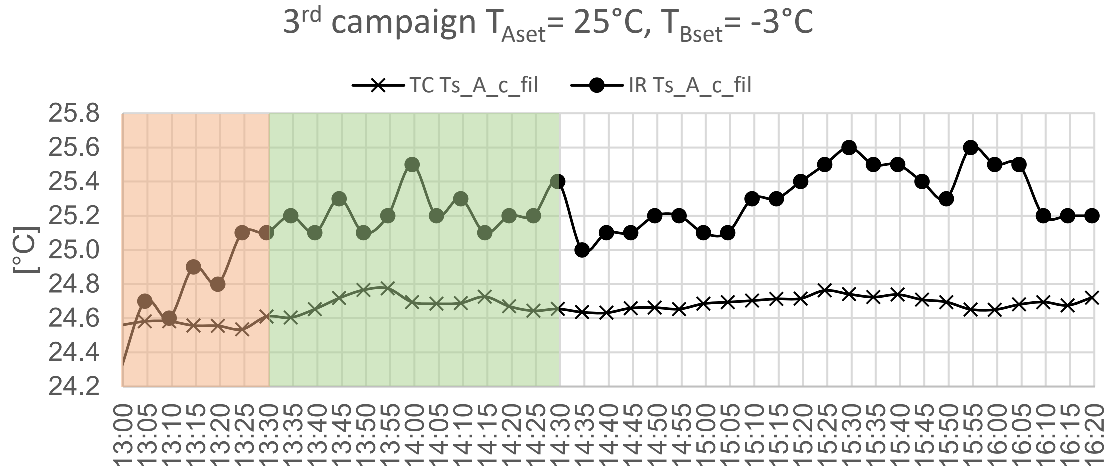

Figure 66_ Comparisons between the temperatures of the thermocouples and those of the IR thermography, filled side.

First, a reference time interval was chosen, excluding the first 30 minutes, which is the period highlighted in red. As is evident from the charts, the IR $T_{s\_A\_c\_fil}$ and $T_{s\_A\_c\_ref}$ lines tend to move from the data obtained by the thermocouples and, therefore, the hour following the discarded period was taken as reference.

Using the TESTO software, the images have been improved following the procedure [14] below:

- Set ε=1 and assess the reflected temperature, T_{refl}, which corresponds with the temperature of the aluminium foil, T_{all};
- Determine the T_{all}-value setting up the T_{refl}-value and the ε_{all}=0.04;
- Change the ε-value of the brick until T_{all}= $T_{surface}$, where $T_{surface}$ is the surface temperature of the center of brick.

The average thermal transmittance, U_{av}, was also assessed, always referring to the improved thermographic images. By using the TESTO software, the average surface temperature, $T_{s\_A\_av}$ for each image was obtained, and employed in order to evaluate the U_{av}-value by Eq. (38) and (39). These two equations were applied to each thermographic image and, afterwards, the 13 values obtained for the reference and filled side were averaged in order to achieve 1 value for each side.

$$U_{av\_fil} = \frac{h_{A_{fil}}(T_{a\_A\_fil} - T_{s\_A\_av\_fil})}{T_{a\_A\_fil,j} - T_{a\_B\_fil,j}} \quad [\mathrm{W/(m^2K)}] \qquad (38)$$

$$U_{av\_ref} = \frac{h_{A_{ref}}(T_{a\_A\_ref} - T_{s\_A\_av\_ref})}{T_{a\_A\_ref} - T_{a\_B\_ref}} \quad [\mathrm{W/(m^2K)}] \qquad (39)$$

6.3.1 Results

The IR images referred to the reference period are shown in Annex C and the T-values of the center of brick are displayed in Table 9, where the $T_{s\_A\_c\_fil}$-values refer to the filled side and the $T_{s\_A\_c\_ref}$-values to the reference side. These data were obtained setting the reflected temperature T_{refl}= 25°C and ε_{brick}=0.93.

3rd Campaign	Ts_A_c_fil [°C]	Ts_A_c_ref [°C]
13:30	25.10	24.50
13:35	25.20	24.60
13:40	25.10	24.60
13:45	25.30	24.50
13:50	25.10	24.70
13:55	25.20	24.70
14:00	25.50	24.50
14:05	25.20	24.50
14:10	25.30	24.60
14:15	25.10	24.50
14:20	25.20	24.50
14:25	25.20	24.40
14:30	25.40	24.50

Table 9_ T-values of IR images.

Employing the procedure explained above, the following values for the filled side were obtained:

- With ε=1, T_{refl}= 26°C was achieved;
- With ε_{all}=0.04 and T_{refl}= 26°C, T_{all}= 24.2 °C was obtained by means of an average of six points (Table 10 and Figure 67);
- With $T_{surface}$= 24.2 °C, ε_{brick}=0.50 was obtained.

As is evident from Figure 68, the difference between the improved surface temperature of the center of filled brick and those recorded by the thermocouples is at most 0.6 °C.

N.	T. [°C]	ε	T_{refl}. [°C]
M1	27.0	0.04	26.0
M2	20.5	0.04	26.0
M3	22.7	0.04	26.0
M4	24.2	0.04	26.0
M5	26.0	0.04	26.0
M6	24.8	0.04	26.0
Tav	**24.2**		

Table 10_ Temperature of the aluminium foil, filled side

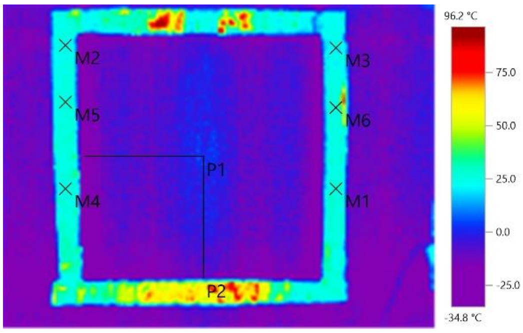

Figure 67_Six temperature measurement points, filled side

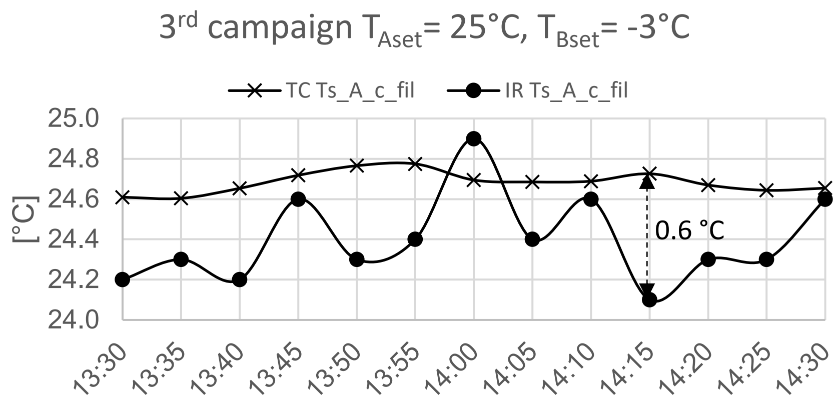

Figure 68_ Improved surface temperatures, filled side.

As regards the reference side, the following data were achieved:

- With ε=1, T_{refl}= 26°C was achieved;
- With ε_{all}=0.04 and T_{refl}= 26°C, T_{all}= 23.8 °C was obtained by means of an average of six points (Table 11 and Figure 69);
- With $T_{surface}$= 23.8 °C, ε_{brick}=0.67 was obtained.

In this case, the maximum difference between the improved surface temperature of the center of filled brick and those recorded by the thermocouples is 0.4 °C, as shown in Figure 70.

N.	T. [°C]	ε	$T_{refl.}$ [°C]
M1	21.3	0.04	26.0
M2	20.0	0.04	26.0
M3	22.7	0.04	26.0
M4	26.1	0.04	26.0
M5	26.7	0.04	26.0
M6	26.2	0.04	26.0
Tav	**23.8**		

Table 11_ Temperature of the aluminium foil, reference side

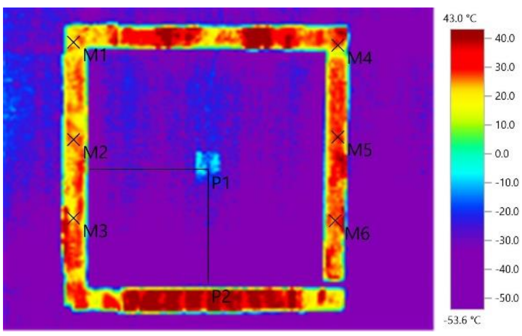

Figure 69_Six temperature measurement points, reference side

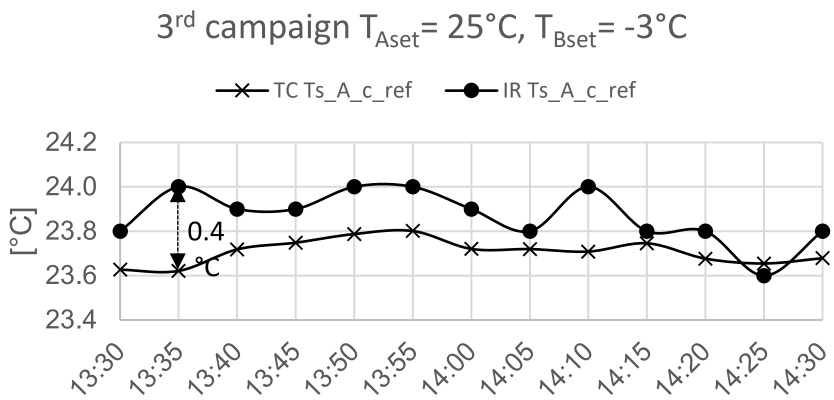

Figure 70_ Improved surface temperatures, reference side.

The results related to the calculations of *h*-values, *C*-values, *U*-values are presented in Figure 71.

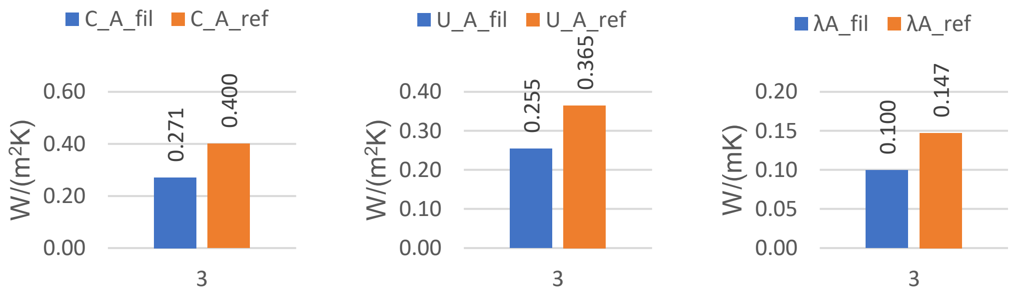

Figure 71_ IR thermography results.

As regards the average value of the thermal transmittance, U_{av}, the results are present in Figure 72 below, whereas Table 20 and Table 21 in Annex D show the complete data. In this case, the percent difference between the filled and the reference side is 37%.

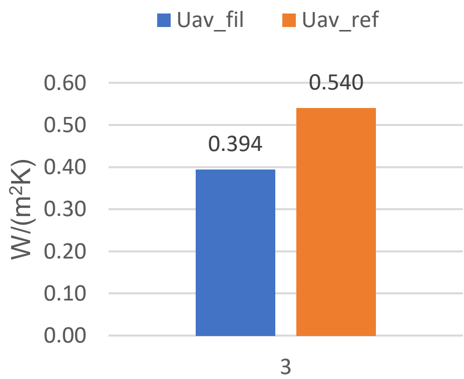

Figure 72_ U_{av}-values.

6.4 Comparison

In order to compare and validate the IR thermography, the following comparisons were carried out. The considered data refer to the third campaign in three conditions:

- With the air and surface temperatures and heat fluxes obtained by HFM method in the case A, as explained in paragraph 6.2 and so-called HFM 3*;
- With the air and surface temperatures and fluxes achieved by HFM method in case B, as explained in paragraph 6.2 and so-called HFM 3**;
- With the air temperatures obtained by the thermocouples and the surface temperatures by IR thermography, as explained in paragraph 6.3 and so-called IR camera 3.

Complete data are shown in Figure 74, whereas the percent difference in the three possible combinations is presented in Figure 75.

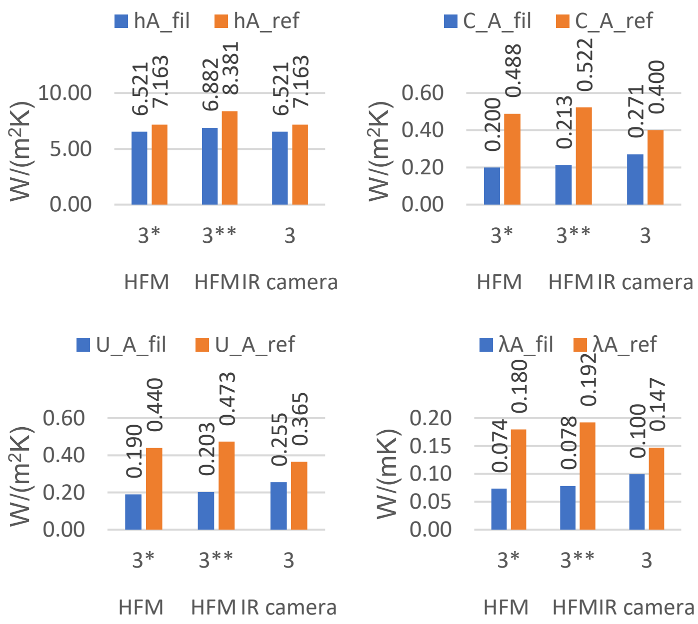

Figure 74_ Third campaign data.

As is evident from the bar chart in the first and second case, HFM 3* and HFM 3**, the percent differences between the filled and reference side are equal, since both the specific heat fluxes and the temperature differences have not changed. Instead, the values obtained by IR camera have a percent difference by nearly half. In other words, the IR thermography method underestimates substantiality both the thermal conductivity, λ_{A_ref}, of the unfilled brick and overestimates the λ_{A_fil}-value of the filled one, as Figure 76 displays.

As the bar charts illustrate, the percent difference between the HFM 3* data and the HFM 3** data differ by about 6%, which means that the operator inside the thermostatic chamber disturbed significantly the environment. A greater percent different with the data of the IR camera can be observed, reaching a difference of about 30% in the reference side (Figure 76).

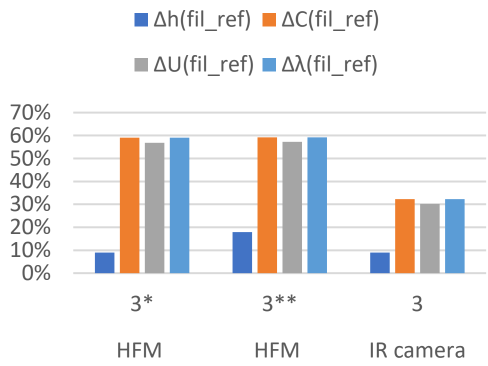

Figure 75_ Percent difference between the filled and the reference side in the three possible combinations.

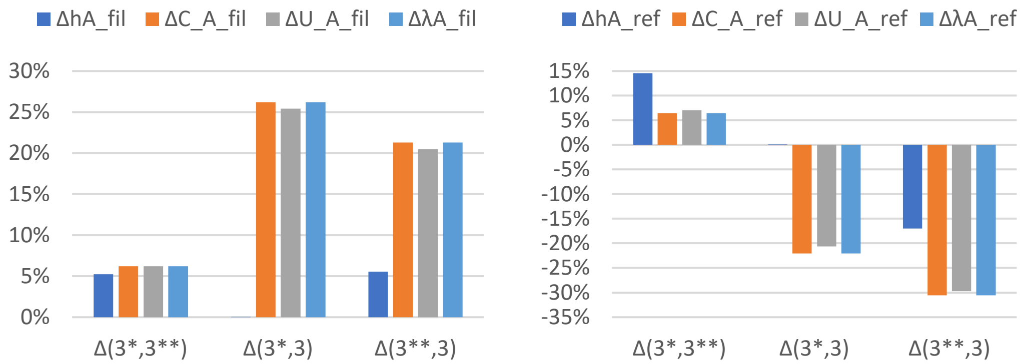

Figure 76_ Percent difference in the three possible combinations.

7 Conclusions

With regard to what has been studied in this thesis, distinct considerations for the first and the second case studies will be conducted in this section.

Taking into account the plasterboard assembly of the first case study, the main consideration concerns the use of the aerogel-base filler. In particular, the advantages emerged are a decrease of linear thermal transmittance of about 23%, according to the numerical simulations. This result widely contributes to the reduction of heat losses in buildings. On the other hand, the employed filler is still in the research phase and presents several issues during the preparation and the coating of it, as explained in the previous chapter.

Moreover, this case has been used in order to validate the methodology proposed in Chapter 4 through numerical simulations and experimental procedures.

As regards the first ones, the percent differences of linear thermal transmittance have been assessed in several cases of R_{add}-values and λ_{filler}-values, as shown in Figure 26.

Indeed, the experimental procedures, referred to one λ_{filler}-value due to the problems with the improved filler, have been provided data with less accuracy than the numerical simulations, as illustrated in Table 7.

Looking at the obtained data, the methodology can be considered validated, according to EN ISO 14683:2014 [2] which requires a typical accuracy of ± 20%.

Concerning the filled brick, the proposed methodology has not been applied due to the hypotheses of it, which are widely explained in Chapter 4. Hence, the linear thermal transmittance has not been assessed by other methods, for example, Asdrubali F. *et al.* [21], since the temperature trend does not match any cases in the literature.

In this case, it is possible to do a comparison between the data obtained by HFM analysis and by thermography.

Taking into account HFM analysis, the *U*-values, *C*-values and *λ*-values decrease when the temperature difference between the two zones reduces. This trend is observed both for unfilled brick and the filled one. The obtained values refer to the center of brick and thus, the equivalent thermal conductivity cannot be assessed.

Moreover, from the comparison between the 3* HFM and 3** HFM cases, namely between the temperatures before and during the IR thermography, it is evident how the *U*-values, *C*-values and *λ*-values do not change substantially. Indeed, the percent difference between filled and reference sides of these values is of about 60% in both cases.

Different results have been provided by the IR thermography, in which the *U*-value, *C*-value and *λ*-value of the unfilled brick are underestimated substantiality, while the values of the filled brick are overestimated compared to HFM method. Hence, the improvement of the IR images is necessary but not enough to compare and validate this thermographic method.

Finally, as regards the average value of the thermal transmittance, the results are not comparable with the others due to the existence of several structural thermal bridges caused by the air cavity or by aerogel-base filler.

8 Bibliography

[1] EN, Thermal bridges in building construction - Heat flows and surface temperatures - Detailed calculations, in: EN ISO 10211, European Committee for Standardization, 2017.

[2] EN, Thermal bridges in building construction - Linear thermal transmittance - Simplified methods and default values, in: EN ISO 14683, European Committee for Standardization, 2014.

[3] EN, Prestazione termica degli edifici – Coefficienti di trasferimento del calore per trasmissione e ventilazione – Metodo di calcolo, in: UNI EN ISO 13789, Ente Nazionale Italiano di Unificazione, 2008.

[4] ISO, Thermal insulation – Building elements – In-situ measurement of thermal resistance and thermal transmittance, in: BS ISO 9869-1, BSI Standard Publication, 2014.

[5] EN, Componenti ed elementi per edilizia – Resistenza termica e trasmittanza termica – Metodo di calcolo, in: UNI EN ISO 6946, Ente Nazionale Italiano di Unificazione, 2008.

[6] EN, Prestazione termica dei materiali e dei prodotti per edilizia – Determinazione della resistenza termica con il metodo della piastra calda con anello di guardia e con il metodo del termoflussimetro – Prodotti con alta e media resistenza termica, in: UNI EN 12667, Ente Nazionale Italiano di Unificazione, 2002.

[7] V. Corrado, E. Fabrizio, Fondamenti di termofisica dell'edificio e climatizzazione, C.L.U.T., Torino, 2014.

[8] Y. A. Çengel, Termodinamica e trasmissione del calore, McGraw-Hill Education, 2009.

[9] [Online] http://www.tainstruments.com/fox-600/

[10] Testo SE & Co. KGaK, Pocket Guide di termografia, 2017.

[11] L. Zalewski, S. Lassue, D. Rousse, K.Boukhalfa, Experimental and numerical characterization of thermal bridges in prefabricated building walls, Energy Conv. And Manag. 51 (2010) 28699-2877.

[12] R. Bassiouny, M. R.O. Ali, E. H. NourEldeeen, Modeling of the thermal behaviour of Egyptian perforated masonry red brick filled with material of low thermal conductivity, Journal of Buil. Engi. 5 (2016) 158-164.

[13] J. Wernery, A. Ben-Ishai, B. Binder, S. Brunner, Aerobrick – An aerogel-filled insulating brick, Procedia Eng. (2017).

[14] I. Nardi, D. Paoletti, D. Ambrosini, T. Rubeis, S. Sfarra, A comparison of different calculation methods in a Guarded Hot Box, Energy Build. 122 (2016) 211-221.

[15] Physibel Bisco, Manual BISCO v11.0w, 2016

[16] C. Sprengard, A. H. Holm, Numerical examination of thermal bridging effects at the edges of vacuum-insulation-panels (VIP) in various constructions, Energy Build. 85 (2014) 638-643.

[17] J. Prata, N. Simoes, A. Tadeu, Heat transfer measurements of a linear thermal bridge in a wooden building corner, Energy Build. 158 (2018) 194-208

[18] G. Baldinelli, F. Bianco, A. Rotili, D. Costarelli, M. Seracini, G. Vinti, F. Asdrubali, L. evangelisti, A model for the improvement of the thermal bridges quantitative assessment by infrared thermography, Applied Energy 211 (2018) 854-864.

[19] F. Isaia, S. Fantucci, A. Capozzoli, M. Perino, Thermal bridges in vacuum insulation panels at buildings scale, Proc. of the ins. of civil engineers: engineering sustainability 170 (2017) 47-60.

[20] A. Lorenzati, S. Fantucci, A. Capozzoli, M.Perino, Experimental and numerical investigation of thermal bridging effects of jointed Vacuum Insulation Panels, Energy Build. 111 (2016) 164-175.

[21] F. Asdrubali, G. Baldinelli, F. Bianchi, A quantitative method to evaluate thermal bridges in buildings, Applied Energy 97 (2012) 365-373.

[22] L. Evangelisti, C. Guattari, F. Asdrubali, Influence of heating systems on the thermal transmittance evaluations: Simulations, experimental measurements, and data post-processing,

[23] Asdrubali F. *et al.* Detection of thermal bridges from thermographic images by means of images processing approximation, Energy Build. 168 (2018) 180-190.

[24] J. Wernery, A. Ben-Ishai, B. Binder, S. Brunner, Aerobrick – An aerogel-filled insulating brick, Procedia Eng. (2017).

[25] B. Nagy, Hydrothermal modelling of masonry blocks filled with thermal insulation, MATEC 163 (2018).

[26] E. Sassine, Z. Younsi, Y. Cherif, A. Chauchois, E. Antczak, Exprimental determination of thermal properties of brick wall for existing construction in the north of France, Journal of Buil. Eng. 14 (2017) 15-23.

[27] N.P. Avdelidis, A. Moropoulou, Emissivity considerations in building thermography, Energy Build. 35 (2003) 663-667.

[28] S. Baghero, P. Cavalletti, A. Chiari, The importance of thermal bridge correction in energy refurbishment of existing buildings, Mathematical Mod. of Eng. Problems 5(3) (2018) 197-204.

[29] J. sadauskiene, J. Ramanauskas, L. Seduikyte, M. Dauksys, A. Vasylius, A simplified methodology for evaluating the impact of point thermal bridges on the high-energy performance of a passive house, Sustainability 7(12) (2015) 16687-16702.

[30] T.G. Theodosiou, A.M. Papadopoulos, The impact of thermal bridges on the energy demand of buildings with double brick wall constructions, Energy Build. 40 (20018) 2083-2089.

[31] A. Capozzoli, A. Gorrino, V. Corrado, A building thermal bridges sensitivity analysis, Applied Energy 107 (2013) 229-243.

[32] F. Favoino, S. Fantucci, V. Serra, M. Perino, Building envelope test cell: development of an indoor test cell for advanced façade systems thermal performance assessment, Advanced building skins (2015).

[33] A. Lacarbonara, Tecniche di misura della trasmittanza termica in opera, Tesi di Laurea Magistrale, Politecnico di Torino (2018).

Annex A

A.1 1D Assembly, R_{add}=0 m^2K/W

BISCO - Input Data
BISCO data file: Assembly 1D_noadd.bsc
Bitmap file: Assembly A.1.bmp
1 pixel = 0.000165 m

Col. -	Width [pixels]	Width [m]	Height [pixels]	Height [m]	Area [pixels]	Zones	Triang.Size [pixels]
107	1540	0.2541	298	0.0492	458920	1	2
164	1540	0.2541	414	0.0683	178640	2	2
196	1540	0.2541	201	0.0332	309540	1	
249	1540	0.2541	201	0.0332	309540	1	

Col. -	Type	CEN-rule	Name	lambda [W/mK]	t [°C]	h [W/m²K]	q [W/m²]
107	MATERIAL		Mineral wool	0.033	0.033		
164	MATERIAL		Plasterboard	0.188	0.188		
196	BC_SIMPL		Lower		15.0	99999	0
249	BC_SIMPL		Upper		35.0	99999	0

BISCO Calculation Results
BISCO data file: Assembly 1D_noadd.bsc
Number of nodes = 183325
Heat flow divergence for total object = 0.000811952
Heat flow divergence for worst node = 0.0944541

Col. -	Type	Name	tmin [°C]	tmax [°C]	flow in [W/m]	flow out [W/m]
107	MATERIAL	Mineral wool	15.6	34.4		
164	MATERIAL	Plasterboard	15	35		
196	BC_SIMPL	Lower	15	15		3.193
249	BC_SIMPL	Upper	35	35	3.193	

A.2 1D Assembly, R_{add}=0.0487 m^2K/W

BISCO - Input Data

BISCO data file: Assembly 1D_redrub5.bsc

Bitmap file: Assembly 1D_redrub5.bmp

1 pixel = 0.000165 m

Col. -	Width [pixels]	Width [m]	Height [pixels]	Height [m]	Area [pixels]	Zones	Triang.Size [pixels]
0	1540	0.2541	472	0.0779	89320	2	2
107	1540	0.2541	298	0.0492	458920	1	2
164	1540	0.2541	414	0.0683	178640	2	2
196	1540	0.2541	172	0.0284	264880	1	
249	1540	0.2541	172	0.0284	264880	1	

Col. -	Type	CEN-rule	Name	lambda [W/mK]	t [°C]	h [W/m²K]	q [W/m²]
0	MATERIAL		Rubber	0.199			
107	MATERIAL		Mineral wool	0.033			
164	MATERIAL		Plasterboard	0.188			
196	BC_SIMPL	NIHIL	Lower		15.0	99999	0
249	BC_SIMPL	NIHIL	Upper		35.0	99999	0

BISCO Calculation Results

BISCO data file: Assembly 1D_redrub5.bsc

Number of nodes = 209515

Heat flow divergence for total object = 0.00074844

Heat flow divergence for worst node = 0.128942

Col. -	Type	Name	tmin [°C]	tmax [°C]	flow in [W/m]	flow out [W/m]
0	MATERIAL	Rubber	15	35		
107	MATERIAL	Mineral wool	15.914	34.086		
164	MATERIAL	Plasterboard	15.293	34.707		
196	BC_SIMPL	Lower	15	15	0	3.099
249	BC_SIMPL	Upper	35	35	3.099	0

A.3 1D Assembly, R_{add}=0.0987 m^2K/W

BISCO - Input Data

BISCO data file: Assembly 1D_redrub10.bsc

Bitmap file: Assembly 1D_redrub10.bmp

1 pixel = 0.000165 m

Col. -	Width [pixels]	Width [m]	Height [pixels]	Height [m]	Area [pixels]	Zones	Triang.Size [pixels]
0	1540	0.2541	532	0.0878	181720	2	2
107	1540	0.2541	298	0.0492	458920	1	2
164	1540	0.2541	414	0.0683	178640	2	2
196	1540	0.2541	142	0.0234	218680	1	
249	1540	0.2541	142	0.0234	218680	1	

Col. -	Type	CEN-rule	Name	lambda [W/mK]	t [°C]	h [W/m²K]	q [W/m²]
0	MATERIAL		Rubber	0.199			
107	MATERIAL		Mineral wool	0.033			
164	MATERIAL		Plasterboard	0.188			
196	BC_SIMPL	NIHIL	Lower		15.0	99999	0
249	BC_SIMPL	NIHIL	Upper		35.0	99999	0

BISCO Calculation Results

BISCO data file: Assembly 1D_redrub10.bsc

Number of nodes = 235704

Heat flow divergence for total object = 0.000969508

Heat flow divergence for worst node = 0.3012

Col. -	Type	Name	tmin [°C]	tmax [°C]	flow in [W/m]	flow out [W/m]
0	MATERIAL	Rubber	15	35		
107	MATERIAL	Mineral wool	16.181	33.819		
164	MATERIAL	Plasterboard	15.579	34.421		
196	BC_SIMPL	Lower	15	15	0	3.008
249	BC_SIMPL	Upper	35	35	3.008	0

A.4 1D Assembly, R_{add}=0.5349 m^2K/W

BISCO - Input Data

BISCO data file: Assembly 1D_blackrub.bsc

Bitmap file: Assembly 1D_blackrub.bmp

1 pixel = 0.000165 m

Col. -	Width [pixels]	Width [m]	Height [pixels]	Height [m]	Area [pixels]	Zones	Triang.Size [pixels]
0	1540	0.2541	582	0.096	258720	2	2
107	1540	0.2541	298	0.0492	458920	1	2
164	1540	0.2541	414	0.0683	178640	2	2
196	1540	0.2541	117	0.0193	180180	1	
249	1540	0.2541	117	0.0193	180180	1	

Col. -	Type	CEN-rule	Name	lambda [W/mK]	t [°C]	h [W/m²K]	q [W/m²]
0	MATERIAL		Rubber	0.052			
107	MATERIAL		Mineral wool	0.033			
164	MATERIAL		Plasterboard	0.188			
196	BC_SIMPL	NIHIL	Lower		15.0	99999	0
249	BC_SIMPL	NIHIL	Upper		35.0	99999	0

BISCO Calculation Results

BISCO data file: Assembly 1D_blackrub.bsc

Number of nodes = 257270

Heat flow divergence for total object = 0.000145379

Heat flow divergence for worst node = 0.29244

Col. -	Type	Name	tmin [°C]	tmax [°C]	flow in [W/m]	flow out [W/m]
0	MATERIAL	Rubber	15	35		
107	MATERIAL	Mineral wool	17.989	32.011		
164	MATERIAL	Plasterboard	17.51	32.49		
196	BC_SIMPL	Lower	15	15	0	2.391
249	BC_SIMPL	Upper	35	35	2.391	0

A.5 2D Assembly, R_{add}=0 m^2K/W

λ_{filler}= 0.30 W/mK

BISCO - Input Data
BISCO data file: Assembly 2D_noadd.bsc
Bitmap file: Assembly 2D_noadd.bmp
1 pixel = 0.000165 m

Col. -	Width [pixels]	Width [m]	Height [pixels]	Height [m]	Area [pixels]	Zones	Triang.Size [pixels]
107	1540	0.2541	298	0.0492	455128	2	2
164	1540	0.2541	414	0.0683	149740	4	2
196	1540	0.2541	201	0.0332	309540	1	
244	297	0.049	298	0.0492	3792	1	2
249	1540	0.2541	201	0.0332	309540	1	
251	740	0.1221	414	0.0683	28900	2	2

Col. -	Type	CEN-rule	Name	lambda [W/mK]	t [°C]	h [W/m²K]	q [W/m²]
107	MATERIAL		Mineral wool	0.033			
164	MATERIAL		Plasterboard	0.188			
196	BC_SIMPL		Lower		15.0	99999	0
244	MATERIAL		Metallic frame	52	35.0	99999	0
249	BC_SIMPL		Upper				
251	MATERIAL		Filler	0.30			

BISCO Calculation Results
BISCO data file: Assembly 2D_noadd.bsc
Number of nodes = 182994
Heat flow divergence for total object = 0.000465048
Heat flow divergence for worst node = 0.295042

Col. -	Type	Name	tmin [°C]	tmax [°C]	flow in [W/m]	flow out [W/m]
107	MATERIAL	Mineral wool	15.596	34.404		
164	MATERIAL	Plasterboard	15.000	35.000		
196	BC_SIMPL	Lower	15.000	15.001	0.000	8.230
244	MATERIAL	Metallic frame	18.303	31.698		
249	BC_SIMPL	Upper	34.999	35.000	8.230	0.000
251	MATERIAL	Filler	15.000	35.000		

λ_{filler}= 0.27 W/mK

BISCO - Input Data

BISCO data file: Assembly 2D_noadd.bsc
Bitmap file: Assembly 2D_noadd.bmp
1 pixel = 0.000165 m

Col. -	Width [pixels]	Width [m]	Height [pixels]	Height [m]	Area [pixels]	Zones	Triang.Size [pixels]
107	1540	0.2541	298	0.0492	455128	2	2
164	1540	0.2541	414	0.0683	149740	4	2
196	1540	0.2541	201	0.0332	309540	1	
244	297	0.049	298	0.0492	3792	1	2
249	1540	0.2541	201	0.0332	309540	1	
251	740	0.1221	414	0.0683	28900	2	2

Col. -	Type	CEN-rule	Name	lambda [W/mK]	t [°C]	h [W/m²K]	q [W/m²]
107	MATERIAL		Mineral wool	0.033			
164	MATERIAL		Plasterboard	0.188			
196	BC_SIMPL		Lower		15.0	99999	0
244	MATERIAL		Metallic frame	52	35.0	99999	0
249	BC_SIMPL		Upper				
251	MATERIAL		Filler	0.27			

BISCO Calculation Results

BISCO data file: Assembly 2D_noadd.bsc
Number of nodes = 182994
Heat flow divergence for total object = 0.000544548
Heat flow divergence for worst node = 0.314317

Col. -	Type	Name	tmin [°C]	tmax [°C]	flow in [W/m]	flow out [W/m]
107	MATERIAL	Mineral wool	15.609	34.391		
164	MATERIAL	Plasterboard	15.000	35.000		
196	BC_SIMPL	Lower	15.000	15.001	0.000	8.162
244	MATERIAL	Metallic frame	18.371	31.630		
249	BC_SIMPL	Upper	34.999	35.000	8.162	0.000
251	MATERIAL	Filler	15.000	35.000		

λ_{filler}= 0.24 W/mK

BISCO - Input Data
BISCO data file: Assembly 2D_noadd.bsc
Bitmap file: Assembly 2D_noadd.bmp
1 pixel = 0.000165 m

Col. -	Width [pixels]	Width [m]	Height [pixels]	Height [m]	Area [pixels]	Zones	Triang.Size [pixels]
107	1540	0.2541	298	0.0492	455128	2	2
164	1540	0.2541	414	0.0683	149740	4	2
196	1540	0.2541	201	0.0332	309540	1	
244	297	0.049	298	0.0492	3792	1	2
249	1540	0.2541	201	0.0332	309540	1	
251	740	0.1221	414	0.0683	28900	2	2

Col. -	Type	CEN-rule	Name	lambda [W/mK]	t [°C]	h [W/m²K]	q [W/m²]
107	MATERIAL		Mineral wool	0.033			
164	MATERIAL		Plasterboard	0.188			
196	BC_SIMPL		Lower		15.0	99999	0
244	MATERIAL		Metallic frame	52	35.0	99999	0
249	BC_SIMPL		Upper				
251	MATERIAL		Filler	0.24			

BISCO Calculation Results
BISCO data file: Assembly 2D_noadd.bsc
Number of nodes = 182994
Heat flow divergence for total object = 0.000908489
Heat flow divergence for worst node = 0.318564

Col. -	Type	Name	tmin [°C]	tmax [°C]	flow in [W/m]	flow out [W/m]
107	MATERIAL	Mineral wool	15.624	34.376		
164	MATERIAL	Plasterboard	15.000	35.000		
196	BC_SIMPL	Lower	15.000	15.001	0.000	8.081
244	MATERIAL	Metallic frame	18.451	31.549		
249	BC_SIMPL	Upper	34.999	35.000	8.081	0.000
251	MATERIAL	Filler	15.000	35.000		

λ_{filler}= 0.21 W/mK

BISCO - Input Data
BISCO data file: Assembly 2D_noadd.bsc
Bitmap file: Assembly 2D_noadd.bmp
1 pixel = 0.000165 m

Col. -	Width [pixels]	Width [m]	Height [pixels]	Height [m]	Area [pixels]	Zones	Triang.Size [pixels]
107	1540	0.2541	298	0.0492	455128	2	2
164	1540	0.2541	414	0.0683	149740	4	2
196	1540	0.2541	201	0.0332	309540	1	
244	297	0.049	298	0.0492	3792	1	2
249	1540	0.2541	201	0.0332	309540	1	
251	740	0.1221	414	0.0683	28900	2	2

Col. -	Type	CEN-rule	Name	lambda [W/mK]	t [°C]	h [W/m²K]	q [W/m²]
107	MATERIAL		Mineral wool	0.033			
164	MATERIAL		Plasterboard	0.188			
196	BC_SIMPL		Lower		15.0	99999	0
244	MATERIAL		Metallic frame	52	35.0	99999	0
249	BC_SIMPL		Upper				
251	MATERIAL		Filler	0.21			

BISCO Calculation Results
BISCO data file: Assembly 2D_noadd.bsc
Number of nodes = 182994
Heat flow divergence for total object = 0.000279072
Heat flow divergence for worst node = 0.374013

Col. -	Type	Name	tmin [°C]	tmax [°C]	flow in [W/m]	flow out [W/m]
107	MATERIAL	Mineral wool	15.639	34.361		
164	MATERIAL	Plasterboard	15.000	35.000		
196	BC_SIMPL	Lower	15.000	15.001	0.000	7.983
244	MATERIAL	Metallic frame	18.550	31.451		
249	BC_SIMPL	Upper	34.999	35.000	7.983	0.000
251	MATERIAL	Filler	15.000	35.000		

λ_{filler}= 0.18 W/mK

BISCO - Input Data

BISCO data file: Assembly 2D_noadd.bsc

Bitmap file: Assembly 2D_noadd.bmp

1 pixel = 0.000165 m

Col. -	Width [pixels]	Width [m]	Height [pixels]	Height [m]	Area [pixels]	Zones	Triang.Size [pixels]
107	1540	0.2541	298	0.0492	455128	2	2
164	1540	0.2541	414	0.0683	149740	4	2
196	1540	0.2541	201	0.0332	309540	1	
244	297	0.049	298	0.0492	3792	1	2
249	1540	0.2541	201	0.0332	309540	1	
251	740	0.1221	414	0.0683	28900	2	2

Col. -	Type	CEN-rule	Name	lambda [W/mK]	t [°C]	h [W/m²K]	q [W/m²]
107	MATERIAL		Mineral wool	0.033			
164	MATERIAL		Plasterboard	0.188			
196	BC_SIMPL		Lower		15.0	99999	0
244	MATERIAL		Metallic frame	52	35.0	99999	0
249	BC_SIMPL		Upper				
251	MATERIAL		Filler	0.18			

BISCO Calculation Results

BISCO data file: Assembly 2D_noadd.bsc

Number of nodes = 182994

Heat flow divergence for total object = 0.000270919

Heat flow divergence for worst node = 0.197423

Col. -	Type	Name	tmin [°C]	tmax [°C]	flow in [W/m]	flow out [W/m]
107	MATERIAL	Mineral wool	15.640	34.360		
164	MATERIAL	Plasterboard	15.000	35.000		
196	BC_SIMPL	Lower	15.000	15.001	0.000	7.859
244	MATERIAL	Metallic frame	18.674	31.326		
249	BC_SIMPL	Upper	34.999	35.000	7.859	0.000
251	MATERIAL	Filler	15.000	35.000		

λ_{filler}= 0.15 W/mK

BISCO - Input Data

BISCO data file: Assembly 2D_noadd.bsc
Bitmap file: Assembly 2D_noadd.bmp
1 pixel = 0.000165 m

Col. -	Width [pixels]	Width [m]	Height [pixels]	Height [m]	Area [pixels]	Zones	Triang.Size [pixels]
107	1540	0.2541	298	0.0492	455128	2	2
164	1540	0.2541	414	0.0683	149740	4	2
196	1540	0.2541	201	0.0332	309540	1	
244	297	0.049	298	0.0492	3792	1	2
249	1540	0.2541	201	0.0332	309540	1	
251	740	0.1221	414	0.0683	28900	2	2

Col. -	Type	CEN-rule	Name	lambda [W/mK]	t [°C]	h [W/m²K]	q [W/m²]
107	MATERIAL		Mineral wool	0.033			
164	MATERIAL		Plasterboard	0.188			
196	BC_SIMPL		Lower		15.0	99999	0
244	MATERIAL		Metallic frame	52	35.0	99999	0
249	BC_SIMPL		Upper				
251	MATERIAL		Filler	0.15			

BISCO Calculation Results

BISCO data file: Assembly 2D_noadd.bsc
Number of nodes = 182994
Heat flow divergence for total object = 0.000583279
Heat flow divergence for worst node = 0.994232

Col. -	Type	Name	tmin [°C]	tmax [°C]	flow in [W/m]	flow out [W/m]
107	MATERIAL	Mineral wool	15.640	34.361		
164	MATERIAL	Plasterboard	15.000	35.000		
196	BC_SIMPL	Lower	15.000	15.001	0.000	7.699
244	MATERIAL	Metallic frame	18.837	31.164		
249	BC_SIMPL	Upper	34.999	35.000	7.699	0.000
251	MATERIAL	Filler	15.000	35.000		

λ_{filler}= 0.12 W/mK

BISCO - Input Data
BISCO data file: Assembly 2D_noadd.bsc
Bitmap file: Assembly 2D_noadd.bmp
1 pixel = 0.000165 m

Col. -	Width [pixels]	Width [m]	Height [pixels]	Height [m]	Area [pixels]	Zones	Triang.Size [pixels]
107	1540	0.2541	298	0.0492	455128	2	2
164	1540	0.2541	414	0.0683	149740	4	2
196	1540	0.2541	201	0.0332	309540	1	
244	297	0.049	298	0.0492	3792	1	2
249	1540	0.2541	201	0.0332	309540	1	
251	740	0.1221	414	0.0683	28900	2	2

Col. -	Type	CEN-rule	Name	lambda [W/mK]	t [°C]	h [W/m²K]	q [W/m²]
107	MATERIAL		Mineral wool	0.033			
164	MATERIAL		Plasterboard	0.188			
196	BC_SIMPL		Lower		15.0	99999	0
244	MATERIAL		Metallic frame	52	35.0	99999	0
249	BC_SIMPL		Upper				
251	MATERIAL		Filler	0.12			

BISCO Calculation Results
BISCO data file: Assembly 2D_noadd.bsc
Number of nodes = 182994
Heat flow divergence for total object = 0.000200489
Heat flow divergence for worst node = 0.105215

Col. -	Type	Name	tmin [°C]	tmax [°C]	flow in [W/m]	flow out [W/m]
107	MATERIAL	Mineral wool	15.640	34.360		
164	MATERIAL	Plasterboard	15.000	35.000		
196	BC_SIMPL	Lower	15.000	15.001	0.000	7.480
244	MATERIAL	Metallic frame	19.059	30.942		
249	BC_SIMPL	Upper	34.999	35.000	7.480	0.000
251	MATERIAL	Filler	15.000	35.000		

λ_{filler}= 0.09 W/mK

BISCO - Input Data
BISCO data file: Assembly 2D_noadd.bsc
Bitmap file: Assembly 2D_noadd.bmp
1 pixel = 0.000165 m

Col. -	Width [pixels]	Width [m]	Height [pixels]	Height [m]	Area [pixels]	Zones	Triang.Size [pixels]
107	1540	0.2541	298	0.0492	455128	2	2
164	1540	0.2541	414	0.0683	149740	4	2
196	1540	0.2541	201	0.0332	309540	1	
244	297	0.049	298	0.0492	3792	1	2
249	1540	0.2541	201	0.0332	309540	1	
251	740	0.1221	414	0.0683	28900	2	2

Col. -	Type	CEN-rule	Name	lambda [W/mK]	t [°C]	h [W/m²K]	q [W/m²]
107	MATERIAL		Mineral wool	0.033			
164	MATERIAL		Plasterboard	0.188			
196	BC_SIMPL		Lower		15.0	99999	0
244	MATERIAL		Metallic frame	52	35.0	99999	0
249	BC_SIMPL		Upper				
251	MATERIAL		Filler	0.09			

BISCO Calculation Results
BISCO data file: Assembly 2D_noadd.bsc
Number of nodes = 182994
Heat flow divergence for total object = 0.00087301
Heat flow divergence for worst node = 0.342445

Col. -	Type	Name	tmin [°C]	tmax [°C]	flow in [W/m]	flow out [W/m]
107	MATERIAL	Mineral wool	15.640	34.360		
164	MATERIAL	Plasterboard	15.000	35.000		
196	BC_SIMPL	Lower	15.000	15.001	0.000	7.162
244	MATERIAL	Metallic frame	19.387	30.614		
249	BC_SIMPL	Upper	34.999	35.000	7.162	0.000
251	MATERIAL	Filler	15.000	35.000		

λ_{filler}= 0.06 W/mK

BISCO - Input Data

BISCO data file: Assembly 2D_noadd.bsc

Bitmap file: Assembly 2D_noadd.bmp

1 pixel = 0.000165 m

Col. -	Width [pixels]	Width [m]	Height [pixels]	Height [m]	Area [pixels]	Zones	Triang.Size [pixels]
107	1540	0.2541	298	0.0492	455128	2	2
164	1540	0.2541	414	0.0683	149740	4	2
196	1540	0.2541	201	0.0332	309540	1	
244	297	0.049	298	0.0492	3792	1	2
249	1540	0.2541	201	0.0332	309540	1	
251	740	0.1221	414	0.0683	28900	2	2

Col. -	Type	CEN-rule	Name	lambda [W/mK]	t [°C]	h [W/m²K]	q [W/m²]
107	MATERIAL		Mineral wool	0.033			
164	MATERIAL		Plasterboard	0.188			
196	BC_SIMPL		Lower		15.0	99999	0
244	MATERIAL		Metallic frame	52	35.0	99999	0
249	BC_SIMPL		Upper				
251	MATERIAL		Filler	0.06			

BISCO Calculation Results

BISCO data file: Assembly 2D_noadd.bsc

Number of nodes = 182994

Heat flow divergence for total object = 0.00088597

Heat flow divergence for worst node = 0.666546

Col. -	Type	Name	tmin [°C]	tmax [°C]	flow in [W/m]	flow out [W/m]
107	MATERIAL	Mineral wool	15.640	34.360		
164	MATERIAL	Plasterboard	15.000	35.000		
196	BC_SIMPL	Lower	15.000	15.001	0.000	6.646
244	MATERIAL	Metallic frame	19.925	30.076		
249	BC_SIMPL	Upper	34.999	35.000	6.646	0.000
251	MATERIAL	Filler	15.000	35.000		

λ_{filler}= 0.03 W/mK

BISCO - Input Data

BISCO data file: Assembly 2D_noadd.bsc
Bitmap file: Assembly 2D_noadd.bmp
1 pixel = 0.000165 m

Col. -	Width [pixels]	Width [m]	Height [pixels]	Height [m]	Area [pixels]	Zones	Triang.Size [pixels]
107	1540	0.2541	298	0.0492	455128	2	2
164	1540	0.2541	414	0.0683	149740	4	2
196	1540	0.2541	201	0.0332	309540	1	
244	297	0.049	298	0.0492	3792	1	2
249	1540	0.2541	201	0.0332	309540	1	
251	740	0.1221	414	0.0683	28900	2	2

Col. -	Type	CEN-rule	Name	lambda [W/mK]	t [°C]	h [W/m²K]	q [W/m²]
107	MATERIAL		Mineral wool	0.033			
164	MATERIAL		Plasterboard	0.188			
196	BC_SIMPL		Lower		15.0	99999	0
244	MATERIAL		Metallic frame	52	35.0	99999	0
249	BC_SIMPL		Upper				
251	MATERIAL		Filler	0.03			

BISCO Calculation Results

BISCO data file: Assembly 2D_noadd.bsc
Number of nodes = 182994
Heat flow divergence for total object = 0.000116877
Heat flow divergence for worst node = 0.711192

-	Type	Name	tmin [°C]	tmax [°C]	flow in [W/m]	flow out [W/m]
107	MATERIAL	Mineral wool	15.640	34.360		
164	MATERIAL	Plasterboard	15.000	35.000		
196	BC_SIMPL	Lower	15.000	15.000	0.000	5.635
244	MATERIAL	Metallic frame	20.995	29.006		
249	BC_SIMPL	Upper	35.000	35.000	5.635	0.000
251	MATERIAL	Filler	15.000	35.000		

A.6 2D Assembly, R_{add}=0.0487 m^{2}K/W

λ_{filler}= 0.30 W/mK

BISCO - Input Data

BISCO data file: Assembly 2D_redrub5.bsc

Bitmap file: Assembly 2D_redrub5.bmp

1 pixel = 0.000165 m

Col. -	Width [pixels]	Width [m]	Height [pixels]	Height [m]	Area [pixels]	Zones	Triang.Size [pixels]
0	1540	0.2541	472	0.0779	89320	2	2
107	1540	0.2541	298	0.0492	455128	2	2
164	1540	0.2541	414	0.0683	149740	4	2
196	1540	0.2541	172	0.0284	264880	1	
244	297	0.049	298	0.0492	3792	1	2
249	1540	0.2541	172	0.0284	264880	1	
251	740	0.1221	414	0.0683	28900	2	2

Col. -	Type	CEN-rule	Name	lambda [W/mK]	t [°C]	h [W/m²K]	q [W/m²]
0	MATERIAL		Rubber	0.199			
107	MATERIAL		Mineral wool	0.033			
164	MATERIAL		Plasterboard	0.188			
196	BC_SIMPL		Lower		15.0	99999	0
244	MATERIAL		Metallic frame	52	35.0	99999	0
249	BC_SIMPL		Upper				
251	MATERIAL		Filler	0.30			

BISCO Calculation Results

BISCO data file: Assembly 2D_redrub5.bsc

Number of nodes = 209184

Heat flow divergence for total object = 0.00072669

Heat flow divergence for worst node = 0.115979

Col. -	Type	Name	tmin [°C]	tmax [°C]	flow in [W/m]	flow out [W/m]
0	MATERIAL	Rubber	15.000	35.000		
107	MATERIAL	Mineral wool	15.915	34.086		
164	MATERIAL	Plasterboard	15.294	34.706		
196	BC_SIMPL	Lower	15.000	15.001	0.000	7.183
244	MATERIAL	Metallic frame	19.314	30.687		
249	BC_SIMPL	Upper	34.999	35.000	7.183	0.000
251	MATERIAL	Filler	15.323	34.678		

λ_{filler}= 0.27 W/mK

BISCO - Input Data

BISCO data file: Assembly 2D_redrub5.bsc

Bitmap file: Assembly 2D_redrub5.bmp

1 pixel = 0.000165 m

Col. -	Width [pixels]	Width [m]	Height [pixels]	Height [m]	Area [pixels]	Zones	Triang.Size [pixels]
0	1540	0.2541	472	0.0779	89320	2	2
107	1540	0.2541	298	0.0492	455128	2	2
164	1540	0.2541	414	0.0683	149740	4	2
196	1540	0.2541	172	0.0284	264880	1	
244	297	0.049	298	0.0492	3792	1	2
249	1540	0.2541	172	0.0284	264880	1	
251	740	0.1221	414	0.0683	28900	2	2

Col. -	Type	CEN-rule	Name	lambda [W/mK]	t [°C]	h [W/m²K]	q [W/m²]
0	MATERIAL		Rubber	0.199			
107	MATERIAL		Mineral wool	0.033			
164	MATERIAL		Plasterboard	0.188			
196	BC_SIMPL		Lower		15.0	99999	0
244	MATERIAL		Metallic frame	52	35.0	99999	0
249	BC_SIMPL		Upper				
251	MATERIAL		Filler	0.27			

BISCO Calculation Results

BISCO data file: Assembly 2D_redrub5.bsc

Number of nodes = 209184

Heat flow divergence for total object = 0.000871356

Heat flow divergence for worst node = 0.118656

Col. -	Type	Name	tmin [°C]	tmax [°C]	flow in [W/m]	flow out [W/m]
0	MATERIAL	Rubber	15.000	35.000		
107	MATERIAL	Mineral wool	15.915	34.086		
164	MATERIAL	Plasterboard	15.294	34.706		
196	BC_SIMPL	Lower	15.000	15.001	0.000	7.137
244	MATERIAL	Metallic frame	19.361	30.640		
249	BC_SIMPL	Upper	34.999	35.000	7.137	0.000
251	MATERIAL	Filler	15.321	34.679		

λ_{filler}= 0.24 W/mK

BISCO - Input Data

BISCO data file: Assembly 2D_redrub5.bsc

Bitmap file: Assembly 2D_redrub5.bmp

1 pixel = 0.000165 m

Col. -	Width [pixels]	Width [m]	Height [pixels]	Height [m]	Area [pixels]	Zones	Triang.Size [pixels]
0	1540	0.2541	472	0.0779	89320	2	2
107	1540	0.2541	298	0.0492	455128	2	2
164	1540	0.2541	414	0.0683	149740	4	2
196	1540	0.2541	172	0.0284	264880	1	
244	297	0.049	298	0.0492	3792	1	2
249	1540	0.2541	172	0.0284	264880	1	
251	740	0.1221	414	0.0683	28900	2	2

Col. -	Type	CEN-rule	Name	lambda [W/mK]	t [°C]	h [W/m²K]	q [W/m²]
0	MATERIAL		Rubber	0.199			
107	MATERIAL		Mineral wool	0.033			
164	MATERIAL		Plasterboard	0.188			
196	BC_SIMPL		Lower		15.0	99999	0
244	MATERIAL		Metallic frame	52	35.0	99999	0
249	BC_SIMPL		Upper				
251	MATERIAL		Filler	0.24			

BISCO Calculation Results

BISCO data file: Assembly 2D_redrub5.bsc

Number of nodes = 209184

Heat flow divergence for total object = 0.000934147

Heat flow divergence for worst node = 0.165955

Col. -	Type	Name	tmin [°C]	tmax [°C]	flow in [W/m]	flow out [W/m]
0	MATERIAL	Rubber	15.000	35.000		
107	MATERIAL	Mineral wool	15.915	34.086		
164	MATERIAL	Plasterboard	15.294	34.706		
196	BC_SIMPL	Lower	15.000	15.001	0.000	7.083
244	MATERIAL	Metallic frame	19.418	30.583		
249	BC_SIMPL	Upper	34.999	35.000	7.083	0.000
251	MATERIAL	Filler	15.320	34.680		

λ_{filler}= 0.21 W/mK

BISCO - Input Data

BISCO data file: Assembly 2D_redrub5.bsc

Bitmap file: Assembly 2D_redrub5.bmp

1 pixel = 0.000165 m

Col. -	Width [pixels]	Width [m]	Height [pixels]	Height [m]	Area [pixels]	Zones	Triang.Size [pixels]
0	1540	0.2541	472	0.0779	89320	2	2
107	1540	0.2541	298	0.0492	455128	2	2
164	1540	0.2541	414	0.0683	149740	4	2
196	1540	0.2541	172	0.0284	264880	1	
244	297	0.049	298	0.0492	3792	1	2
249	1540	0.2541	172	0.0284	264880	1	
251	740	0.1221	414	0.0683	28900	2	2

Col. -	Type	CEN-rule	Name	lambda [W/mK]	t [°C]	h [W/m²K]	q [W/m²]
0	MATERIAL		Rubber	0.199			
107	MATERIAL		Mineral wool	0.033			
164	MATERIAL		Plasterboard	0.188			
196	BC_SIMPL		Lower		15.0	99999	0
244	MATERIAL		Metallic frame	52	35.0	99999	0
249	BC_SIMPL		Upper				
251	MATERIAL		Filler	0.21			

BISCO Calculation Results

BISCO data file: Assembly 2D_redrub5.bsc

Number of nodes = 209184

Heat flow divergence for total object = 5.32922e-005

Heat flow divergence for worst node = 0.187202

Col. -	Type	Name	tmin [°C]	tmax [°C]	flow in [W/m]	flow out [W/m]
0	MATERIAL	Rubber	15.000	35.000		
107	MATERIAL	Mineral wool	15.915	34.086		
164	MATERIAL	Plasterboard	15.294	34.706		
196	BC_SIMPL	Lower	15.000	15.001	0.000	7.016
244	MATERIAL	Metallic frame	19.487	30.514		
249	BC_SIMPL	Upper	34.999	35.000	7.016	0.000
251	MATERIAL	Filler	15.319	34.681		

λ_{filler}= 0.18 W/mK

BISCO - Input Data

BISCO data file: Assembly 2D_redrub5.bsc

Bitmap file: Assembly 2D_redrub5.bmp

1 pixel = 0.000165 m

Col. -	Width [pixels]	Width [m]	Height [pixels]	Height [m]	Area [pixels]	Zones	Triang.Size [pixels]
0	1540	0.2541	472	0.0779	89320	2	2
107	1540	0.2541	298	0.0492	455128	2	2
164	1540	0.2541	414	0.0683	149740	4	2
196	1540	0.2541	172	0.0284	264880	1	
244	297	0.049	298	0.0492	3792	1	2
249	1540	0.2541	172	0.0284	264880	1	
251	740	0.1221	414	0.0683	28900	2	2

Col. -	Type	CEN-rule	Name	lambda [W/mK]	t [°C]	h [W/m²K]	q [W/m²]
0	MATERIAL		Rubber	0.199			
107	MATERIAL		Mineral wool	0.033			
164	MATERIAL		Plasterboard	0.188			
196	BC_SIMPL		Lower		15.0	99999	0
244	MATERIAL		Metallic frame	52	35.0	99999	0
249	BC_SIMPL		Upper				
251	MATERIAL		Filler	0.18			

BISCO Calculation Results

BISCO data file: Assembly 2D_redrub5.bsc

Number of nodes = 209184

Heat flow divergence for total object = 0.000228166

Heat flow divergence for worst node = 0.61078

Col. -	Type	Name	tmin [°C]	tmax [°C]	flow in [W/m]	flow out [W/m]
0	MATERIAL	Rubber	15.000	35.000		
107	MATERIAL	Mineral wool	15.915	34.085		
164	MATERIAL	Plasterboard	15.294	34.706		
196	BC_SIMPL	Lower	15.000	15.001	0.000	6.932
244	MATERIAL	Metallic frame	19.574	30.427		
249	BC_SIMPL	Upper	34.999	35.000	6.932	0.000
251	MATERIAL	Filler	15.318	34.682		

λ_{filler}= 0.15 W/mK

BISCO - Input Data

BISCO data file: Assembly 2D_redrub5.bsc

Bitmap file: Assembly 2D_redrub5.bmp

1 pixel = 0.000165 m

Col. -	Width [pixels]	Width [m]	Height [pixels]	Height [m]	Area [pixels]	Zones	Triang.Size [pixels]
0	1540	0.2541	472	0.0779	89320	2	2
107	1540	0.2541	298	0.0492	455128	2	2
164	1540	0.2541	414	0.0683	149740	4	2
196	1540	0.2541	172	0.0284	264880	1	
244	297	0.049	298	0.0492	3792	1	2
249	1540	0.2541	172	0.0284	264880	1	
251	740	0.1221	414	0.0683	28900	2	2

Col. -	Type	CEN-rule	Name	lambda [W/mK]	t [°C]	h [W/m²K]	q [W/m²]
0	MATERIAL		Rubber	0.199			
107	MATERIAL		Mineral wool	0.033			
164	MATERIAL		Plasterboard	0.188			
196	BC_SIMPL		Lower		15.0	99999	0
244	MATERIAL		Metallic frame	52	35.0	99999	0
249	BC_SIMPL		Upper				
251	MATERIAL		Filler	0.15			

BISCO Calculation Results

BISCO data file: Assembly 2D_redrub5.bsc

Number of nodes = 209184

Heat flow divergence for total object = 8.97944e-005

Heat flow divergence for worst node = 0.762114

Col. -	Type	Name	tmin [°C]	tmax [°C]	flow in [W/m]	flow out [W/m]
0	MATERIAL	Rubber	15.000	35.000		
107	MATERIAL	Mineral wool	15.915	34.085		
164	MATERIAL	Plasterboard	15.294	34.706		
196	BC_SIMPL	Lower	15.000	15.001	0.000	6.821
244	MATERIAL	Metallic frame	19.688	30.313		
249	BC_SIMPL	Upper	34.999	35.000	6.821	0.000
251	MATERIAL	Filler	15.317	34.683		

λ_{filler}= 0.12 W/mK

BISCO - Input Data

BISCO data file: Assembly 2D_redrub5.bsc
Bitmap file: Assembly 2D_redrub5.bmp
1 pixel = 0.000165 m

Col. -	Width [pixels]	Width [m]	Height [pixels]	Height [m]	Area [pixels]	Zones	Triang.Size [pixels]
0	1540	0.2541	472	0.0779	89320	2	2
107	1540	0.2541	298	0.0492	455128	2	2
164	1540	0.2541	414	0.0683	149740	4	2
196	1540	0.2541	172	0.0284	264880	1	
244	297	0.049	298	0.0492	3792	1	2
249	1540	0.2541	172	0.0284	264880	1	
251	740	0.1221	414	0.0683	28900	2	2

Col. -	Type	CEN-rule	Name	lambda [W/mK]	t [°C]	h [W/m²K]	q [W/m²]
0	MATERIAL		Rubber	0.199			
107	MATERIAL		Mineral wool	0.033			
164	MATERIAL		Plasterboard	0.188			
196	BC_SIMPL		Lower		15.0	99999	0
244	MATERIAL		Metallic frame	52	35.0	99999	0
249	BC_SIMPL		Upper				
251	MATERIAL		Filler	0.12			

BISCO Calculation Results

BISCO data file: Assembly 2D_redrub5.bsc
Number of nodes = 209184
Heat flow divergence for total object = 0.000416938
Heat flow divergence for worst node = 0.210255

Col. -	Type	Name	tmin [°C]	tmax [°C]	flow in [W/m]	flow out [W/m]
0	MATERIAL	Rubber	15.000	35.000		
107	MATERIAL	Mineral wool	15.915	34.085		
164	MATERIAL	Plasterboard	15.294	34.706		
196	BC_SIMPL	Lower	15.000	15.001	0.000	6.668
244	MATERIAL	Metallic frame	19.847	30.154		
249	BC_SIMPL	Upper	34.999	35.000	6.668	0.000
251	MATERIAL	Filler	15.312	34.688		

λ_{filler}= 0.09 W/mK

BISCO - Input Data

BISCO data file: Assembly 2D_redrub5.bsc

Bitmap file: Assembly 2D_redrub5.bmp

1 pixel = 0.000165 m

Col. -	Width [pixels]	Width [m]	Height [pixels]	Height [m]	Area [pixels]	Zones	Triang.Size [pixels]
0	1540	0.2541	472	0.0779	89320	2	2
107	1540	0.2541	298	0.0492	455128	2	2
164	1540	0.2541	414	0.0683	149740	4	2
196	1540	0.2541	172	0.0284	264880	1	
244	297	0.049	298	0.0492	3792	1	2
249	1540	0.2541	172	0.0284	264880	1	
251	740	0.1221	414	0.0683	28900	2	2

Col. -	Type	CEN-rule	Name	lambda [W/mK]	t [°C]	h [W/m²K]	q [W/m²]
0	MATERIAL		Rubber	0.199			
107	MATERIAL		Mineral wool	0.033			
164	MATERIAL		Plasterboard	0.188			
196	BC_SIMPL		Lower		15.0	99999	0
244	MATERIAL		Metallic frame	52	35.0	99999	0
249	BC_SIMPL		Upper				
251	MATERIAL		Filler	0.09			

BISCO Calculation Results

BISCO data file: Assembly 2D_redrub5.bsc

Number of nodes = 209184

Heat flow divergence for total object = 0.000709654

Heat flow divergence for worst node = 0.099608

Col. -	Type	Name	tmin [°C]	tmax [°C]	flow in [W/m]	flow out [W/m]
0	MATERIAL	Rubber	15.000	35.000		
107	MATERIAL	Mineral wool	15.915	34.085		
164	MATERIAL	Plasterboard	15.294	34.706		
196	BC_SIMPL	Lower	15.000	15.001	0.000	6.440
244	MATERIAL	Metallic frame	20.085	29.916		
249	BC_SIMPL	Upper	34.999	35.000	6.440	0.000
251	MATERIAL	Filler	15.305	34.695		

λ_{filler}= 0.06 W/mK

BISCO - Input Data

BISCO data file: Assembly 2D_redrub5.bsc

Bitmap file: Assembly 2D_redrub5.bmp

1 pixel = 0.000165 m

Col. -	Width [pixels]	Width [m]	Height [pixels]	Height [m]	Area [pixels]	Zones	Triang.Size [pixels]
0	1540	0.2541	472	0.0779	89320	2	2
107	1540	0.2541	298	0.0492	455128	2	2
164	1540	0.2541	414	0.0683	149740	4	2
196	1540	0.2541	172	0.0284	264880	1	
244	297	0.049	298	0.0492	3792	1	2
249	1540	0.2541	172	0.0284	264880	1	
251	740	0.1221	414	0.0683	28900	2	2

Col. -	Type	CEN-rule	Name	lambda [W/mK]	t [°C]	h [W/m²K]	q [W/m²]
0	MATERIAL		Rubber	0.199			
107	MATERIAL		Mineral wool	0.033			
164	MATERIAL		Plasterboard	0.188			
196	BC_SIMPL		Lower		15.0	99999	0
244	MATERIAL		Metallic frame	52	35.0	99999	0
249	BC_SIMPL		Upper				
251	MATERIAL		Filler	0.06			

BISCO Calculation Results

BISCO data file: Assembly 2D_redrub5.bsc

Number of nodes = 235373

Heat flow divergence for total object = 0.000448399

Heat flow divergence for worst node = 0.327272

Col. -	Type	Name	tmin [°C]	tmax [°C]	flow in [W/m]	flow out [W/m]
0	MATERIAL	Rubber	15.000	35.000		
107	MATERIAL	Mineral wool	15.915	34.085		
164	MATERIAL	Plasterboard	15.294	34.706		
196	BC_SIMPL	Lower	15.000	15.001	0.000	6.057
244	MATERIAL	Metallic frame	20.487	29.514		
249	BC_SIMPL	Upper	34.999	35.000	6.057	0.000
251	MATERIAL	Filler	15.294	34.706		

λ_{filler}= 0.03 W/mK

BISCO - Input Data

BISCO data file: Assembly 2D_redrub5.bsc

Bitmap file: Assembly 2D_redrub5.bmp

1 pixel = 0.000165 m

Col. -	Width [pixels]	Width [m]	Height [pixels]	Height [m]	Area [pixels]	Zones	Triang.Size [pixels]
0	1540	0.2541	472	0.0779	89320	2	2
107	1540	0.2541	298	0.0492	455128	2	2
164	1540	0.2541	414	0.0683	149740	4	2
196	1540	0.2541	172	0.0284	264880	1	
244	297	0.049	298	0.0492	3792	1	2
249	1540	0.2541	172	0.0284	264880	1	
251	740	0.1221	414	0.0683	28900	2	2

Col. -	Type	CEN-rule	Name	lambda [W/mK]	t [°C]	h [W/m²K]	q [W/m²]
0	MATERIAL		Rubber	0.199			
107	MATERIAL		Mineral wool	0.033			
164	MATERIAL		Plasterboard	0.188			
196	BC_SIMPL		Lower		15.0	99999	0
244	MATERIAL		Metallic frame	52	35.0	99999	0
249	BC_SIMPL		Upper				
251	MATERIAL		Filler	0.03			

BISCO Calculation Results

BISCO data file: Assembly 2D_redrub5.bsc

Number of nodes = 209184

Heat flow divergence for total object = 0.000865252

Heat flow divergence for worst node = 0.188001

Col. -	Type	Name	tmin [°C]	tmax [°C]	flow in [W/m]	flow out [W/m]
0	MATERIAL	Rubber	15.000	35.000		
107	MATERIAL	Mineral wool	15.916	34.084		
164	MATERIAL	Plasterboard	15.294	34.706		
196	BC_SIMPL	Lower	15.000	15.000	0.000	5.261
244	MATERIAL	Metallic frame	21.330	28.670		
249	BC_SIMPL	Upper	35.000	35.000	5.261	0.000
251	MATERIAL	Filler	15.269	34.731		

A.7 2D Assembly, R_{add}=0.0987 m^2K/W

λ_{filler}= 0.30 W/mK

BISCO - Input Data

BISCO data file: Assembly 2D_redrub10.bsc

Bitmap file: Assembly 2D_redrub10.bmp

1 pixel = 0.000165 m

Col. -	Width [pixels]	Width [m]	Height [pixels]	Height [m]	Area [pixels]	Zones	Triang.Size [pixels]
0	1540	0.2541	532	0.0878	181720	2	2
107	1540	0.2541	298	0.0492	455128	2	2
164	1540	0.2541	414	0.0683	149740	4	2
196	1540	0.2541	142	0.0234	218680	1	
244	297	0.049	298	0.0492	3792	1	2
249	1540	0.2541	142	0.0234	218680	1	
251	740	0.1221	414	0.0683	28900	2	2

Col. -	Type	CEN-rule	Name	lambda [W/mK]	t [°C]	h [W/m²K]	q [W/m²]
0	MATERIAL		Rubber	0.199			
107	MATERIAL		Mineral wool	0.033			
164	MATERIAL		Plasterboard	0.188			
196	BC_SIMPL		Lower		15.0	99999	0
244	MATERIAL		Metallic frame	52	35.0	99999	0
249	BC_SIMPL		Upper				
251	MATERIAL		Filler	0.30			

BISCO Calculation Results

BISCO data file: Assembly 2D_redrub10.bsc

Number of nodes = 235373

Heat flow divergence for total object = 1.76634e-006

Heat flow divergence for worst node = 0.262851

Col. -	Type	Name	tmin [°C]	tmax [°C]	flow in [W/m]	flow out [W/m]
0	MATERIAL	Rubber	15.000	35.000		
107	MATERIAL	Mineral wool	16.183	33.817		
164	MATERIAL	Plasterboard	15.580	34.420		
196	BC_SIMPL	Lower	15.000	15.001	0.000	6.454
244	MATERIAL	Metallic frame	20.018	29.983		
249	BC_SIMPL	Upper	34.999	35.000	6.454	0.000
251	MATERIAL	Filler	15.691	34.309		

λ_{filler}= 0.27 W/mK

BISCO - Input Data

BISCO data file: Assembly 2D_redrub10.bsc

Bitmap file: Assembly 2D_redrub10.bmp

1 pixel = 0.000165 m

Col. -	Width [pixels]	Width [m]	Height [pixels]	Height [m]	Area [pixels]	Zones	Triang.Size [pixels]
0	1540	0.2541	532	0.0878	181720	2	2
107	1540	0.2541	298	0.0492	455128	2	2
164	1540	0.2541	414	0.0683	149740	4	2
196	1540	0.2541	142	0.0234	218680	1	
244	297	0.049	298	0.0492	3792	1	2
249	1540	0.2541	142	0.0234	218680	1	
251	740	0.1221	414	0.0683	28900	2	2

Col. -	Type	CEN-rule	Name	lambda [W/mK]	t [°C]	h [W/m²K]	q [W/m²]
0	MATERIAL		Rubber	0.199			
107	MATERIAL		Mineral wool	0.033			
164	MATERIAL		Plasterboard	0.188			
196	BC_SIMPL		Lower		15.0	99999	0
244	MATERIAL		Metallic frame	52	35.0	99999	0
249	BC_SIMPL		Upper				
251	MATERIAL		Filler	0.27			

BISCO Calculation Results

BISCO data file: Assembly 2D_redrub10.bsc

Number of nodes = 235373

Heat flow divergence for total object = 8.77597e-005

Heat flow divergence for worst node = 0.329497

Col. -	Type	Name	tmin [°C]	tmax [°C]	flow in [W/m]	flow out [W/m]
0	MATERIAL	Rubber	15.000	35.000		
107	MATERIAL	Mineral wool	16.183	33.817		
164	MATERIAL	Plasterboard	15.580	34.420		
196	BC_SIMPL	Lower	15.000	15.001	0.000	6.419
244	MATERIAL	Metallic frame	20.054	29.947		
249	BC_SIMPL	Upper	34.999	35.000	6.419	0.000
251	MATERIAL	Filler	15.686	34.314		

λ_{filler}= 0.24 W/mK

BISCO - Input Data

BISCO data file: Assembly 2D_redrub10.bsc
Bitmap file: Assembly 2D_redrub10.bmp
1 pixel = 0.000165 m

Col. -	Width [pixels]	Width [m]	Height [pixels]	Height [m]	Area [pixels]	Zones	Triang.Size [pixels]
0	1540	0.2541	532	0.0878	181720	2	2
107	1540	0.2541	298	0.0492	455128	2	2
164	1540	0.2541	414	0.0683	149740	4	2
196	1540	0.2541	142	0.0234	218680	1	
244	297	0.049	298	0.0492	3792	1	2
249	1540	0.2541	142	0.0234	218680	1	
251	740	0.1221	414	0.0683	28900	2	2

Col. -	Type	CEN-rule	Name	lambda [W/mK]	t [°C]	h [W/m²K]	q [W/m²]
0	MATERIAL		Rubber	0.199			
107	MATERIAL		Mineral wool	0.033			
164	MATERIAL		Plasterboard	0.188			
196	BC_SIMPL		Lower		15.0	99999	0
244	MATERIAL		Metallic frame	52	35.0	99999	0
249	BC_SIMPL		Upper				
251	MATERIAL		Filler	0.24			

BISCO Calculation Results

BISCO data file: Assembly 2D_redrub10.bsc
Number of nodes = 235373
Heat flow divergence for total object = 0.000913419
Heat flow divergence for worst node = 0.341993

Col. -	Type	Name	tmin [°C]	tmax [°C]	flow in [W/m]	flow out [W/m]
0	MATERIAL	Rubber	15.000	35.000		
107	MATERIAL	Mineral wool	16.183	33.817		
164	MATERIAL	Plasterboard	15.580	34.420		
196	BC_SIMPL	Lower	15.000	15.001	0.000	6.377
244	MATERIAL	Metallic frame	20.098	29.903		
249	BC_SIMPL	Upper	34.999	35.000	6.378	0.000
251	MATERIAL	Filler	15.681	34.319		

λ_{filler}= 0.21 W/mK

BISCO - Input Data

BISCO data file: Assembly 2D_redrub10.bsc

Bitmap file: Assembly 2D_redrub10.bmp

1 pixel = 0.000165 m

Col. -	Width [pixels]	Width [m]	Height [pixels]	Height [m]	Area [pixels]	Zones	Triang.Size [pixels]
0	1540	0.2541	532	0.0878	181720	2	2
107	1540	0.2541	298	0.0492	455128	2	2
164	1540	0.2541	414	0.0683	149740	4	2
196	1540	0.2541	142	0.0234	218680	1	
244	297	0.049	298	0.0492	3792	1	2
249	1540	0.2541	142	0.0234	218680	1	
251	740	0.1221	414	0.0683	28900	2	2

Col. -	Type	CEN-rule	Name	lambda [W/mK]	t [°C]	h [W/m²K]	q [W/m²]
0	MATERIAL		Rubber	0.199			
107	MATERIAL		Mineral wool	0.033			
164	MATERIAL		Plasterboard	0.188			
196	BC_SIMPL		Lower		15.0	99999	0
244	MATERIAL		Metallic frame	52	35.0	99999	0
249	BC_SIMPL		Upper				
251	MATERIAL		Filler	0.21			

BISCO Calculation Results

BISCO data file: Assembly 2D_redrub10.bsc

Number of nodes = 235373

Heat flow divergence for total object = 0.000920133

Heat flow divergence for worst node = 0.219391

Col. -	Type	Name	tmin [°C]	tmax [°C]	flow in [W/m]	flow out [W/m]
0	MATERIAL	Rubber	15.000	35.000		
107	MATERIAL	Mineral wool	16.183	33.817		
164	MATERIAL	Plasterboard	15.580	34.420		
196	BC_SIMPL	Lower	15.000	15.001	0.000	6.327
244	MATERIAL	Metallic frame	20.151	29.850		
249	BC_SIMPL	Upper	34.999	35.000	6.327	0.000
251	MATERIAL	Filler	15.677	34.323		

λ_{filler}= 0.18 W/mK

BISCO - Input Data

BISCO data file: Assembly 2D_redrub10.bsc

Bitmap file: Assembly 2D_redrub10.bmp

1 pixel = 0.000165 m

Col. -	Width [pixels]	Width [m]	Height [pixels]	Height [m]	Area [pixels]	Zones	Triang.Size [pixels]
0	1540	0.2541	532	0.0878	181720	2	2
107	1540	0.2541	298	0.0492	455128	2	2
164	1540	0.2541	414	0.0683	149740	4	2
196	1540	0.2541	142	0.0234	218680	1	
244	297	0.049	298	0.0492	3792	1	2
249	1540	0.2541	142	0.0234	218680	1	
251	740	0.1221	414	0.0683	28900	2	2

Col. -	Type	CEN-rule	Name	lambda [W/mK]	t [°C]	h [W/m²K]	q [W/m²]
0	MATERIAL		Rubber	0.199			
107	MATERIAL		Mineral wool	0.033			
164	MATERIAL		Plasterboard	0.188			
196	BC_SIMPL		Lower		15.0	99999	0
244	MATERIAL		Metallic frame	52	35.0	99999	0
249	BC_SIMPL		Upper				
251	MATERIAL		Filler	0.18			

BISCO Calculation Results

BISCO data file: Assembly 2D_redrub10.bsc

Number of nodes = 235373

Heat flow divergence for total object = 0.000490031

Heat flow divergence for worst node = 0.326829

Col. -	Type	Name	tmin [°C]	tmax [°C]	flow in [W/m]	flow out [W/m]
0	MATERIAL	Rubber	15.000	35.000		
107	MATERIAL	Mineral wool	16.183	33.817		
164	MATERIAL	Plasterboard	15.580	34.420		
196	BC_SIMPL	Lower	15.000	15.001	0.000	6.263
244	MATERIAL	Metallic frame	20.217	29.784		
249	BC_SIMPL	Upper	34.999	35.000	6.263	0.000
251	MATERIAL	Filler	15.673	34.327		

λ_{filler}= 0.15 W/mK

BISCO - Input Data

BISCO data file: Assembly 2D_redrub10.bsc

Bitmap file: Assembly 2D_redrub10.bmp

1 pixel = 0.000165 m

Col. -	Width [pixels]	Width [m]	Height [pixels]	Height [m]	Area [pixels]	Zones	Triang.Size [pixels]
0	1540	0.2541	532	0.0878	181720	2	2
107	1540	0.2541	298	0.0492	455128	2	2
164	1540	0.2541	414	0.0683	149740	4	2
196	1540	0.2541	142	0.0234	218680	1	
244	297	0.049	298	0.0492	3792	1	2
249	1540	0.2541	142	0.0234	218680	1	
251	740	0.1221	414	0.0683	28900	2	2

Col. -	Type	CEN-rule	Name	lambda [W/mK]	t [°C]	h [W/m²K]	q [W/m²]
0	MATERIAL		Rubber	0.199			
107	MATERIAL		Mineral wool	0.033			
164	MATERIAL		Plasterboard	0.188			
196	BC_SIMPL		Lower		15.0	99999	0
244	MATERIAL		Metallic frame	52	35.0	99999	0
249	BC_SIMPL		Upper				
251	MATERIAL		Filler	0.15			

BISCO Calculation Results

BISCO data file: Assembly 2D_redrub10.bsc

Number of nodes = 256939

Heat flow divergence for total object = 0.000919927

Heat flow divergence for worst node = 0.430854

Col. -	Type	Name	tmin [°C]	tmax [°C]	flow in [W/m]	flow out [W/m]
0	MATERIAL	Rubber	15.000	35.000		
107	MATERIAL	Mineral wool	16.183	33.817		
164	MATERIAL	Plasterboard	15.580	34.420		
196	BC_SIMPL	Lower	15.000	15.001	0.000	6.179
244	MATERIAL	Metallic frame	20.305	29.696		
249	BC_SIMPL	Upper	34.999	35.000	6.179	0.000
251	MATERIAL	Filler	15.670	34.330		

λ_{filler}= 0.12 W/mK

BISCO - Input Data

BISCO data file: Assembly 2D_redrub10.bsc

Bitmap file: Assembly 2D_redrub10.bmp

1 pixel = 0.000165 m

Col. -	Width [pixels]	Width [m]	Height [pixels]	Height [m]	Area [pixels]	Zones	Triang.Size [pixels]
0	1540	0.2541	532	0.0878	181720	2	2
107	1540	0.2541	298	0.0492	455128	2	2
164	1540	0.2541	414	0.0683	149740	4	2
196	1540	0.2541	142	0.0234	218680	1	
244	297	0.049	298	0.0492	3792	1	2
249	1540	0.2541	142	0.0234	218680	1	
251	740	0.1221	414	0.0683	28900	2	2

Col. -	Type	CEN-rule	Name	lambda [W/mK]	t [°C]	h [W/m²K]	q [W/m²]
0	MATERIAL		Rubber	0.199			
107	MATERIAL		Mineral wool	0.033			
164	MATERIAL		Plasterboard	0.188			
196	BC_SIMPL		Lower		15.0	99999	0
244	MATERIAL		Metallic frame	52	35.0	99999	0
249	BC_SIMPL		Upper				
251	MATERIAL		Filler	0.12			

BISCO Calculation Results

BISCO data file: Assembly 2D_redrub10.bsc

Number of nodes = 235373

Heat flow divergence for total object = 7.62342e-005

Heat flow divergence for worst node = 0.348101

Col. -	Type	Name	tmin [°C]	tmax [°C]	flow in [W/m]	flow out [W/m]
0	MATERIAL	Rubber	15.000	35.000		
107	MATERIAL	Mineral wool	16.184	33.817		
164	MATERIAL	Plasterboard	15.580	34.420		
196	BC_SIMPL	Lower	15.000	15.001	0.000	6.063
244	MATERIAL	Metallic frame	20.427	29.574		
249	BC_SIMPL	Upper	34.999	35.000	6.063	0.000
251	MATERIAL	Filler	15.665	34.335		

λ_{filler}= 0.09 W/mK

BISCO - Input Data

BISCO data file: Assembly 2D_redrub10.bsc

Bitmap file: Assembly 2D_redrub10.bmp

1 pixel = 0.000165 m

Col. -	Width [pixels]	Width [m]	Height [pixels]	Height [m]	Area [pixels]	Zones	Triang.Size [pixels]
0	1540	0.2541	532	0.0878	181720	2	2
107	1540	0.2541	298	0.0492	455128	2	2
164	1540	0.2541	414	0.0683	149740	4	2
196	1540	0.2541	142	0.0234	218680	1	
244	297	0.049	298	0.0492	3792	1	2
249	1540	0.2541	142	0.0234	218680	1	
251	740	0.1221	414	0.0683	28900	2	2

Col. -	Type	CEN-rule	Name	lambda [W/mK]	t [°C]	h [W/m²K]	q [W/m²]
0	MATERIAL		Rubber	0.199			
107	MATERIAL		Mineral wool	0.033			
164	MATERIAL		Plasterboard	0.188			
196	BC_SIMPL		Lower		15.0	99999	0
244	MATERIAL		Metallic frame	52	35.0	99999	0
249	BC_SIMPL		Upper				
251	MATERIAL		Filler	0.09			

BISCO Calculation Results

BISCO data file: Assembly 2D_redrub10.bsc

Number of nodes = 235373

Heat flow divergence for total object = 0.0008172

Heat flow divergence for worst node = 0.496397

Col. -	Type	Name	tmin [°C]	tmax [°C]	flow in [W/m]	flow out [W/m]
0	MATERIAL	Rubber	15.000	35.000		
107	MATERIAL	Mineral wool	16.184	33.816		
164	MATERIAL	Plasterboard	15.581	34.419		
196	BC_SIMPL	Lower	15.000	15.000	0.000	5.888
244	MATERIAL	Metallic frame	20.610	29.390		
249	BC_SIMPL	Upper	35.000	35.000	5.888	0.000
251	MATERIAL	Filler	15.657	34.343		

λ_{filler}= 0.06 W/mK

BISCO - Input Data

BISCO data file: Assembly 2D_redrub10.bsc

Bitmap file: Assembly 2D_redrub10.bmp

1 pixel = 0.000165 m

Col. -	Width [pixels]	Width [m]	Height [pixels]	Height [m]	Area [pixels]	Zones	Triang.Size [pixels]
0	1540	0.2541	532	0.0878	181720	2	2
107	1540	0.2541	298	0.0492	455128	2	2
164	1540	0.2541	414	0.0683	149740	4	2
196	1540	0.2541	142	0.0234	218680	1	
244	297	0.049	298	0.0492	3792	1	2
249	1540	0.2541	142	0.0234	218680	1	
251	740	0.1221	414	0.0683	28900	2	2

Col. -	Type	CEN-rule	Name	lambda [W/mK]	t [°C]	h [W/m²K]	q [W/m²]
0	MATERIAL		Rubber	0.199			
107	MATERIAL		Mineral wool	0.033			
164	MATERIAL		Plasterboard	0.188			
196	BC_SIMPL		Lower		15.0	99999	0
244	MATERIAL		Metallic frame	52	35.0	99999	0
249	BC_SIMPL		Upper				
251	MATERIAL		Filler	0.06			

BISCO Calculation Results

BISCO data file: Assembly 2D_redrub10.bsc

Number of nodes = 235373

Heat flow divergence for total object = 0.000448399

Heat flow divergence for worst node = 0.327272

Col. -	Type	Name	tmin [°C]	tmax [°C]	flow in [W/m]	flow out [W/m]
0	MATERIAL	Rubber	15.000	35.000		
107	MATERIAL	Mineral wool	16.185	33.815		
164	MATERIAL	Plasterboard	15.581	34.419		
196	BC_SIMPL	Lower	15.000	15.000	0.000	5.589
244	MATERIAL	Metallic frame	20.925	29.075		
249	BC_SIMPL	Upper	35.000	35.000	5.589	0.000
251	MATERIAL	Filler	15.644	34.357		

λ_{filler}= 0.03 W/mK

BISCO - Input Data

BISCO data file: Assembly 2D_redrub10.bsc

Bitmap file: Assembly 2D_redrub10.bmp

1 pixel = 0.000165 m

Col. -	Width [pixels]	Width [m]	Height [pixels]	Height [m]	Area [pixels]	Zones	Triang.Size [pixels]
0	1540	0.2541	532	0.0878	181720	2	2
107	1540	0.2541	298	0.0492	455128	2	2
164	1540	0.2541	414	0.0683	149740	4	2
196	1540	0.2541	142	0.0234	218680	1	
244	297	0.049	298	0.0492	3792	1	2
249	1540	0.2541	142	0.0234	218680	1	
251	740	0.1221	414	0.0683	28900	2	2

Col. -	Type	CEN-rule	Name	lambda [W/mK]	t [°C]	h [W/m²K]	q [W/m²]
0	MATERIAL		Rubber	0.199			
107	MATERIAL		Mineral wool	0.033			
164	MATERIAL		Plasterboard	0.188			
196	BC_SIMPL		Lower		15.0	99999	0
244	MATERIAL		Metallic frame	52	35.0	99999	0
249	BC_SIMPL		Upper				
251	MATERIAL		Filler	0.03			

BISCO Calculation Results

BISCO data file: Assembly 2D_redrub10.bsc

Number of nodes = 235373

Heat flow divergence for total object = 0.00080891

Heat flow divergence for worst node = 0.198188

Col. -	Type	Name	tmin [°C]	tmax [°C]	flow in [W/m]	flow out [W/m]
0	MATERIAL	Rubber	15.000	35.000		
107	MATERIAL	Mineral wool	16.186	33.814		
164	MATERIAL	Plasterboard	15.582	34.418		
196	BC_SIMPL	Lower	15.000	15.000	0.000	4.941
244	MATERIAL	Metallic frame	21.611	28.390		
249	BC_SIMPL	Upper	35.000	35.000	4.941	0.000
251	MATERIAL	Filler	15.610	34.390		

A.8 2D Assembly, R_{add}=0.5349 m^2K/W

λ_{filler}= 0.30 W/mK

BISCO - Input Data

BISCO data file: Assembly 2D_blackrub.bsc
Bitmap file: Assembly 2D_blackrub.bmp
1 pixel = 0.000165 m

Col. -	Width [pixels]	Width [m]	Height [pixels]	Height [m]	Area [pixels]	Zones	Triang.Size [pixels]
0	1540	0.2541	582	0.096	258720	2	2
107	1540	0.2541	298	0.0492	455128	2	2
164	1540	0.2541	414	0.0683	149740	4	2
196	1540	0.2541	117	0.0193	180180	1	
244	297	0.049	298	0.0492	3792	1	2
249	1540	0.2541	117	0.0193	180180	1	
251	740	0.1221	414	0.0683	28900	2	2

Col. -	Type	CEN-rule	Name	lambda [W/mK]	t [°C]	h [W/m²K]	q [W/m²]
0	MATERIAL		Rubber	0.052			
107	MATERIAL		Mineral wool	0.033			
164	MATERIAL		Plasterboard	0.188			
196	BC_SIMPL		Lower		15.0	99999	0
244	MATERIAL		Metallic frame	52	35.0	99999	0
249	BC_SIMPL		Upper				
251	MATERIAL		Filler	0.30			

BISCO Calculation Results

BISCO data file: Assembly 2D_blackrub.bsc
Number of nodes = 256939
Heat flow divergence for total object = 0.000983233
Heat flow divergence for worst node = 0.162567

Col. -	Type	Name	tmin [°C]	tmax [°C]	flow in [W/m]	flow out [W/m]
0	MATERIAL	Rubber	15.000	35.000		
107	MATERIAL	Mineral wool	18.059	31.941		
164	MATERIAL	Plasterboard	17.576	32.424		
196	BC_SIMPL	Lower	15.000	15.000	0.000	3.776
244	MATERIAL	Metallic frame	22.426	27.575		
249	BC_SIMPL	Upper	35.000	35.000	3.776	0.000
251	MATERIAL	Filler	18.248	31.751		

λ_{filler}= 0.27 W/mK

BISCO - Input Data

BISCO data file: Assembly 2D_blackrub.bsc

Bitmap file: Assembly 2D_blackrub.bmp

1 pixel = 0.000165 m

Col. -	Width [pixels]	Width [m]	Height [pixels]	Height [m]	Area [pixels]	Zones	Triang.Size [pixels]
0	1540	0.2541	582	0.096	258720	2	2
107	1540	0.2541	298	0.0492	455128	2	2
164	1540	0.2541	414	0.0683	149740	4	2
196	1540	0.2541	117	0.0193	180180	1	
244	297	0.049	298	0.0492	3792	1	2
249	1540	0.2541	117	0.0193	180180	1	
251	740	0.1221	414	0.0683	28900	2	2

Col. -	Type	CEN-rule	Name	lambda [W/mK]	t [°C]	h [W/m²K]	q [W/m²]
0	MATERIAL		Rubber	0.052			
107	MATERIAL		Mineral wool	0.033			
164	MATERIAL		Plasterboard	0.188			
196	BC_SIMPL		Lower		15.0	99999	0
244	MATERIAL		Metallic frame	52	35.0	99999	0
249	BC_SIMPL		Upper				
251	MATERIAL		Filler	0.27			

BISCO Calculation Results

BISCO data file: Assembly 2D_blackrub.bsc

Number of nodes = 256939

Heat flow divergence for total object = 0.000803223

Heat flow divergence for worst node = 0.334529

Col. -	Type	Name	tmin [°C]	tmax [°C]	flow in [W/m]	flow out [W/m]
0	MATERIAL	Rubber	15.000	35.000		
107	MATERIAL	Mineral wool	18.057	31.942		
164	MATERIAL	Plasterboard	17.574	32.425		
196	BC_SIMPL	Lower	15.000	15.000	0.000	3.764
244	MATERIAL	Metallic frame	22.441	27.559		
249	BC_SIMPL	Upper	35.000	35.000	3.764	0.000
251	MATERIAL	Filler	18.219	31.781		

λ_{filler}= 0.24 W/mK

BISCO - Input Data

BISCO data file: Assembly 2D_blackrub.bsc

Bitmap file: Assembly 2D_blackrub.bmp

1 pixel = 0.000165 m

Col. -	Width [pixels]	Width [m]	Height [pixels]	Height [m]	Area [pixels]	Zones	Triang.Size [pixels]
0	1540	0.2541	582	0.096	258720	2	2
107	1540	0.2541	298	0.0492	455128	2	2
164	1540	0.2541	414	0.0683	149740	4	2
196	1540	0.2541	117	0.0193	180180	1	
244	297	0.049	298	0.0492	3792	1	2
249	1540	0.2541	117	0.0193	180180	1	
251	740	0.1221	414	0.0683	28900	2	2

Col. -	Type	CEN-rule	Name	lambda [W/mK]	t [°C]	h [W/m²K]	q [W/m²]
0	MATERIAL		Rubber	0.052			
107	MATERIAL		Mineral wool	0.033			
164	MATERIAL		Plasterboard	0.188			
196	BC_SIMPL		Lower		15.0	99999	0
244	MATERIAL		Metallic frame	52	35.0	99999	0
249	BC_SIMPL		Upper				
251	MATERIAL		Filler	0.24			

BISCO Calculation Results

BISCO data file: Assembly 2D_blackrub.bsc

Number of nodes = 256939

Heat flow divergence for total object = 0.00086627

Heat flow divergence for worst node = 0.301628

Col. -	Type	Name	tmin [°C]	tmax [°C]	flow in [W/m]	flow out [W/m]
0	MATERIAL	Rubber	15.000	35.000		
107	MATERIAL	Mineral wool	18.055	31.944		
164	MATERIAL	Plasterboard	17.572	32.427		
196	BC_SIMPL	Lower	15.000	15.000	0.000	3.750
244	MATERIAL	Metallic frame	22.458	27.542		
249	BC_SIMPL	Upper	35.000	35.000	3.750	0.000
251	MATERIAL	Filler	18.189	31.811		

λ_{filler}= 0.21 W/mK

BISCO - Input Data

BISCO data file: Assembly 2D_blackrub.bsc

Bitmap file: Assembly 2D_blackrub.bmp

1 pixel = 0.000165 m

Col. -	Width [pixels]	Width [m]	Height [pixels]	Height [m]	Area [pixels]	Zones	Triang.Size [pixels]
0	1540	0.2541	582	0.096	258720	2	2
107	1540	0.2541	298	0.0492	455128	2	2
164	1540	0.2541	414	0.0683	149740	4	2
196	1540	0.2541	117	0.0193	180180	1	
244	297	0.049	298	0.0492	3792	1	2
249	1540	0.2541	117	0.0193	180180	1	
251	740	0.1221	414	0.0683	28900	2	2

Col. -	Type	CEN-rule	Name	lambda [W/mK]	t [°C]	h [W/m²K]	q [W/m²]
0	MATERIAL		Rubber	0.052			
107	MATERIAL		Mineral wool	0.033			
164	MATERIAL		Plasterboard	0.188			
196	BC_SIMPL		Lower		15.0	99999	0
244	MATERIAL		Metallic frame	52	35.0	99999	0
249	BC_SIMPL		Upper				
251	MATERIAL		Filler	0.21			

BISCO Calculation Results

BISCO data file: Assembly 2D_blackrub.bsc

Number of nodes = 256939

Heat flow divergence for total object = 0.000500233

Heat flow divergence for worst node = 0.369759

Col. -	Type	Name	tmin [°C]	tmax [°C]	flow in [W/m]	flow out [W/m]
0	MATERIAL	Rubber	15.000	35.000		
107	MATERIAL	Mineral wool	18.053	31.946		
164	MATERIAL	Plasterboard	17.570	32.429		
196	BC_SIMPL	Lower	15.000	15.000	0.000	3.734
244	MATERIAL	Metallic frame	22.478	27.523		
249	BC_SIMPL	Upper	35.000	35.000	3.734	0.000
251	MATERIAL	Filler	18.158	31.841		

λ_{filler}= 0.18 W/mK

BISCO - Input Data

BISCO data file: Assembly 2D_blackrub.bsc

Bitmap file: Assembly 2D_blackrub.bmp

1 pixel = 0.000165 m

Col. -	Width [pixels]	Width [m]	Height [pixels]	Height [m]	Area [pixels]	Zones	Triang.Size [pixels]
0	1540	0.2541	582	0.096	258720	2	2
107	1540	0.2541	298	0.0492	455128	2	2
164	1540	0.2541	414	0.0683	149740	4	2
196	1540	0.2541	117	0.0193	180180	1	
244	297	0.049	298	0.0492	3792	1	2
249	1540	0.2541	117	0.0193	180180	1	
251	740	0.1221	414	0.0683	28900	2	2

Col. -	Type	CEN-rule	Name	lambda [W/mK]	t [°C]	h [W/m²K]	q [W/m²]
0	MATERIAL		Rubber	0.052			
107	MATERIAL		Mineral wool	0.033			
164	MATERIAL		Plasterboard	0.188			
196	BC_SIMPL		Lower		15.0	99999	0
244	MATERIAL		Metallic frame	52	35.0	99999	0
249	BC_SIMPL		Upper				
251	MATERIAL		Filler	0.18			

BISCO Calculation Results

BISCO data file: Assembly 2D_blackrub.bsc

Number of nodes = 256939

Heat flow divergence for total object = 0.000523715

Heat flow divergence for worst node = 0.405033

Col. -	Type	Name	tmin [°C]	tmax [°C]	flow in [W/m]	flow out [W/m]
0	MATERIAL	Rubber	15.000	35.000		
107	MATERIAL	Mineral wool	18.052	31.947		
164	MATERIAL	Plasterboard	17.569	32.430		
196	BC_SIMPL	Lower	15.000	15.000	0.000	3.715
244	MATERIAL	Metallic frame	22.500	27.500		
249	BC_SIMPL	Upper	35.000	35.000	3.715	0.000
251	MATERIAL	Filler	18.127	31.873		

λ_{filler}= 0.15 W/mK

BISCO - Input Data

BISCO data file: Assembly 2D_blackrub.bsc
Bitmap file: Assembly 2D_blackrub.bmp
1 pixel = 0.000165 m

Col. -	Width [pixels]	Width [m]	Height [pixels]	Height [m]	Area [pixels]	Zones	Triang.Size [pixels]
0	1540	0.2541	582	0.096	258720	2	2
107	1540	0.2541	298	0.0492	455128	2	2
164	1540	0.2541	414	0.0683	149740	4	2
196	1540	0.2541	117	0.0193	180180	1	
244	297	0.049	298	0.0492	3792	1	2
249	1540	0.2541	117	0.0193	180180	1	
251	740	0.1221	414	0.0683	28900	2	2

Col. -	Type	CEN-rule	Name	lambda [W/mK]	t [°C]	h [W/m²K]	q [W/m²]
0	MATERIAL		Rubber	0.052			
107	MATERIAL		Mineral wool	0.033			
164	MATERIAL		Plasterboard	0.188			
196	BC_SIMPL		Lower		15.0	99999	0
244	MATERIAL		Metallic frame	52	35.0	99999	0
249	BC_SIMPL		Upper				
251	MATERIAL		Filler	0.15			

BISCO Calculation Results

BISCO data file: Assembly 2D_blackrub.bsc
Number of nodes = 256939
Heat flow divergence for total object = 0.000919927
Heat flow divergence for worst node = 0.430854

Col. -	Type	Name	tmin [°C]	tmax [°C]	flow in [W/m]	flow out [W/m]
0	MATERIAL	Rubber	15.000	35.000		
107	MATERIAL	Mineral wool	18.050	31.949		
164	MATERIAL	Plasterboard	17.567	32.432		
196	BC_SIMPL	Lower	15.000	15.000	0.000	3.691
244	MATERIAL	Metallic frame	22.528	27.473		
249	BC_SIMPL	Upper	35.000	35.000	3.691	0.000
251	MATERIAL	Filler	18.094	31.906		

λ_{filler}= 0.12 W/mK

BISCO - Input Data

BISCO data file: Assembly 2D_blackrub.bsc

Bitmap file: Assembly 2D_blackrub.bmp

1 pixel = 0.000165 m

Col. -	Width [pixels]	Width [m]	Height [pixels]	Height [m]	Area [pixels]	Zones	Triang.Size [pixels]
0	1540	0.2541	582	0.096	258720	2	2
107	1540	0.2541	298	0.0492	455128	2	2
164	1540	0.2541	414	0.0683	149740	4	2
196	1540	0.2541	117	0.0193	180180	1	
244	297	0.049	298	0.0492	3792	1	2
249	1540	0.2541	117	0.0193	180180	1	
251	740	0.1221	414	0.0683	28900	2	2

Col. -	Type	CEN-rule	Name	lambda [W/mK]	t [°C]	h [W/m²K]	q [W/m²]
0	MATERIAL		Rubber	0.052			
107	MATERIAL		Mineral wool	0.033			
164	MATERIAL		Plasterboard	0.188			
196	BC_SIMPL		Lower		15.0	99999	0
244	MATERIAL		Metallic frame	52	35.0	99999	0
249	BC_SIMPL		Upper				
251	MATERIAL		Filler	0.12			

BISCO Calculation Results

BISCO data file: Assembly 2D_blackrub.bsc

Number of nodes = 256939

Heat flow divergence for total object = 0.000101292

Heat flow divergence for worst node = 0.4867

Col. -	Type	Name	tmin [°C]	tmax [°C]	flow in [W/m]	flow out [W/m]
0	MATERIAL	Rubber	15.000	35.000		
107	MATERIAL	Mineral wool	18.049	31.950		
164	MATERIAL	Plasterboard	17.566	32.433		
196	BC_SIMPL	Lower	15.000	15.000	0.000	3.659
244	MATERIAL	Metallic frame	22.565	27.436		
249	BC_SIMPL	Upper	35.000	35.000	3.659	0.000
251	MATERIAL	Filler	18.061	31.939		

λ_{filler}= 0.09 W/mK

BISCO - Input Data

BISCO data file: Assembly 2D_blackrub.bsc

Bitmap file: Assembly 2D_blackrub.bmp

1 pixel = 0.000165 m

Col. -	Width [pixels]	Width [m]	Height [pixels]	Height [m]	Area [pixels]	Zones	Triang.Size [pixels]
0	1540	0.2541	582	0.096	258720	2	2
107	1540	0.2541	298	0.0492	455128	2	2
164	1540	0.2541	414	0.0683	149740	4	2
196	1540	0.2541	117	0.0193	180180	1	
244	297	0.049	298	0.0492	3792	1	2
249	1540	0.2541	117	0.0193	180180	1	
251	740	0.1221	414	0.0683	28900	2	2

Col. -	Type	CEN-rule	Name	lambda [W/mK]	t [°C]	h [W/m²K]	q [W/m²]
0	MATERIAL		Rubber	0.052			
107	MATERIAL		Mineral wool	0.033			
164	MATERIAL		Plasterboard	0.188			
196	BC_SIMPL		Lower		15.0	99999	0
244	MATERIAL		Metallic frame	52	35.0	99999	0
249	BC_SIMPL		Upper				
251	MATERIAL		Filler	0.09			

BISCO Calculation Results

BISCO data file: Assembly 2D_blackrub.bsc

Number of nodes = 256939

Heat flow divergence for total object = 0.000616488

Heat flow divergence for worst node = 0.485052

Col. -	Type	Name	tmin [°C]	tmax [°C]	flow in [W/m]	flow out [W/m]
0	MATERIAL	Rubber	15.000	35.000		
107	MATERIAL	Mineral wool	18.048	31.950		
164	MATERIAL	Plasterboard	17.566	32.433		
196	BC_SIMPL	Lower	15.000	15.000	0.000	3.611
244	MATERIAL	Metallic frame	22.617	27.384		
249	BC_SIMPL	Upper	35.000	35.000	3.611	0.000
251	MATERIAL	Filler	18.021	31.978		

λ_{filler}= 0.06 W/mK

BISCO - Input Data

BISCO data file: Assembly 2D_blackrub.bsc

Bitmap file: Assembly 2D_blackrub.bmp

1 pixel = 0.000165 m

Col. -	Width [pixels]	Width [m]	Height [pixels]	Height [m]	Area [pixels]	Zones	Triang.Size [pixels]
0	1540	0.2541	582	0.096	258720	2	2
107	1540	0.2541	298	0.0492	455128	2	2
164	1540	0.2541	414	0.0683	149740	4	2
196	1540	0.2541	117	0.0193	180180	1	
244	297	0.049	298	0.0492	3792	1	2
249	1540	0.2541	117	0.0193	180180	1	
251	740	0.1221	414	0.0683	28900	2	2

Col. -	Type	CEN-rule	Name	lambda [W/mK]	t [°C]	h [W/m²K]	q [W/m²]
0	MATERIAL		Rubber	0.052			
107	MATERIAL		Mineral wool	0.033			
164	MATERIAL		Plasterboard	0.188			
196	BC_SIMPL		Lower		15.0	99999	0
244	MATERIAL		Metallic frame	52	35.0	99999	0
249	BC_SIMPL		Upper				
251	MATERIAL		Filler	0.06			

BISCO Calculation Results

BISCO data file: Assembly 2D_blackrub.bsc

Number of nodes = 256939

Heat flow divergence for total object = 0.000472034

Heat flow divergence for worst node = 0.672389

Col. -	Type	Name	tmin [°C]	tmax [°C]	flow in [W/m]	flow out [W/m]
0	MATERIAL	Rubber	15.000	35.000		
107	MATERIAL	Mineral wool	18.051	31.949		
164	MATERIAL	Plasterboard	17.568	32.432		
196	BC_SIMPL	Lower	15.000	15.000	0.000	3.527
244	MATERIAL	Metallic frame	22.707	27.294		
249	BC_SIMPL	Upper	35.000	35.000	3.527	0.000
251	MATERIAL	Filler	17.961	32.039		

λ_{filler}= 0.03 W/mK

BISCO - Input Data

BISCO data file: Assembly 2D_blackrub.bsc

Bitmap file: Assembly 2D_blackrub.bmp

1 pixel = 0.000165 m

Col. -	Width [pixels]	Width [m]	Height [pixels]	Height [m]	Area [pixels]	Zones	Triang.Size [pixels]
0	1540	0.2541	582	0.096	258720	2	2
107	1540	0.2541	298	0.0492	455128	2	2
164	1540	0.2541	414	0.0683	149740	4	2
196	1540	0.2541	117	0.0193	180180	1	
244	297	0.049	298	0.0492	3792	1	2
249	1540	0.2541	117	0.0193	180180	1	
251	740	0.1221	414	0.0683	28900	2	2

Col. -	Type	CEN-rule	Name	lambda [W/mK]	t [°C]	h [W/m²K]	q [W/m²]
0	MATERIAL		Rubber	0.052			
107	MATERIAL		Mineral wool	0.033			
164	MATERIAL		Plasterboard	0.188			
196	BC_SIMPL		Lower		15.0	99999	0
244	MATERIAL		Metallic frame	52	35.0	99999	0
249	BC_SIMPL		Upper				
251	MATERIAL		Filler	0.03			

BISCO Calculation Results

BISCO data file: Assembly 2D_blackrub.bsc

Number of nodes = 256939

Heat flow divergence for total object = 0.000982136

Heat flow divergence for worst node = 0.688429

Col. -	Type	Name	tmin [°C]	tmax [°C]	flow in [W/m]	flow out [W/m]
0	MATERIAL	Rubber	15.000	35.000		
107	MATERIAL	Mineral wool	18.058	31.941		
164	MATERIAL	Plasterboard	17.575	32.424		
196	BC_SIMPL	Lower	15.000	15.000	0.000	3.323
244	MATERIAL	Metallic frame	22.920	27.081		
249	BC_SIMPL	Upper	35.000	35.000	3.323	0.000
251	MATERIAL	Filler	17.813	32.186		

A.9 NumA procedure results

NumA	λ_{filler} [W/mK]									
	0.30	0.27	0.24	0.21	0.18	0.15	0.12	0.09	0.06	0.03
R_i+R_e [m^{2}K/W]	0									
ΔT [K]	20									
φ_{1D} [W/m]	3.193									
φ_{2D} [W/m]	8.230	8.162	8.081	7.983	7.859	7.699	7.480	7.162	6.646	5.635
Ψ [W/mK]	0.252	0.248	0.244	0.240	0.233	0.225	0.214	0.198	0.173	0.122
R_i+R_e [m^{2}K/W]	0.5349									
ΔT [K]	20									
φ_{1D} [W/m]	2.391									
φ_{2D} [W/m]	3.776	3.764	3.750	3.734	3.715	3.691	3.659	3.611	3.527	3.323
Ψ [W/mK]	0.069	0.069	0.068	0.067	0.066	0.065	0.063	0.061	0.057	0.047
R_i+R_e [m^{2}K/W]	0.04772									
ΔT [K]	20									
φ_{1D} [W/m]	3.131									
φ_{2D} [W/m]	7.494	7.442	7.381	7.306	7.211	7.088	6.917	6.664	6.242	5.382
Ψ [W/mK]	0.218	0.216	0.213	0.209	0.204	0.198	0.189	0.177	0.156	0.113
R_i+R_e [m^{2}K/W]	0.04871									
ΔT [K]	20									
φ_{1D} [W/m]	3.099									
φ_{2D} [W/m]	7.183	7.137	7.083	7.016	6.932	6.821	6.668	6.440	6.057	5.261
Ψ [W/mK]	0.204	0.202	0.199	0.196	0.192	0.186	0.178	0.167	0.148	0.108
R_i+R_e [m^{2}K/W]	0.09778									
ΔT [K]	20									
φ_{1D} [W/m]	3.008									
φ_{2D} [W/m]	6.454	6.419	6.378	6.327	6.263	6.179	6.063	5.888	5.589	4.941
Ψ [W/mK]	0.172	0.171	0.169	0.166	0.163	0.159	0.153	0.144	0.129	0.097

Table 12_ Ψ-values by NumA procedure.

A.10 NumB procedure results

T_{up} [°C]	35
$R_{add,up}$ [m^2K/W]	0.267
ϕ_{1D} [W/m]	2.447
ϕ_{1D} [W/m^2]	9.632

		1	2	3	4	5	6	7	8	9	10	11	12	13	14	15	16	17
	x_i [mm]	0	31.750	63.500	79.375	95.250	103.190	111.130	119.065	127.000	134.940	142.880	150.815	158.750	174.625	190.500	222.250	254.000
λ_{filler}=0.30 W/mK	$T_{i,up}$ [°C]	32.424	32.340	31.878	31.227	30.050	29.290	28.780	28.506	28.308	28.206	28.217	28.594	29.434	30.889	31.684	32.298	32.405
	ϕ_{tb} [W/m^2]	9.632	9.945	11.673	14.107	18.508	21.351	23.258	24.281	25.022	25.403	25.360	23.951	20.813	15.371	12.397	10.103	9.702
	d_i [m]	0.016	0.032	0.024	0.016	0.012	0.008	0.008	0.008	0.008	0.008	0.008	0.008	0.012	0.016	0.024	0.032	0.016
	ϕ_{tb} [W/m]	0.153	0.316	0.278	0.224	0.220	0.170	0.185	0.193	0.199	0.202	0.201	0.190	0.248	0.244	0.295	0.321	0.154
	ϕ_{2D} [W/m]	3.792																
	ψ [W/mK]	0.0673																
λ_{filler}=0.27 W/mK	$T_{i,up}$ [°C]	32.425	32.344	31.882	31.255	30.067	29.296	28.785	28.517	28.326	28.218	28.223	28.600	29.451	30.921	31.709	32.303	32.407
	ϕ_{tb} [W/m^2]	9.632	9.935	11.665	14.011	18.457	21.339	23.251	24.252	24.968	25.374	25.355	23.945	20.761	15.260	12.311	10.090	9.699
	d_i [m]	0.016	0.032	0.024	0.016	0.012	0.008	0.008	0.008	0.008	0.008	0.008	0.008	0.012	0.016	0.024	0.032	0.016
	ϕ_{tb} [W/m]	0.153	0.315	0.278	0.222	0.220	0.169	0.185	0.193	0.198	0.201	0.201	0.190	0.247	0.242	0.293	0.320	0.154
	ϕ_{2D} [W/m]	3.783																
	ψ [W/mK]	0.0668																
λ_{filler}=0.24 W/mK	$T_{i,up}$ [°C]	32.427	32.348	31.902	31.285	30.086	29.306	28.795	28.534	28.350	28.234	28.233	28.610	29.472	30.956	31.735	32.308	32.410
	ϕ_{tb} [W/m^2]	9.632	9.927	11.599	13.908	18.396	21.315	23.230	24.208	24.895	25.328	25.333	23.923	20.696	15.139	12.224	10.078	9.697
	d_i [m]	0.016	0.032	0.024	0.016	0.012	0.008	0.008	0.008	0.008	0.008	0.008	0.008	0.012	0.016	0.024	0.032	0.016
	ϕ_{tb} [W/m]	0.153	0.315	0.276	0.221	0.219	0.169	0.184	0.192	0.198	0.201	0.201	0.190	0.246	0.240	0.291	0.320	0.154
	ϕ_{2D} [W/m]	3.7719																
	ψ [W/mK]	0.0663																

λ_{filler}=0.21 W/mK	$T_{i,up}$ [°C]	32.429	32.352	31.894	31.318	30.110	29.321	28.810	28.556	28.382	28.259	28.250	28.626	29.498	30.995	31.760	32.313	32.412
	ϕ_{tb} [W/m^2]	9.632	9.920	11.635	13.793	18.319	21.272	23.185	24.137	24.791	25.253	25.283	23.877	20.610	15.004	12.135	10.066	9.695
	d_i [m]	0.016	0.032	0.024	0.016	0.012	0.008	0.008	0.008	0.008	0.008	0.008	0.008	0.012	0.016	0.024	0.032	0.016
	ϕ_{tb} [W/m]	0.153	0.315	0.277	0.219	0.218	0.169	0.184	0.192	0.197	0.201	0.201	0.190	0.245	0.238	0.289	0.320	0.154
	ϕ_{2D} [W/m]	3.761																
	ψ [W/mK]	0.0657																
λ_{filler}=0.18 W/mK	$T_{i,up}$ [°C]	32.430	32.355	31.941	31.355	30.139	29.344	28.835	28.589	28.424	28.293	28.279	28.652	29.532	31.038	31.786	32.318	32.414
	ϕ_{tb} [W/m^2]	9.632	9.912	11.466	13.663	18.219	21.200	23.107	24.029	24.646	25.137	25.193	23.794	20.494	14.850	12.046	10.054	9.693
	d_i [m]	0.016	0.032	0.024	0.016	0.012	0.008	0.008	0.008	0.008	0.008	0.008	0.008	0.012	0.016	0.024	0.032	0.016
	ϕ_{tb} [W/m]	0.153	0.315	0.273	0.217	0.217	0.168	0.183	0.191	0.196	0.200	0.200	0.189	0.244	0.236	0.287	0.319	0.154
	ϕ_{2D} [W/m]	3.741																
	ψ [W/mK]	0.0647																
λ_{filler}=0.15 W/mK	$T_{i,up}$ [°C]	32.432	32.359	31.960	31.398	30.179	29.379	28.874	28.638	28.484	28.345	28.324	28.694	29.579	31.089	31.812	32.322	32.416
	ϕ_{tb} [W/m^2]	9.632	9.906	11.402	13.510	18.081	21.079	22.973	23.860	24.435	24.956	25.035	23.648	20.330	14.668	11.956	10.043	9.691
	d_i [m]	0.016	0.032	0.024	0.016	0.012	0.008	0.008	0.008	0.008	0.008	0.008	0.008	0.012	0.016	0.024	0.032	0.016
	ϕ_{tb} [W/m]	0.153	0.315	0.271	0.215	0.215	0.167	0.182	0.189	0.194	0.198	0.199	0.188	0.242	0.233	0.285	0.319	0.154
	ϕ_{2D} [W/m]	3.719																
	ψ [W/mK]	0.0636																
λ_{filler}=0.12 W/mK	$T_{i,up}$ [°C]	32.433	32.360	31.977	31.451	30.217	29.451	28.932	28.703	28.570	28.429	28.402	28.778	29.666	31.151	31.836	32.327	32.418
	ϕ_{tb} [W/m^2]	9.632	9.904	11.343	13.317	17.943	20.820	22.766	23.626	24.124	24.653	24.753	23.343	20.010	14.439	11.869	10.028	9.688
	d_i [m]	0.016	0.032	0.024	0.016	0.012	0.008	0.008	0.008	0.008	0.008	0.008	0.008	0.012	0.016	0.024	0.032	0.016
	ϕ_{tb} [W/m]	0.153	0.314	0.270	0.211	0.214	0.165	0.181	0.188	0.192	0.196	0.197	0.185	0.238	0.229	0.283	0.318	0.154
	ϕ_{2D} [W/m]	3.688																
	ψ [W/mK]	0.0621																
λ_{filler}=0.09 W/mK	$T_{i,up}$ [°C]	32.433	32.362	31.989	31.522	30.321	29.535	29.051	28.839	28.715	28.563	28.534	28.887	29.754	31.236	31.857	32.328	32.419
	ϕ_{tb} [W/m^2]	9.632	9.899	11.296	13.049	17.558	20.505	22.320	23.116	23.581	24.152	24.262	22.935	19.684	14.123	11.792	10.025	9.686
	d_i [m]	0.016	0.032	0.024	0.016	0.012	0.008	0.008	0.008	0.008	0.008	0.008	0.008	0.012	0.016	0.024	0.032	0.016
	ϕ_{tb} [W/m]	0.153	0.314	0.269	0.207	0.209	0.163	0.177	0.184	0.187	0.192	0.193	0.182	0.234	0.224	0.281	0.318	0.154
	ϕ_{2D} [W/m]	3.641																
	ψ [W/mK]	0.0597																

λ_{filler}=0.06 W/mK	$T_{i,up}$ [°C]	32.432	32.359	31.989	31.637	30.480	29.734	29.278	29.084	28.980	28.828	28.801	29.135	29.954	31.372	31.869	32.327	32.418
	ϕ_{tb} [W/m^2]	9.632	9.906	11.295	12.613	16.954	19.753	21.461	22.188	22.578	23.148	23.250	21.996	18.925	13.607	11.745	10.026	9.684
	d_i [m]	0.016	0.032	0.024	0.016	0.012	0.008	0.008	0.008	0.008	0.008	0.008	0.008	0.012	0.016	0.024	0.032	0.016
	ϕ_{tb} [W/m]	0.153	0.315	0.269	0.200	0.202	0.157	0.170	0.176	0.179	0.184	0.185	0.175	0.225	0.216	0.280	0.318	0.154
	ϕ_{2D} [W/m]	3.558																
	ψ [W/mK]	0.0556																
λ_{filler}=0.03 W/mK	$T_{i,up}$ [°C]	32.425	32.342	31.949	31.905	30.893	30.268	29.886	29.726	29.649	29.520	29.508	29.792	30.468	31.684	31.839	32.312	32.411
	ϕ_{tb} [W/m^2]	9.632	9.940	11.411	11.575	15.359	17.699	19.125	19.726	20.011	20.496	20.539	19.476	16.950	12.401	11.823	10.052	9.681
	d_i [m]	0.016	0.032	0.024	0.016	0.012	0.008	0.008	0.008	0.008	0.008	0.008	0.008	0.012	0.016	0.024	0.032	0.016
	ϕ_{tb} [W/m]	0.153	0.316	0.272	0.184	0.183	0.141	0.152	0.157	0.159	0.163	0.163	0.155	0.202	0.197	0.282	0.319	0.154
	ϕ_{2D} [W/m]	3.349																
	ψ [W/mK]	0.0451																

Table 13_ NumB results, R_{add}=0.5349 m^{2}K/W.

T_{up} [°C]	35
$R_{add,up}$ [m^{2}K/W]	0.024
ϕ_{1D} [W/m]	3.062
ϕ_{1D} [W/m^2]	12.054

		1	2	3	4	5	6	7	8	9	10	11	12	13	14	15	16	17
	x_i [mm]	0	31.750	63.500	79.375	95.250	103.190	111.130	119.065	127.000	134.940	142.880	150.815	158.750	174.625	190.500	222.250	254.000
λ_{filler} 0.30 W/mK	$T_{i,up}$ [°C]	34.706	34.706	34.696	34.601	34.197	33.800	33.502	33.337	33.173	33.078	32.999	33.224	33.830	34.512	34.678	34.705	34.706
	ϕ_{tb} [W/m^2]	12.054	12.064	12.463	16.369	32.950	49.266	61.518	68.283	75.017	78.934	82.165	72.925	48.040	20.036	13.224	12.094	12.058
	d_i [m]	0.016	0.032	0.024	0.016	0.012	0.008	0.008	0.008	0.008	0.008	0.008	0.008	0.012	0.016	0.024	0.032	0.016
	ϕ_{tb} [W/m]	0.191	0.383	0.297	0.260	0.392	0.391	0.488	0.542	0.596	0.627	0.652	0.579	0.572	0.318	0.315	0.384	0.191
	ϕ_{2D} [W/m]	7.1798																
	ψ [W/mK]	0.2059																

λ_{filler} 0.27 W/mK	$T_{i,up}$ [°C]	34.706	34.706	34.695	34.604	34.201	33.804	33.510	33.353	33.202	33.099	33.016	33.237	33.840	34.516	34.677	34.705	34.706
	ϕ_{tb} [W/m^2]	12.054	12.068	12.527	16.268	32.802	49.090	61.176	67.606	73.811	78.061	81.468	72.391	47.633	19.855	13.270	12.098	12.058
	d_i [m]	0.016	0.032	0.024	0.016	0.012	0.008	0.008	0.008	0.008	0.008	0.008	0.008	0.012	0.016	0.024	0.032	0.016
	ϕ_{tb} [W/m]	0.191	0.383	0.298	0.258	0.391	0.390	0.486	0.537	0.586	0.620	0.647	0.575	0.567	0.315	0.316	0.384	0.191
	ϕ_{2D} [W/m]	7.1358																
	ψ [W/mK]	0.2037																
λ_{filler} 0.24 W/mK	$T_{i,up}$ [°C]	34.706	34.706	34.693	34.606	34.205	33.810	33.521	33.373	33.236	33.124	33.038	33.254	33.852	34.521	34.675	34.705	34.706
	ϕ_{tb} [W/m^2]	12.054	12.073	12.611	16.168	32.633	48.847	60.731	66.803	72.440	77.014	80.570	71.685	47.154	19.671	13.339	12.104	12.058
	d_i [m]	0.016	0.032	0.024	0.016	0.012	0.008	0.008	0.008	0.008	0.008	0.008	0.008	0.012	0.016	0.024	0.032	0.016
	ϕ_{tb} [W/m]	0.191	0.383	0.300	0.257	0.389	0.388	0.482	0.530	0.575	0.611	0.640	0.569	0.562	0.312	0.318	0.384	0.191
	ϕ_{2D} [W/m]	7.0838																
	ψ [W/mK]	0.2011																
λ_{filler} 0.21 W/mK	$T_{i,up}$ [°C]	34.706	34.706	34.690	34.609	34.210	33.819	33.535	33.397	33.275	33.156	33.066	33.277	33.866	34.526	34.673	34.705	34.706
	ϕ_{tb} [W/m^2]	12.054	12.079	12.724	16.063	32.432	48.501	60.125	65.812	70.835	75.713	79.378	70.729	46.564	19.478	13.439	12.109	12.058
	d_i [m]	0.016	0.032	0.024	0.016	0.012	0.008	0.008	0.008	0.008	0.008	0.008	0.008	0.012	0.016	0.024	0.032	0.016
	ϕ_{tb} [W/m]	0.191	0.384	0.303	0.255	0.386	0.385	0.477	0.523	0.562	0.601	0.630	0.562	0.555	0.309	0.320	0.384	0.191
	ϕ_{2D} [W/m]	7.0195																
	ψ [W/mK]	0.1979																
λ_{filler} 0.18 W/mK	$T_{i,up}$ [°C]	34.706	34.706	34.686	34.611	34.216	33.831	33.556	33.427	33.321	33.196	33.105	33.309	33.884	34.530	34.669	34.705	34.706
	ϕ_{tb} [W/m^2]	12.054	12.087	12.878	15.953	32.184	48.008	59.295	64.563	68.928	74.067	77.782	69.426	45.827	19.276	13.586	12.118	12.057
	d_i [m]	0.016	0.032	0.024	0.016	0.012	0.008	0.008	0.008	0.008	0.008	0.008	0.008	0.012	0.016	0.024	0.032	0.016
	ϕ_{tb} [W/m]	0.191	0.384	0.307	0.253	0.383	0.381	0.471	0.513	0.547	0.588	0.618	0.551	0.546	0.306	0.323	0.385	0.191
	ϕ_{2D} [W/m]	6.9389																
	ψ [W/mK]	0.1939																

λ_{filler} 0.15 W/mK	$T_{i,up}$ [°C]	34.706	34.705	34.681	34.614	34.224	33.848	33.584	33.467	33.378	33.248	33.159	33.353	33.907	34.536	34.664	34.704	34.706
	ϕ_{tb} [W/m^2]	12.054	12.100	13.098	15.833	31.860	47.284	58.122	62.927	66.587	71.908	75.584	67.607	44.866	19.055	13.806	12.131	12.057
	d_i [m]	0.016	0.032	0.024	0.016	0.012	0.008	0.008	0.008	0.008	0.008	0.008	0.008	0.012	0.016	0.024	0.032	0.016
	ϕ_{tb} [W/m]	0.191	0.384	0.312	0.251	0.379	0.375	0.461	0.500	0.529	0.571	0.600	0.537	0.534	0.303	0.329	0.385	0.191
	ϕ_{2D} [W/m]	6.8338																
	ψ [W/mK]	0.1886																
λ_{filler} 0.12 W/mK	$T_{i,up}$ [°C]	34.706	34.705	34.673	34.618	34.235	33.875	33.627	33.522	33.452	33.321	33.235	33.417	33.939	34.542	34.655	34.704	34.706
	ϕ_{tb} [W/m^2]	12.054	12.117	13.425	15.689	31.391	46.164	56.372	60.648	63.557	68.919	72.425	64.957	43.530	18.790	14.145	12.149	12.056
	d_i [m]	0.016	0.032	0.024	0.016	0.012	0.008	0.008	0.008	0.008	0.008	0.008	0.008	0.012	0.016	0.024	0.032	0.016
	ϕ_{tb} [W/m]	0.191	0.385	0.320	0.249	0.374	0.367	0.448	0.482	0.505	0.547	0.575	0.516	0.518	0.298	0.337	0.386	0.191
	ϕ_{2D} [W/m]	6.6880																
	ψ [W/mK]	0.1813																
λ_{filler} 0.09 W/mK	$T_{i,up}$ [°C]	34.706	34.704	34.660	34.623	34.254	33.920	33.694	33.605	33.554	33.428	33.352	33.516	33.988	34.551	34.641	34.703	34.706
	ϕ_{tb} [W/m^2]	12.054	12.140	13.959	15.483	30.625	44.312	53.589	57.236	59.358	64.500	67.631	60.889	41.516	18.425	14.712	12.176	12.057
	d_i [m]	0.016	0.032	0.024	0.016	0.012	0.008	0.008	0.008	0.008	0.008	0.008	0.008	0.012	0.016	0.024	0.032	0.016
	ϕ_{tb} [W/m]	0.191	0.385	0.332	0.246	0.365	0.352	0.426	0.454	0.471	0.512	0.537	0.483	0.494	0.293	0.350	0.387	0.191
	ϕ_{2D} [W/m]	6.4709																
	ψ [W/mK]	0.1705																
λ_{filler} 0.06 W/mK	$T_{i,up}$ [°C]	34.706	34.703	34.635	34.633	34.290	34.003	33.814	33.744	33.712	33.604	33.545	33.682	34.072	34.567	34.615	34.702	34.706
	ϕ_{tb} [W/m^2]	12.054	12.193	14.962	15.078	29.114	40.888	48.671	51.516	52.831	57.269	59.697	54.079	38.061	17.753	15.788	12.233	12.058
	d_i [m]	0.016	0.032	0.024	0.016	0.012	0.008	0.008	0.008	0.008	0.008	0.008	0.008	0.012	0.016	0.024	0.032	0.016
	ϕ_{tb} [W/m]	0.191	0.387	0.356	0.239	0.347	0.325	0.386	0.409	0.419	0.455	0.474	0.429	0.453	0.282	0.376	0.388	0.191
	ϕ_{2D} [W/m]	6.1097																
	ψ [W/mK]	0.1524																

λ_{filler} 0.03 W/mK	$T_{i,up}$ [°C]	34.706	34.700	34.578	34.672	34.407	34.211	34.078	34.033	34.022	33.954	33.920	33.994	34.234	34.606	34.550	34.698	34.706
	ϕ_{tb} [W/m²]	12.054	12.282	17.306	13.441	24.292	32.327	37.799	39.649	40.105	42.853	44.278	41.236	31.391	16.160	18.426	12.367	12.058
	d_i [m]	0.016	0.032	0.024	0.016	0.012	0.008	0.008	0.008	0.008	0.008	0.008	0.008	0.012	0.016	0.024	0.032	0.016
	ϕ_{tb} [W/m]	0.191	0.390	0.412	0.213	0.289	0.257	0.300	0.315	0.318	0.340	0.352	0.327	0.374	0.257	0.439	0.393	0.191
	ϕ_{2D} [W/m]	5.3588																
	ψ [W/mK]	0.1149																

Table 14_ NumB results, R_{add}=0.0487 m²K/W.

T_{up} [°C]	35
$R_{add,up}$ [°C]	0.0489
ϕ_{1D} [W/m]	3.0121
ϕ_{1D} [W/m²]	11.8586

		1	2	3	4	5	6	7	8	9	10	11	12	13	14	15	16	17
	x_i [mm]	0	31.750	63.500	79.375	95.250	103.190	111.130	119.065	127.000	134.940	142.880	150.815	158.750	174.625	190.500	222.250	254.000
λ_{filler} 0.30 W/mK	$T_{i,up}$ [°C]	34.420	34.416	34.345	34.119	33.429	32.873	32.440	32.189	31.981	31.862	31.816	32.142	32.906	33.935	34.289	34.411	34.419
	ϕ_{tb} [W/m²]	11.859	11.952	13.396	18.018	32.140	43.509	52.366	57.501	61.741	64.175	65.118	58.452	42.838	21.786	14.542	12.038	11.876
	d_i [m]	0.016	0.032	0.024	0.016	0.012	0.008	0.008	0.008	0.008	0.008	0.008	0.008	0.012	0.016	0.024	0.032	0.016
	ϕ_{tb} [W/m]	0.188	0.379	0.319	0.286	0.383	0.345	0.416	0.457	0.490	0.510	0.517	0.464	0.510	0.346	0.346	0.382	0.189
	ϕ_{2D} [W/m]	6.5276																
	ψ [W/mK]	0.1758																
λ_{filler} 0.27 W/mK	$T_{i,up}$ [°C]	34.420	34.416	34.346	34.126	33.437	32.881	32.452	32.210	32.014	31.887	31.835	32.158	32.920	33.946	34.292	34.411	34.419
	ϕ_{tb} [W/m²]	11.859	11.954	13.381	17.868	31.971	43.343	52.118	57.070	61.070	63.666	64.728	58.137	42.536	21.556	14.489	12.039	11.876
	d_i [m]	0.016	0.032	0.024	0.016	0.012	0.008	0.008	0.008	0.008	0.008	0.008	0.008	0.012	0.016	0.024	0.032	0.016
	ϕ_{tb} [W/m]	0.188	0.380	0.319	0.284	0.381	0.344	0.414	0.453	0.485	0.506	0.514	0.462	0.507	0.342	0.345	0.382	0.189
	ϕ_{2D} [W/m]	6.4927																
	ψ [W/mK]	0.1740																
λ_{filler}	$T_{i,up}$ [°C]	34.420	34.415	34.346	34.134	33.447	32.892	32.468	32.236	32.053	31.918	31.861	32.179	32.938	33.958	34.294	34.411	34.419

	ϕ_{tb} [W/m^2]	11.859	11.956	13.376	17.709	31.772	43.119	51.785	56.538	60.276	63.031	64.202	57.705	42.170	21.310	14.447	12.040	11.876
	d_i [m]	0.016	0.032	0.024	0.016	0.012	0.008	0.008	0.008	0.008	0.008	0.008	0.008	0.012	0.016	0.024	0.032	0.016
	ϕ_{tb} [W/m]	0.188	0.380	0.318	0.281	0.378	0.342	0.411	0.449	0.479	0.500	0.510	0.458	0.502	0.338	0.344	0.382	0.189
	ϕ_{2D} [W/m]	6.4510																
	ψ [W/mK]	0.1719																
λ_{filler} 0.21 W/mK	$T_{i,up}$ [°C]	34.420	34.415	34.345	34.142	33.458	32.906	32.490	32.268	32.099	31.957	31.895	32.207	32.960	33.971	34.295	34.411	34.419
	ϕ_{tb} [W/m^2]	11.859	11.960	13.387	17.538	31.533	42.813	51.337	55.871	59.321	62.225	63.492	57.114	41.717	21.045	14.420	12.042	11.875
	d_i [m]	0.016	0.032	0.024	0.016	0.012	0.008	0.008	0.008	0.008	0.008	0.008	0.008	0.012	0.016	0.024	0.032	0.016
	ϕ_{tb} [W/m]	0.188	0.380	0.319	0.279	0.376	0.340	0.408	0.444	0.471	0.494	0.504	0.453	0.497	0.334	0.343	0.382	0.189
	ϕ_{2D} [W/m]	6.4000																
	ψ [W/mK]	0.1694																
λ_{filler} 0.18 W/mK	$T_{i,up}$ [°C]	34.420	34.415	34.344	34.151	33.472	32.927	32.519	32.310	32.156	32.008	31.943	32.247	32.988	33.985	34.295	34.411	34.419
	ϕ_{tb} [W/m^2]	11.859	11.967	13.421	17.352	31.237	42.388	50.722	55.010	58.144	61.178	62.516	56.292	41.140	20.753	14.417	12.048	11.875
	d_i [m]	0.016	0.032	0.024	0.016	0.012	0.008	0.008	0.008	0.008	0.008	0.008	0.008	0.012	0.016	0.024	0.032	0.016
	ϕ_{tb} [W/m]	0.188	0.380	0.320	0.276	0.372	0.337	0.403	0.437	0.462	0.486	0.496	0.447	0.490	0.330	0.343	0.383	0.189
	ϕ_{2D} [W/m]	6.3361																
	ψ [W/mK]	0.1662																
λ_{filler} 0.15 W/mK	$T_{i,up}$ [°C]	34.420	34.414	34.340	34.161	33.491	32.957	32.562	32.366	32.229	32.077	32.009	32.304	33.025	34.001	34.293	34.410	34.419
	ϕ_{tb} [W/m^2]	11.859	11.979	13.491	17.144	30.852	41.778	49.850	53.858	56.644	59.770	61.144	55.127	40.378	20.421	14.453	12.058	11.875
	d_i [m]	0.016	0.032	0.024	0.016	0.012	0.008	0.008	0.008	0.008	0.008	0.008	0.008	0.012	0.016	0.024	0.032	0.016
	ϕ_{tb} [W/m]	0.188	0.380	0.321	0.272	0.367	0.332	0.396	0.428	0.450	0.475	0.485	0.438	0.481	0.324	0.344	0.383	0.189
	ϕ_{2D} [W/m]	6.2529																
	ψ [W/mK]	0.1620																

λ_{filler}	$T_{i,up}$ [°C]	34.420	34.413	34.334	34.174	33.517	33.002	32.625	32.445	32.328	32.174	32.108	32.388	33.077	34.021	34.288	34.409	34.419

	ϕ_{tb} [W/m^2]	11.859	11.994	13.619	16.884	30.301	40.842	48.535	52.212	54.611	57.757	59.105	53.381	39.294	20.010	14.548	12.073	11.875
	d_i [m]	0.016	0.032	0.024	0.016	0.012	0.008	0.008	0.008	0.008	0.008	0.008	0.008	0.012	0.016	0.024	0.032	0.016
	ϕ_{tb} [W/m]	0.188	0.381	0.324	0.268	0.361	0.324	0.385	0.415	0.434	0.459	0.469	0.424	0.468	0.318	0.346	0.383	0.189
	ϕ_{2D} [W/m]	6.1360																
	ψ [W/mK]	0.1562																
λ_{filler} 0.09 W/mK	$T_{i,up}$ [°C]	34.420	34.411	34.321	34.191	33.559	33.075	32.727	32.567	32.471	32.322	32.262	32.521	33.157	34.047	34.277	34.408	34.419
	ϕ_{tb} [W/m^2]	11.859	12.023	13.863	16.534	29.447	39.325	46.439	49.704	51.667	54.700	55.928	50.640	37.648	19.459	14.763	12.103	11.876
	d_i [m]	0.016	0.032	0.024	0.016	0.012	0.008	0.008	0.008	0.008	0.008	0.008	0.008	0.012	0.016	0.024	0.032	0.016
	ϕ_{tb} [W/m]	0.188	0.382	0.330	0.263	0.351	0.312	0.369	0.395	0.410	0.434	0.444	0.402	0.448	0.309	0.352	0.384	0.189
	ϕ_{2D} [W/m]	5.9615																
	ψ [W/mK]	0.1475																
λ_{filler} 0.06 W/mK	$T_{i,up}$ [°C]	34.419	34.408	34.296	34.219	33.635	33.211	32.910	32.778	32.706	32.576	32.530	32.753	33.297	34.091	34.253	34.404	34.418
	ϕ_{tb} [W/m^2]	11.859	12.078	14.368	15.941	27.862	36.523	42.665	45.365	46.825	49.480	50.424	45.859	34.772	18.549	15.247	12.160	11.878
	d_i [m]	0.016	0.032	0.024	0.016	0.012	0.008	0.008	0.008	0.008	0.008	0.008	0.008	0.012	0.016	0.024	0.032	0.016
	ϕ_{tb} [W/m]	0.188	0.383	0.342	0.253	0.332	0.290	0.339	0.360	0.372	0.393	0.400	0.364	0.414	0.295	0.363	0.386	0.189
	ϕ_{2D} [W/m]	5.6634																
	ψ [W/mK]	0.1326																
λ_{filler} 0.03 W/mK	$T_{i,up}$ [°C]	34.418	34.400	34.229	34.293	33.829	33.528	33.320	33.232	33.192	33.107	33.087	33.243	33.608	34.198	34.186	34.396	34.417
	ϕ_{tb} [W/m^2]	11.859	12.217	15.711	14.396	23.846	29.982	34.224	36.004	36.825	38.548	38.955	35.787	28.347	16.339	16.570	12.301	11.874
	d_i [m]	0.016	0.032	0.024	0.016	0.012	0.008	0.008	0.008	0.008	0.008	0.008	0.008	0.012	0.016	0.024	0.032	0.016
	ϕ_{tb} [W/m]	0.188	0.388	0.374	0.229	0.284	0.238	0.272	0.286	0.292	0.306	0.309	0.284	0.338	0.259	0.395	0.391	0.189
	ϕ_{2D} [W/m]	5.0212																
	ψ [W/mK]	0.1005																

Table 15_ NumB results, R_{add}=0.0978 m^{2}K/W.

NumB	λ$_{filler}$ [W/mK]									
	0.30	0.27	0.24	0.21	0.18	0.15	0.12	0.09	0.06	0.03
R_i+R_e [m^{2}K/W]	0.5349									
ΔT [K]	20									
$φ_{1D}$ [W/m]	2.447									
$φ_{2D}$ [W/m]	3.792	3.783	3.772	3.761	3.741	3.719	3.688	3.641	3.558	3.349
Ψ [W/mK]	0.067	0.067	0.066	0.066	0.065	0.064	0.062	0.060	0.056	0.045
R_i+R_e [m^{2}K/W]	0.0477									
ΔT [K]	20									
$φ_{1D}$ [W/m]	2.066									
$φ_{2D}$ [W/m]	5.008	4.977	4.935	4.891	4.832	4.755	4.652	4.489	4.229	3.706
Ψ [W/mK]	0.147	0.146	0.143	0.141	0.138	0.134	0.129	0.121	0.108	0.082
R_i+R_e [m^{2}K/W]	0.0487									
ΔT [K]	20									
$φ_{1D}$ [W/m]	3.062									
$φ_{2D}$ [W/m]	7.180	7.136	7.084	7.020	6.939	6.834	6.688	6.471	6.110	5.359
Ψ [W/mK]	0.206	0.204	0.201	0.198	0.194	0.189	0.181	0.170	0.152	0.115
R_i+R_e [m^{2}K/W]	0.0978									
ΔT [K]	20									
$φ_{1D}$ [W/m]	3.012									
$φ_{2D}$ [W/m]	6.528	6.493	6.451	6.400	6.336	6.253	6.136	5.961	5.663	5.021
Ψ [W/mK]	0.176	0.174	0.172	0.169	0.166	0.162	0.156	0.147	0.133	0.100

Table 16_ Ψ-values by NumB procedure.

Annex B

1	2	3	4	5	6	7	8	16	15	14	13	12	11	10	9	
T_{1up}	T_{2up}	T_{3up}	T_{4up}	T_{5up}	T_{6up}	T_{7up}	T_{8up}	T_{1low}	T_{2low}	T_{3low}	T_{4low}	T_{5low}	T_{6low}	T_{7low}	T_{8low}	
22.79	22.78	22.79	22.74	22.66	22.52	22.43	22.36	25.67	22.80	22.76	22.69	22.58	22.49	22.41	22.34	
25.13	25.17	25.07	24.98	24.81	24.51	24.35	24.21	26.95	25.16	25.01	24.72	24.47	24.24	24.15	24.08	
26.97	27.00	26.84	26.67	26.29	25.89	25.64	25.44	28.30	26.94	26.66	26.14	25.73	25.40	25.29	25.25	
28.30	28.31	28.06	27.82	27.28	26.81	26.49	26.25	28.82	28.17	27.78	27.10	26.58	26.19	26.06	26.04	
29.32	29.28	28.99	28.66	27.98	27.46	27.10	26.84	29.76	29.04	28.58	27.78	27.19	26.76	26.62	26.61	
30.07	29.99	29.65	29.27	28.50	27.94	27.55	27.27	30.09	29.67	29.15	28.28	27.64	27.20	27.05	27.04	
30.62	30.52	30.14	29.72	28.89	28.31	27.91	27.61	30.30	30.14	29.58	28.66	27.99	27.53	27.38	27.37	
31.03	30.92	30.50	30.05	29.18	28.59	28.17	27.87	30.55	30.48	29.89	28.95	28.26	27.79	27.64	27.63	
31.34	31.20	30.77	30.30	29.40	28.80	28.37	28.07	30.92	30.74	30.13	29.16	28.46	27.99	27.83	27.83	
31.56	31.42	30.96	30.48	29.56	28.96	28.53	28.22	31.08	30.92	30.30	29.33	28.62	28.14	27.98	27.98	
31.73	31.58	31.11	30.62	29.69	29.08	28.65	28.34	31.61	31.07	30.44	29.45	28.74	28.26	28.10	28.10	
31.85	31.70	31.23	30.73	29.79	29.18	28.74	28.44	31.59	31.17	30.54	29.55	28.83	28.35	28.19	28.19	
31.94	31.79	31.32	30.81	29.87	29.26	28.82	28.51	31.41	31.26	30.62	29.62	28.90	28.42	28.26	28.26	
32.01	31.86	31.38	30.87	29.92	29.31	28.87	28.56	31.01	31.32	30.68	29.68	28.96	28.48	28.32	28.32	
32.07	31.91	31.43	30.93	29.97	29.36	28.92	28.61	31.89	31.37	30.73	29.72	29.00	28.52	28.36	28.36	
32.10	31.95	31.47	30.96	30.00	29.39	28.95	28.64	31.00	31.40	30.76	29.76	29.04	28.56	28.39	28.39	
32.14	31.99	31.51	30.99	30.03	29.42	28.98	28.67	31.61	31.43	30.79	29.78	29.06	28.58	28.42	28.42	
32.16	32.01	31.53	31.01	30.05	29.44	29.00	28.69	32.04	31.45	30.81	29.80	29.08	28.60	28.44	28.44	
32.18	32.03	31.55	31.03	30.07	29.46	29.01	28.70	32.06	31.47	30.82	29.82	29.10	28.62	28.46	28.46	
32.19	32.04	31.56	31.04	30.08	29.47	29.03	28.72	32.07	31.48	30.84	29.83	29.11	28.63	28.47	28.47	
32.21	32.06	31.57	31.06	30.09	29.48	29.04	28.73	32.08	31.49	30.85	29.84	29.12	28.64	28.48	28.48	
32.21	32.07	31.58	31.07	30.10	29.49	29.05	28.74	32.09	31.50	30.86	29.85	29.13	28.65	28.49	28.49	
32.22	32.08	31.59	31.07	30.11	29.49	29.05	28.74	32.10	31.51	30.86	29.86	29.14	28.66	28.49	28.50	
32.23	32.08	31.59	31.08	30.11	29.50	29.05	28.74	30.97	31.51	30.87	29.86	29.14	28.65	28.50	28.50	
32.156	**32.007**	**31.524**	**31.010**	**30.048**	**29.437**	**28.995**	**28.685**	**31.720**	**31.448**	**30.806**	**29.800**	**29.080**	**28.599**	**28.438**	**28.439**	**Avarage value of the last 10 data**

Table 17_ Thermocouples temperatures by ExpB procedure.

ExpA	λ_{filler} [W/mK]
	0.2758
R_i+R_e [m^2K/W]	0.5349
ΔT [K]	20
φ_{1D} [W/m]	2.435
φ_{2D} [W/m]	3.823
Ψ [W/mK]	0.0694

Table 18_ Ψ-value by ExpA procedure.

	ExpB	1	2	3	4	5	6	7	8	9	10	11	12	13	14	15	16	17
	x_i [mm]	0	31.750	63.500	79.375	95.250	103.190	111.130	119.065	127.000	134.940	142.880	150.815	158.750	174.625	190.500	222.250	254.000
λ_{filler} 0.2758 W/mK	$T_{i,up}$ [°C]	32.156	32.007	31.524	31.010	30.048	29.437	28.995	28.685	28.439	28.438	28.599	29.080	29.800	30.806	31.448	31.720	32.156
	ϕ_{tb} [W/m^2]	10.632	11.190	12.998	14.919	18.515	20.799	22.451	23.610	24.531	24.535	23.933	22.135	19.443	15.680	13.280	12.264	10.632
	d_i [m]	0.016	0.032	0.024	0.016	0.012	0.008	0.008	0.008	0.008	0.008	0.008	0.008	0.012	0.016	0.024	0.032	/
	ϕ_{tb} [W/m]	0.169	0.355	0.309	0.237	0.221	0.165	0.178	0.187	0.195	0.195	0.190	0.176	0.232	0.249	0.316	0.389	0.169
	ϕ_{2D} [W/m]	3.932																
	φ_{1D} [W/m^2]	10.632																
	φ_{1D} [W/m]	2.701																
	ψ [W/mK]	0.0616																

Table 19_ Ψ-value by ExpB procedure.

Annex C

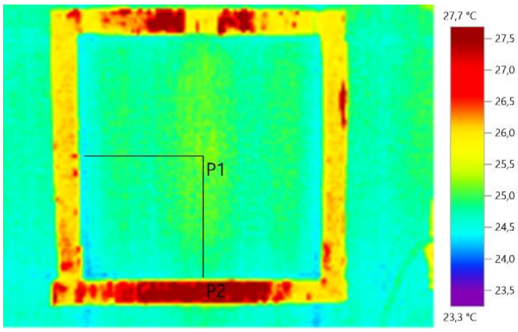

Figure 78_ IR thermography, filled side 13:30

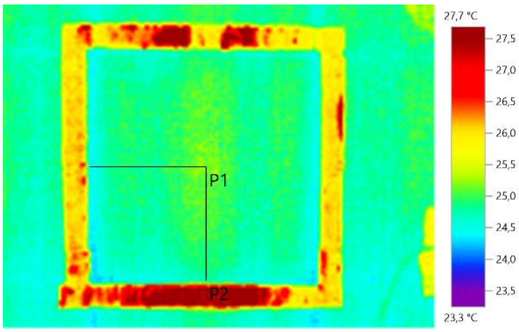

Figure 79_ IR thermography, filled side 13:35

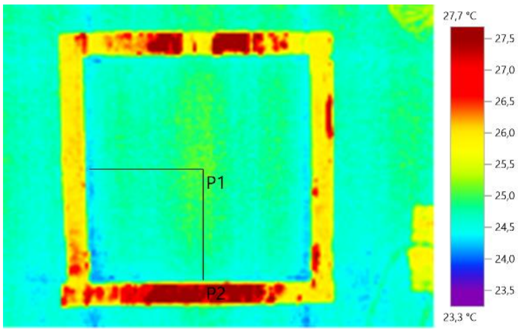

Figure 80_ IR thermography, filled side 13:40

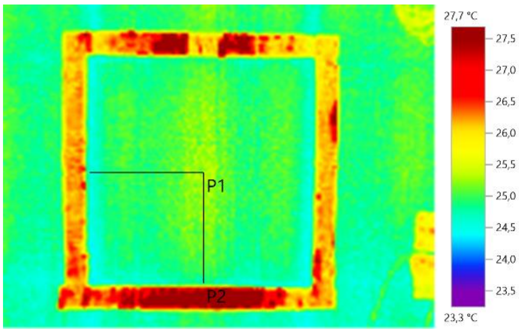

Figure 81_ IR thermography, filled side 13:45

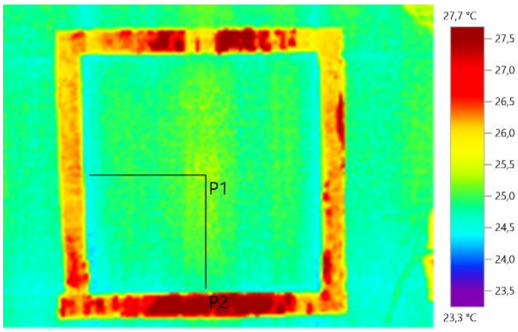

Figure 82_ IR thermography, filled side 13:50

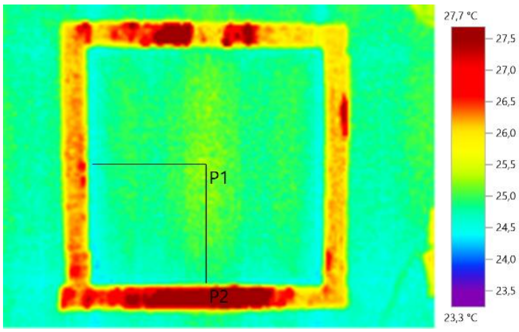

Figure 83_ IR thermography, filled side 13:55

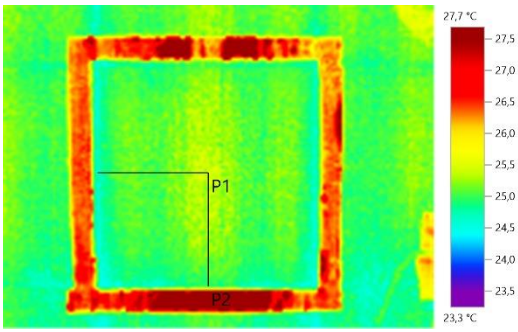

Figure 84_ IR thermography, filled side 14:00

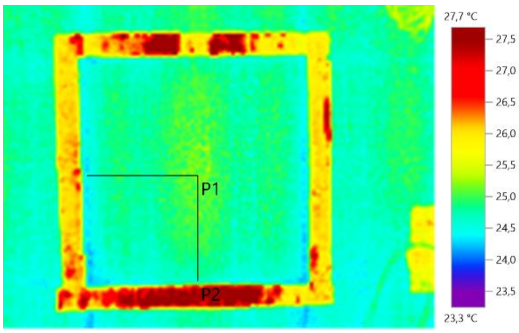

Figure 85_ IR thermography, filled side 14:05

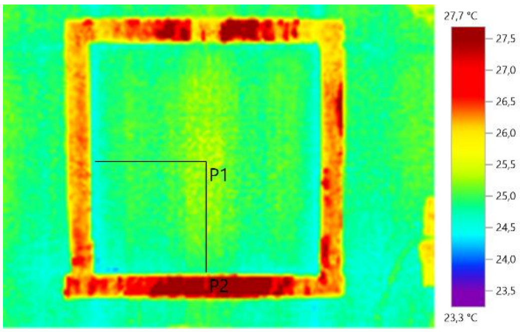

Figure 86_ IR thermography, filled side 14:10

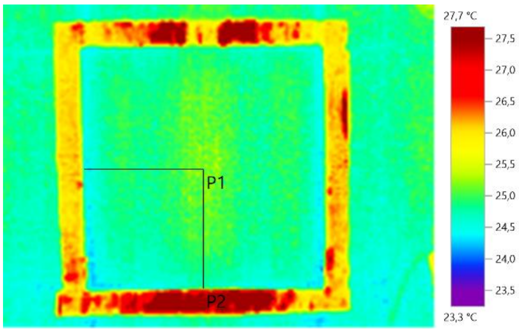

Figure 87_ IR thermography, filled side 14:15

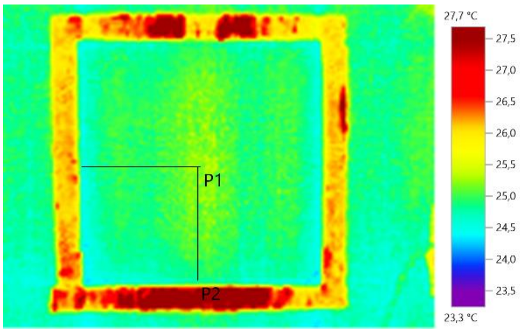

Figure 88_ IR thermography, filled side 14:20

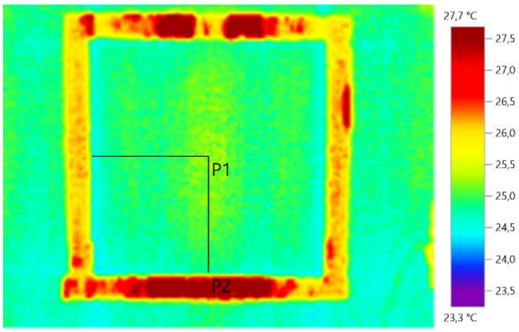

Figure 89_ IR thermography, filled side 14:25

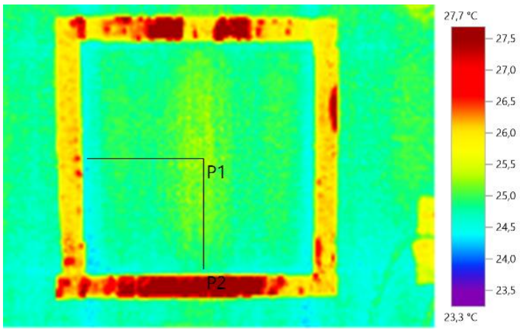

Figure 90_ IR thermography, filled side 14:30

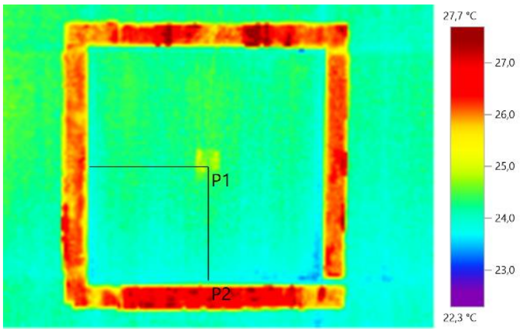

Figure 91_ IR thermography, reference side 13:30

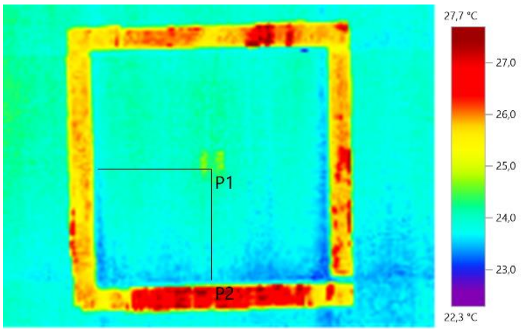

Figure 92_ IR thermography, reference side 13:35

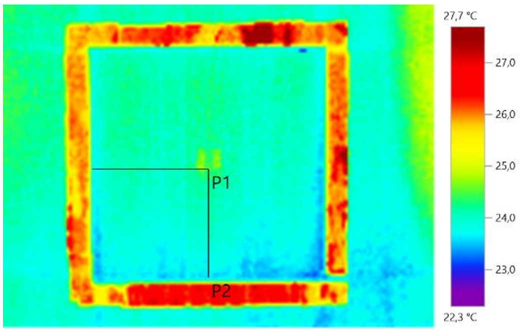

Figure 93_ IR thermography, reference side 13:40

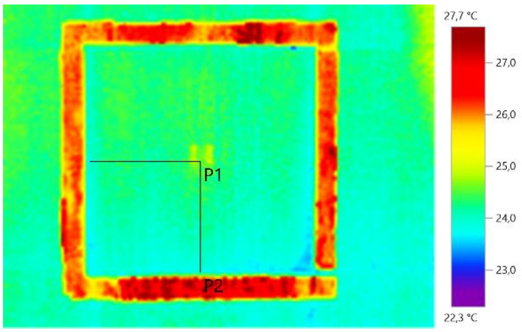

Figure 94_ IR thermography, reference side 13:45

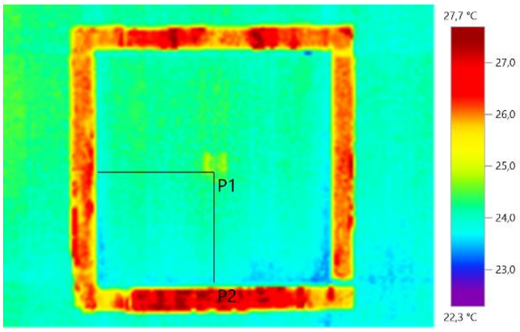

Figure 95_ IR thermography, reference side 13:50

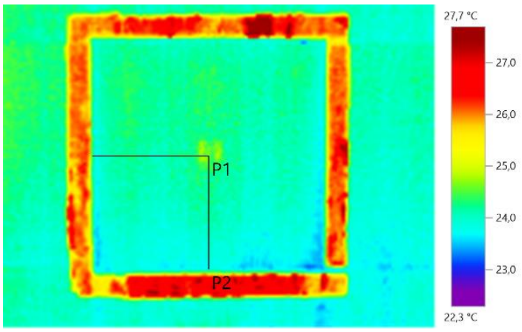

Figure 96_ IR thermography, reference side 13:55

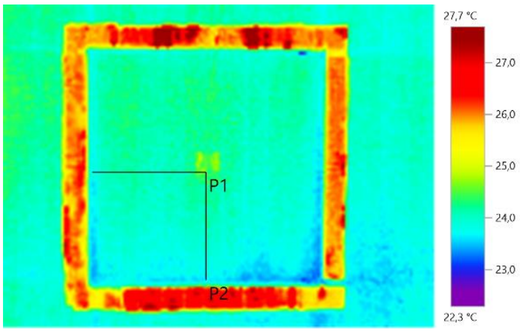

Figure 97_ IR thermography, reference side 14:00

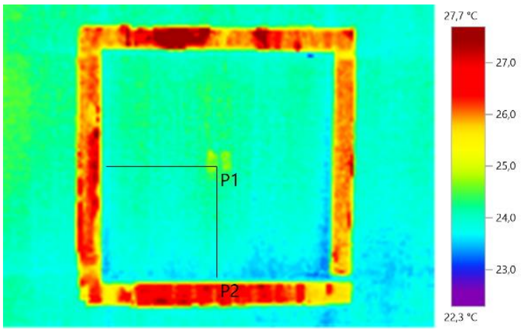

Figure 98_ IR thermography, reference side 14:05

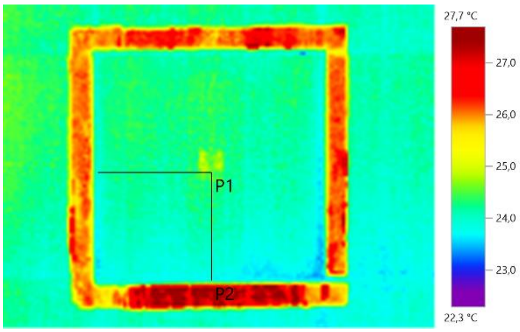

Figure 99_ IR thermography, reference side 14:10

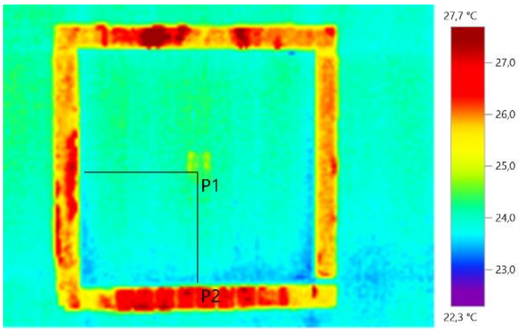

Figure 100_ IR thermography, reference side 14:15

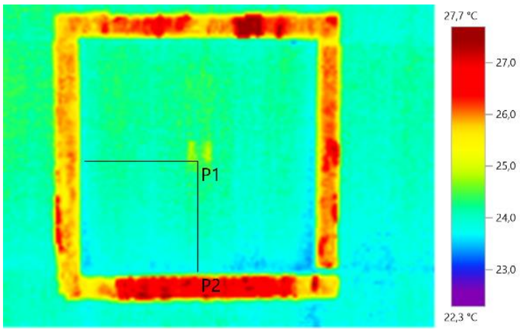

Figure 101_ IR thermography, reference side 14:20

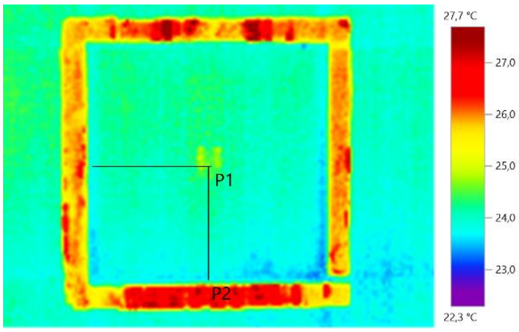

Figure 102_ IR thermography, reference side 14:25

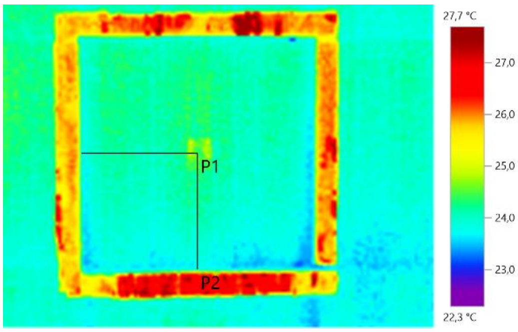

Figure 103_ IR thermography, reference side 14:30

Annex D

	IR	TC	TC		
	Tav_A_c_ref [°C]	Ta_A_ref [°C]	Ta_B_ref [°C]	h_{A_ref} [W/m^{2}K]	U_A_ref [W/m^{2}K]
13:30	23.30	25.280	-5.996	7.163	0.453
13:35	22.90	25.253	-2.823	7.163	0.600
13:40	23.10	25.423	-4.604	7.163	0.554
13:45	23.30	25.371	-2.217	7.163	0.538
13:50	23.20	25.483	-3.246	7.163	0.569
13:55	23.20	25.514	-5.250	7.163	0.539
14:00	23.10	25.399	-2.762	7.163	0.585
14:05	23.10	25.424	-4.277	7.163	0.560
14:10	23.30	25.346	-3.160	7.163	0.514
14:15	23.10	25.331	-3.043	7.163	0.563
14:20	23.20	25.258	-5.089	7.163	0.486
14:25	23.10	25.241	-2.295	7.163	0.557
14:30	23.20	25.226	-3.612	7.163	0.503
					0.540

Table 20_ U_{av}-value, reference side.

	IR	TC	TC		
	Tav_A_c_fil [°C]	Ta_A_fil [°C]	Ta_B_fil [°C]	h_{A_fil} [W/m^{2}K]	U_A_fil [W/m^{2}K]
13:30	23.60	25.490	-6.282	6.521	0.388
13:35	23.70	25.480	-2.892	6.521	0.409
13:40	23.50	25.577	-4.631	6.521	0.448
13:45	23.90	25.590	-2.405	6.521	0.394
13:50	23.80	25.667	-3.306	6.521	0.420
13:55	23.80	25.720	-5.776	6.521	0.397
14:00	24.10	25.601	-2.771	6.521	0.345
14:05	23.60	25.553	-4.328	6.521	0.426
14:10	23.90	25.526	-3.684	6.521	0.363
14:15	23.70	25.628	-3.098	6.521	0.438
14:20	23.80	25.456	-5.195	6.521	0.352
14:25	23.80	25.434	-2.355	6.521	0.383
14:30	23.80	25.419	-3.608	6.521	0.364
					0.394

Table 21_ U_{av}-value, filled side.